DEVELOPMENT OF CONDUCTIVE POLYMER BASED TACTILE SENSORS FOR WEARABLE BIO-MEDICAL DEVICES

W.H.P. Sampath

168073T

Degree of Master of Science

Department of Mechanical Engineering

University of Moratuwa
Sri Lanka

March 2021

DEVELOPMENT OF CONDUCTIVE POLYMER BASED TACTILE SENSORS FOR WEARABLE BIO-MEDICAL DEVICES

Walgama Hewage Peshan Sampath

168073T

Thesis submitted in partial fulfillment of the requirements for the degree
Master of Science

Department of Mechanical Engineering

University of Moratuwa
Sri Lanka

March 2021

DECLARATION

I declare that this is my own work and this dissertation does not incorporate without acknowledgement any material previously submitted for a Degree or Diploma in any other University or institute of higher learning and to the best of my knowledge and belief it does not contain any material previously published or written by another person except where the acknowledgement is made in the text.

Also, I hereby grant to University of Moratuwa the non-exclusive right to reproduce and distribute my dissertation, in whole or in part in print, electronic or other medium. I retain the right to use this content in whole or part in future works (such as articles or books).

Signature: Date:

The above candidate has carried out research for the MSc thesis under my supervision.

Signature of the Supervisor(s): Date:

Prof. Y.W.R. Amarasinghe

Prof. D.V. Dao

Prof. A. Mitani

Abstract

Tactile sensors are devices which acquire data from the physical world through sense of touch. These acquired data may be related to either, surface roughness, texture, force, or any other tactile parameter. Even though, tactile sensor systems are identified as a feasible method to acquire force feedback in robotics and automation systems, due to the requirement of physical interaction between the sensor and application, development of tactile sensors does not come to the spotlight during the past decades. Rather, researchers were more focused on developing non-contact sensors for various sensing modalities when comparing with the tactile sensors. Currently, importance of tactile sensors has come to the spotlight, as development of robotics, automation and biomedical applications are limited due to lack of tactile feedback. Also, many application areas are identified, where tactile sensors can be incorporated such as robotics, industrial automation, biomedical imaging, biomedical robotics, etc.

With the recent advancements of the medical industry, wearable devices are used to support in controlling long-term or repetitive diseases or a disease that comes with time (i.e. chronic diseases) such as heart related diseases, diabetes and asthma by providing information on vital signs. Those vital signs can be heart rate, blood pressure, temperature in the body, blood oxygen level, etc. Other than that wearable biomedical devices are capable of producing smart and intelligent patient monitoring required for several diseases that capable of providing real-time feedback and assist in clinical based decision making. Tactile sensors are useful in measuring and monitoring point based and an area based force/pressure values in biomedical industry.

Under this research, a novel tactile sensor has been developed using a conductive polymer-based sensing element. The incorporated sensing element is manufactured by polymer compression moulding, where the compound is based on silicone rubber and has enhancements by silica and carbon black, with Silane-69 as the coupling agent. Characteristics of the sensing element have been observed using its sensitivity and range.

For the force scaling purpose and point based force/pressure measuring, a novel 3D printed cylindrical arch spring structure was developed for this highly customizable tactile sensor by adopting commonly available ABSplus material in 3D printing technology. By considering critical dimensions of the structure, finite element analysis was carried out to achieve nearly optimized results. A special electrical routing arrangement was also designed to reduce the routing complexities. A microcontroller based signal conditioning circuit was introduced to the system for the purpose of acquiring data. The concept was further improved to use as a tactile sensor array and hence a 3-DoF tactile sensor with a 3D printed square type spring system was also developed in this research.

Under this research, a flexible conductive polymer based sensor that consists of a flexible electrodes sewn on a garment using conductive yarns, also developed. The flexible tactile sensor has been incorporated into a knee brace and tested for its performances of monitoring forces generated at the patella of the knee. The developed sensor attached knee brace is capable of differentiating human activities and posses.

***Keywords*- wearables, conductive polymer, tactile sensor, spring structures, 3D printing, knee brace**

DEDICATION

To the three pillars of my life,

loving wife,

my parents,

and my teachers...

ACKNOWLEDGEMENTS

I am deeply grateful to the Head of the Department of Mechanical Engineering and all the academic and non-academic staff of the department for their constant encouragement in the period of research. Especially my research supervisor, Prof. Y.W.R Amarasighe and co-supervisors, Prof. D.V. Dao and Prof. A. Mitani, who gave me the best support and attention towards my work. Without their keen supervision, none of this would have been possible for myself alone. I consider me very fortunate for being able to work with such resourceful individuals.

I also like to extend my sincere gratitude to Mr. V.S.C. Weragoda of the Department of Material Science and Engineering for helping me in the process of testing tactile sensors. I would like to express my gratitude to the Centre for Advanced Mechatronic Systems (CFAMS), University of Moratuwa for providing academic and financial assistance under the recommendation of the Vice-chancellor and the Dean, Faculty of Graduate Studies of the University of Moratuwa. Further, would like to acknowledge the Senate Research Committee (SRC), University of Moratuwa for providing financial assistance to this research.

I'm deeply grateful to my loving parents, Mr. W.H. Piyasoma and Ms. I.H.S. Weerathunga and my loving wife for all the support given to me. Furthermore, I would like to express my gratitude to Mr. B.A.D.J.C.K. Basnayake, Mr. T.A.U. Roshan and Mr. A.H.T.E. De Silva for their assistance given me throughout my research.

Moreover, I'm particularly grateful to Prof. R.A.R.C. Gopura and Dr. A.G.B.P. Jayasekara who were in the progress review panel appointed for this research, for their valuable comments and advice given to me throughout this research.

Last but not the least, I owe my thankfulness to Mr. R.A.D.N.S. Ranasinghe, Mr. K.D.C. Jeewantha, and Mr. M.N.M. Musammil of the Mechatronic Systems Laboratory and Ms. T.L.K. Kumari of the Applied Mechanics Laboratory of the Department of Mechanical Engineering for providing me with their assistance, tools and facility required for the conduction of my research works whenever required.

Walgama Hewage Peshan Sampath
MSc Postgraduate,
Department of Mechanical Engineering,
University of Moratuwa.

TABLE OF FIGURES

LIST OF FIGURES

LIST OF TABLES

LIST OF ABBREVIATIONS

Abbreviation	Description
ADC	Analogue to Digital Converter
BAN	Body Area Network
CNC	Computer Numerical Control
DAQ	Data Acquisition
FSR	Force Sensitive Resistors
EDAX	Energy-Dispersive X-ray
FEA	Finite Element Analysis
GUI	Graphical User Interface
LabVIEW	Laboratory Virtual Instrument Engineering Workbench
MEMS	Micro Electro Mechanical Systems
PLA	Polylactic Acid
RTV	Room Temperature Vulcanizing
SEM	Scanning Electron Microscope
USB	Universal Serial Bus
USD	United State Dollars
VISA	Virtual Instrument Software Architecture

LIST OF APPENDICES

CHAPTER 1

INTRODUCTION

Tactile sensing that is capable of sensing the physical parameters by interacting with the physical environment, is another popular mode of sensing used in fields like robotics, industrial automation, aerospace, etc. Unlike non-contact sensors (temperature, vision, motion), tactile sensors haven't developed much over the past decades. Nevertheless, at the present many industrial and commercial applications now appear to be on the cusp of accepting tactile sensing technology. The tactile parameters that can be measured through such tactile sensor may vary from force, pressure, surface roughness, surface texture, temperature, etc. There are many transducer techniques available so far regarding the tactile sensors, such as capacitive, piezoresistive, piezoelectric, strain gauges, etc. They have their advantages and disadvantages [1].

The conductive polymer is one of the sensing technique used in piezoresistive tactile sensors. Conductive polymers have received significant attention in both science and engineering community due to their attractiveness in a wide range of electrical conductivity, which can be achieved with various doping levels while maintaining their mechanical flexibility and high thermal stability [2]. By incorporating conductive polymer based tactile sensing elements to a wearable bio-medical device, data related to human haptic such as interaction, exploration, manipulation, and extraction of object properties such as texture, shape, hardness, and temperature can be acquired for further analysis and predictions.

This research intends to develop conductive polymer based tactile sensors that illustrate mechanical flexibility in production. A combination of conductive polymer based material and a rigid or flexible structure can be used to provide quantitative measurements to physicians by developing a bio-medical monitoring platform/device and was identified as one of the intentions of this research.

This research work mainly focuses on the development of conductive polymers for tactile sensors and incorporate them for biomedical devices. The Figure 1.1 shows the structure of this research thesis as a summary.

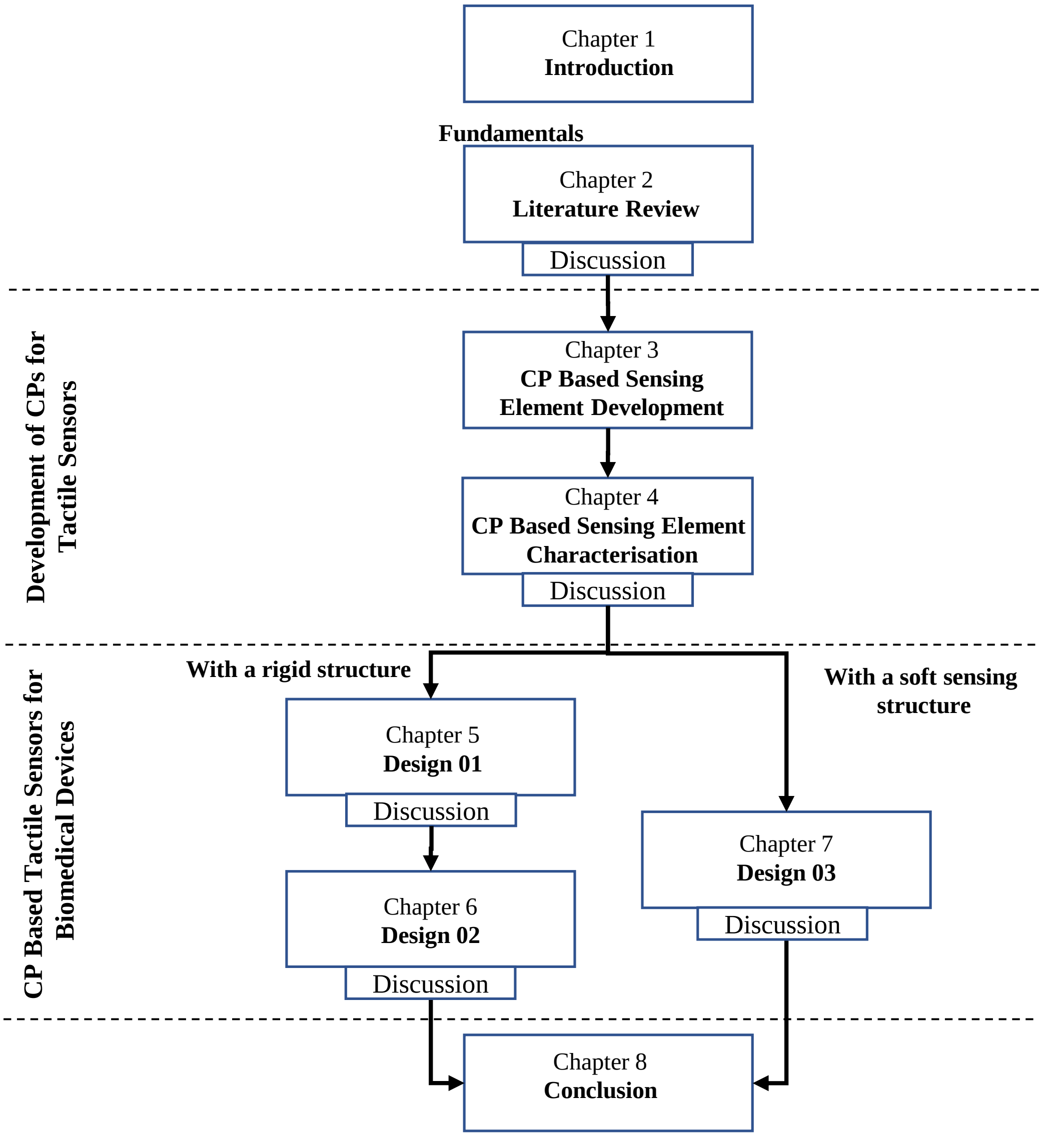

Figure 1.1: The structure of the thesis.

When developing tactile sensors, it is vital to conduct a literature review, regarding tactile sensors and to identify the current stage of development regarding them. Hence, Chapter 2 of this thesis consists of the details about the conducted literature review. Further, the prospective manufacturing methods of tactile sensors using conductive polymers are also discussed in the literature review.

The Chapter 3 of this thesis consists of the details about the development of the conductive polymer based sensing elements. The fabrication of sensing elements was discussed with the suitable materials and steps followed during the fabrication process. The Chapter 4 consists of the detailed characterization of the sensing element in terms of mechanical and material properties. Possible applications of the developed conductive polymer based sensing element were discussed in Chapter 3.

Chapter 5 and 6 contain details related to the development of a rigid sensing structures based on 3D printing technology. After identifying restrictions of using for biomedical applications, the Chapter 7 contains details of the flexible structure that incorporated a conductive polymer based sensing element to use with a knee brace for biomedical applications.

CHAPTER 2

LITERATURE REVIEW

2.1 Tactile Sensing and Tactile Sensors

2.1.1 What is tactile sensing?

Usually, the sensory information from various and multiple sensory modalities such as touch, vision, hearing etc. are required to cooperate and distinguish the environment. This sensory information could come from a single modality or concurrently from numerous sensory modalities to acquire powerful percept. Numerous sensory modalities may cooperate or combine in perfect ways to acquire a robust percept as in human [3]. The tactile sensing measures the parameters related to physical contact with the environment.

2.1.2 What are tactile sensors?

Tactile sensors are capable of capturing electronic sensing signals using tactile sensing principles and measuring tactile parameters with the assistance of physical touch. Tactile parameters may often include temperature, vibration, softness, texture, shape, shear, and normal force [4]. Even though pressure and torque are not identified as tactile parameters in this list, they are important parameters that can be sensed through physical touch [4–6].

2.1.3 Past trends and advancements

Even though tactile sensing came to the attention of researchers in the 1970s, tactile sensors have not been developed much compared to the non-contact sensors [7, 8], due to the direct physical contact forces/impacts that have to be manipulated by the sensors/sensor-structures themselves. With the recent advances in the robotics and automation field, there is a requirement for tactile sensing feedback systems that performs better with respect to force range, dynamic range, frequency response, and special resolution [9]. Henceforth, a large amount of research has been carried out on the subject of tactile sensing and numerous devices have been developed for different applications [5, 10, 11]. Besides, application areas of tactile sensing have been expanded as new fields of applications have emerged in recent times.

The advancements in the research and developments related to tactile sensors has a solidly increasing trend and details were mentioned under the Table 2.1. Counts of papers published per decade using search terms "tactile AND sensor" was tabled as follows:

Table 2.1: Past trends and advancements of the researches and developments in tactile sensors.

Year	**Scopus**	**IEEE**	**ScienceDirect**	**Springerlink**
1970-1979	43	11	–	146
1980-1789	537	169	–	654
1990-1999	724	636	1823	1267
2000-2009	1752	1298	2867	2839
2010-Present	4376	2912	6213	7295

Although human tactile sensing or more specifically human skin provided a reference point to researchers when developing tactile force sensors, tactile sensors are only capable of sensing a lesser number of tactile parameters simultaneously [12]. Current tactile force sensors face difficulty in meeting the demands of force sensors required in modern sophisticated measurement systems and control systems.

2.2 Different Types of Tactile Sensing Principles

Frequently researched tactile transduction techniques are mostly based on capacitive, piezoresistive, piezoelectric and optical methods. These sensing principles have their advantages and disadvantages.

Capacitive tactile sensors

The working principle of a capacitive type tactile sensor is to measure the variation in capacitance occurred due to the applied mechanical changes to the geometry of the capacitor. The capacitance (C) of a parallel plate capacitor could be determined using [13]:

$$C = \frac{A\varepsilon_0\varepsilon_1}{d} \tag{2.1}$$

where ε_0 and ε_1 are the permittivity of free space and dielectric material respectively. A and d are the overlapped area and the layer gap of two parallel plates respectively.

In general, capacitive sensors showcase a good frequency response, high spatial resolution and large dynamic ranges. However capacitive sensors might be susceptible to different types of noises.

Piezoresistive tactile sensors

Piezoresistive tactile sensing is achieved by mechanically changing resistivity/ conductivity of a sensing element and measuring the variation by an external circuit. Typically, piezoresistive metal or semi conductive foils are used as the sensing element for commercial strain gauges. Piezoresistive effect for a conductive (semi-conductive) material can be described as [13]:

$$\frac{\Delta R}{R} = (1 + 2\sigma + \pi E)\chi \tag{2.2}$$

The equation for the electrical resistance can be given by:

$$R = \rho \frac{L}{A} \tag{2.3}$$

The mathematical relationship for piezoresistive coefficient along a crystal orientation can be written as:

$$\pi = \frac{\Delta\rho}{\rho} T \tag{2.4}$$

The relationship between stress (T) and strain of a piezoresistive element can be described as:

$$\pi = \frac{T}{\chi} \tag{2.5}$$

where,

R : electrical resistance of a conductive structure along longitudinal direction

ΔR : change of resistance as a result of applied strain.

σ : Poisson's ratio of the material.

π : piezoresistive coefficient.

E : Young's modulus

χ : the longitudinal strain.

Piezoresistive sensing methods are robust against noise, and a better choice for array based applications. By considering the limitations, piezoresistive sensing technology is greatly affected by hysteresis, resulting in lower frequency response, so it is limited to use for dynamic measurements with marginal spatial resolution.

Piezoelectric tactile sensors

The different sensing principles for piezoelectric tactile sensors can be considered as passive and active. Passive tactile sensing make use of direct piezoelectric effect. Electrical charge is generated because of the material polarization under external stresses. So the generated electrical charge density D_i at i orientation/ direction can be expressed as [13]:

$$D_i = d_{ijk}\ \chi_{jk} \tag{2.6}$$

where d_{ijk} is the direct piezoelectric coefficient of the material and χ_{jk} is the externally applied stress.

Piezoelectric sensors exhibit a very good high-frequency response. Due to that, they are suitable to measure vibrations. But limited performance in measuring dynamic forces. Usually used as sandwich structures where piezoelectric layers are deposited in between two electrode layers.

Optical tactile sensors

Optical tactile sensing is obtained by coupling geometric change of electromagnetic wave guide with the modulation of wavelength, the intensity of the wave, polarization or phase. Optical tactile sensing is immune to electronic noise and generally have high spatial resolution and a wide dynamic response range. Optical tactile sensing can be used for sensing compliance, surface roughness, shear and vertical stress.

Comparison on tactile sensing techniques and typical examples

A brief comparison of these tactile sensing techniques and their relative advantages and disadvantages are summarized in the Table 2.2 with typical examples.

Table 2.2: Summary of tactile sensing technologies.

Sensing technique	**Advantage**	**Disadvantage**	**Typical example**
Capacitive	Excellent sensitivity Good spatial resolution Large dynamic range High repeatability	Noise susceptible Complexity of measurement electronics	Pressure Profile systems, Robotouch [14, 15]

Resistive: Quantum Tunneling Composites	Good sensitivity Wide dynamic range	Hysteresis Absorption of gases	Peratech QTC [16]
Resistive: Strain gauge	Good sensitivity Wide dynamic range	Expensive	[17]
Resistive: Deformable contact area	Flexible Thin	Hysteresis Absorption of gases	Inaba: Inastomer [18]
Resistive: Conductive fabric	Flexible Robust	Unable to resolve more than one contact point	[19]
Resistive: Piezoresistive conductive polymer	High sensitivity Good spacial resolution Repeatability Low cost	Low sensing range Hysteresis occur at certain range	Tekscan Flexiforce [20]
Piezoelectric	High frequency response High sensitivity High dynamic range	Hysteresis Absorption of gases	Peratech QTC [21, 22]
Optical: Resistive	Good sensing range Good reliability High repeatability High spacial resolution Immunity from EMI	Buly in size Non-comfortable Complex in fabrication	[23]

2.3 Components of Tactile Sensor

2.3.1 Sensing element

The core component of the tactile sensor is the sensing element and the performance of the tactile sensor is mostly rely on the characteristics of the sensing element.

Materials for capacitive tactile sensors

Various material types were used to fabricate capacitive sensing structures. Additionally the possibility for the formation of sandwich, parallel capacitors and good mechanical properties are essential for those materials. Polysilicon has been widely used material for capacitive tactile sensors [24, 25]. Polymer materials that posses chemical stability and elastic properties upto a certain extent (such as Polydimethylsiloxane (PDMS) [26, 27] and SU-8 [28]) are also becoming popular among researchers. Those polymer materials are common in the field of flexible tactile sensor devices [26, 27]. The polymer materials can be used for di-electrical intermediate layers [29], movable sensing plates, or the 3D contact promoters in flexible tactile sensors [26, 27].

Materials for piezoresistive tactile sensors

The piezoresistive sensing materials are required to pose both electrical resistivity and mechanical elasticity. Few types of metals, semiconductors and polymer materials can be considered for piezoresistive materials. The single crystal silicon and polysilicon [30–32] were used mostly during the early stage of tactile sensors. Currently, piezoresistivity in carbon nanomaterials such as multi-walled carbon nanotube and graphene related materials [33, 34] are also using for piezoresistive materials. Carbon black micro/nanoparticles [35] were also attractive methods used in recent researches.

Materials for piezoelectric tactile sensors

Limited number of natural and synthetic materials exhibit piezoelectric properties that are suitable for tactile sensors. Out of those materials quartz [36], zinc oxide [36,37] and lead zirconated titanate (PZT) [38,39] are commonly used materials. Polyvinylidene fluoride (PVDF) [40, 41] is the most popular material used for flexible piezoelectric tactile sensors.

2.3.2 Packaging or mechanical structures

As per the researchers, a mechanical structure mainly protects the sensing element. The structure also caters as a platform to transmit the applied force towards the sensing element while diminishing the amount of force applied to the sensor structure.

Here, a few of those related researches were considered. The sensor and the structure shown in Figure 2.1 was developed by Choi et al. [42] to integrate it to the fingertips of an anthropomorphic robot hand called SKKU Hand [43]. Lanes of resistive ink and strips made of polyvinylidene fluoride (PVDF) were used on top of the base material - polyester films. The sensor also can be bent due to the flexible quality of chosen materials.

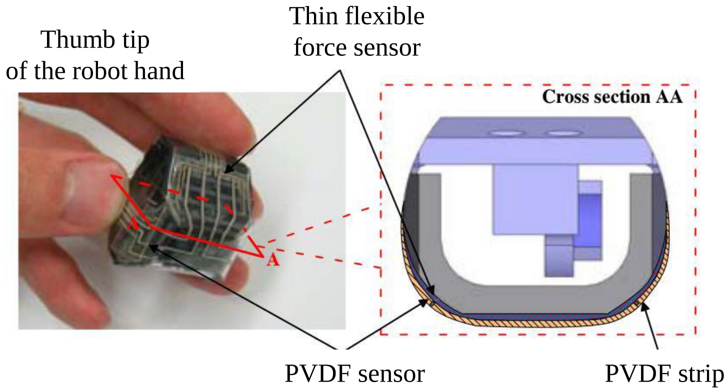

Figure 2.1: Tactile sensor module for integration into the fingertips of a robotic hand.

The BioTac, a finger-shaped sensor array developed by Wettels et al. [44] capable of providing information on contact forces, micro vibrations and thermal fluxes simultaneously. The main element of this sensor (shown in Figure 2.2) is an electrically conductive fluid that filled in the cavities of the structure while the contact surface is made from an elastomeric skin. During an excitation at the surface, vibration is transmitted through the fluid to a pressure sensor.

Tan et al. [45] developed an optical fiber slide tactile sensor based on the inner modulation mechanism of optical fibers (model shown in Figure 2.3) in order to use with an underwater robots. This sensor has a spring-shaft mechanism that can transmit the excitation identified by the roller at the contact region.

The research work by Zhang et al. [46] describes a novel approach for underwater dexterous hand structure whose fingertip is equipped with underwater tactile force sensor array. It is capable of identifying the location of the grasping sample and force perception. [46]. This was designed as a differential pressure capsule-shaped tactile

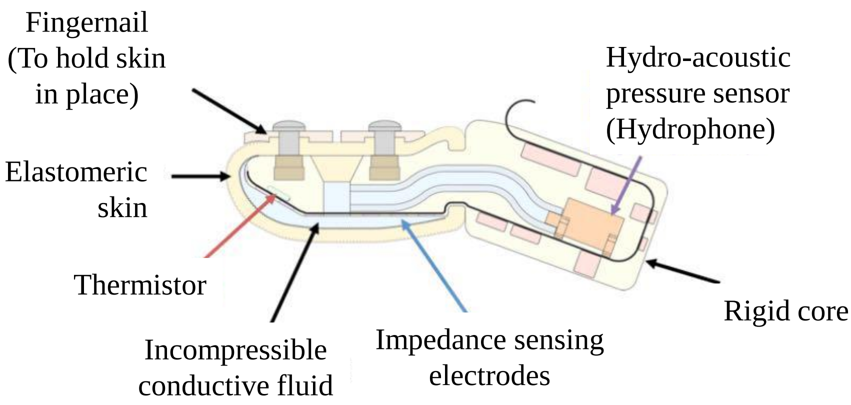

Figure 2.2: Multi-model tactile sensor for robot hand development.

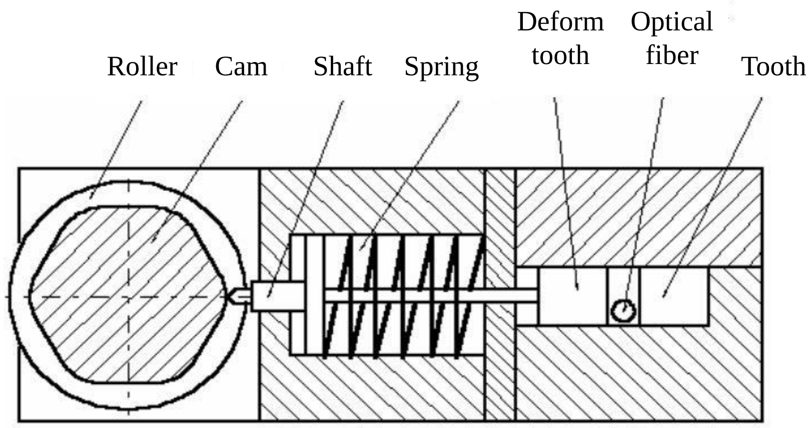

Figure 2.3: Tactile sensor developed by Tan et al. based on microbending fiber-optic sensing.

sensor. External tactile stimuli are transmitted to strain elements through a silicone oil medium. Here, a silicone cup plays a vital role as a medium to the tactile force transmission.

One of the previous works leading to this research, tactile sensor development work conducted by Udayanga et al. [47, 48] is shown in Figure 2.5. This sensor uses an external spring-piston mechanism as an agent to transmit the force and reduce the amount of force applying to the QTC sensing element.

It can be mainly seen that outer protection or a covering is provided to the sensing element by the structure while acting as a tactile force applying platform to the sensor.

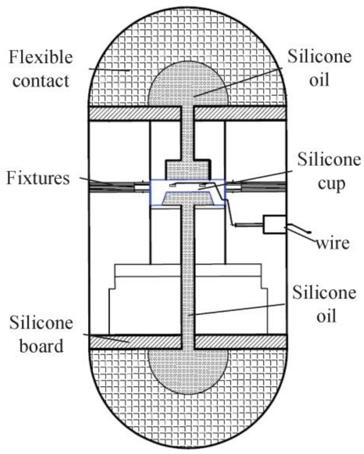

Figure 2.4: Tactile force sensor developed by Zhang et al. for underwater dexterous hand intelligent grasping.

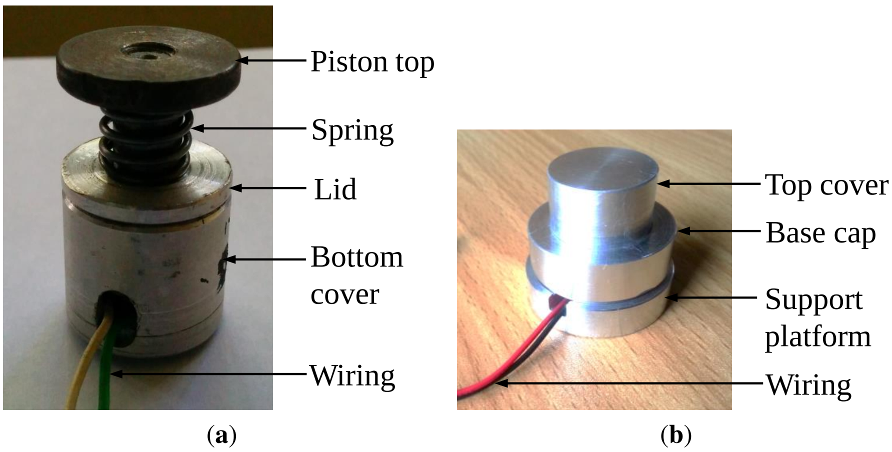

Figure 2.5: QTC based tactile sensors developed by Udayanga et al.: (**a**) unenclosed sensor; (**b**) enclosed sensor.

Further, the structure caters as a system to transmit and focus the tactile force into the sensing element. In each design, structures are designed so that it allows the control in tactile force and the total deflection/variation at the sensing element. In most of the aforementioned researches, the out structure facilitates the control unit or the electric circuitry. In the design architecture of Udayanga et al. [47,48], Zhang et al. [46] and Tan et al. [45] structures provide some amount of elasticity to the sensor while providing the capability to releasing back to the initial state or position after the removal of the tactile force. In addition to that, the tactile sensor developed by Udayanga et al. [47,48] provides overload protection to the sensor itself.

The identified materials used by the researchers considered for the aforementioned structures are discussed under the Table 2.3.

Table 2.3: Different materials used for tactile sensing structures.

Research		Sensing element	Materials used
Choi et al.	[42]	PVDF	base material - polyester films outer structure - PVDF resistive ink layers
Wettels et al.	[44]	Hydrophone	contact surface - elastomeric skin
Udayanga et al.	[47, 48]	QTC	metal structure - Aluminium alloy 1060

In these research works, traditional manufacturing methods were used for most of the structures and structures are simple in configuration. In contrast with traditional manufacturing methods, additive manufacturing methods like 3D printing exhibits abilities to achieve complex geometries at a relatively low cost. With the recent advancements, 3D printing technology and 3D printing materials can also identify as potential manufacturing method and materials for structure development.

2.3.3 Circuitry

Generally, sensors produce an electrical signal corresponding to the changes in the inputs. Therefore, the circuitry that is associated with different sensors should be able to acquire electrical signals and treat the acquired signal appropriately. The acquired sensor signal may be amplified, filtered or modified to the desired output voltage. But the signal conditioning may not be necessary for all the sensors. Most of the sensors required a sufficient amount of input voltage and can't perform independently.

2.4 Conductive polymers for tactile sensors

Tactile sensors that have wider input ranges and wrap a larger area can be developed by arranging single force/tactile sensors on a flexible substrate [49, 50] that involves higher cost components due to the required number of force/tactile sensors for the assembling purpose. A batch fabrication is required to reduce the cost involved with this.

The use of sensors similar to Tekscan Flexiforce [20] for large surface applications seems beyond the limit due to the high cost of materials like metallic microparticles (silver). Further, the tactile sensor developed by Someya et al. [51] using polydimethylsiloxane (PDMS) conductive graphite particles and the fabrication consisted of a gold layer deposition (vacuum evaporated) and polyimide layers (cured at 180^0C) increasing the fabrication cost.

In the context of tactile sensors with a larger area, conductive polymers play an important role as the material cost and fabrication cost are relatively lesser. Conductive polymers are a class of organic materials that pose electrical and optical properties similar to semiconductors and metals. Conductive polymers can be prepared using simple, adaptable, and cost-effective methods. Various procedures have been developed to enhance and tune the conductive polymers to integrate and interface them into biomedical applications, including biomaterials and biosensors [52].

Conductive polymer based piezoresistive force sensors have benefits of good sensitivity, low noise, simplicity in electronics, low-cost manufacturing and physical flexibility of the sensing element. If the conductive polymer based piezoresistive force sensing element equips the intra-electron tunnelling effect, other than the classical percolation piezoresistivity, the sensitivity would be further enhanced.

2.4.1 Philosophy of conductive polymers

Carbon black material can be used as the conductive phase of conductor-filled polymer composites. With a suitable amount of carbon black, the composites gain flexibility and piezoresistivity. These type of materials can be used as the sensing element of a tactile force sensor. The study on the relation between the composite resistance and external pressure/ force is important to design this kind of sensors.

To describe the changes taking place with effective conductive paths of a carbon black filled silicone rubber composite when it is subjected to a uniaxial pressure/force, Luheng et al. [53] used a shell structure model as illustrated in Figure 2.6.

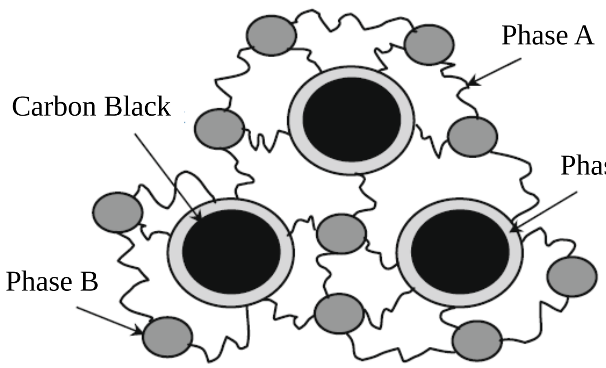

Figure 2.6: Shell structure model of carbon black filled silicone rubber composite.

In this shell model, the rubber molecule chain that is not absorbed by carbon black is described as phase A and it posses active micro-Brownian motion. A cross-linked rubber molecule chain whose motion has been restricted is described as phase B. Rubber molecule chain absorbed by the carbon black surface posses a low level of activity in terms of motion, is described as phase C. In this model, elastic “phase A” and “phase B” are bonded to “phase C”, form a three dimensional network [53].

Carbon black has a comparatively lesser amount of resistivity than the resistivity of silicon rubber and consequently carbon black acts as a conductive phase. The tunnelling effect is the cause for the local conductive paths that initiated when the gap between carbon black particles is small enough. The effective conductive paths are formed when the local conductive paths penetrate the insulating matrix (as shown in Figure 2.7), and contribute towards the conductivity of the composite. When the composite subjected to external compressive forces, gap sizes in existing effective conductive paths can be changed or new effective conductive paths can be formed and resultant will be a reduction in resistance. Apart from that destruction of effective conductive paths that increase the resistance of the composite can be occurred [53].

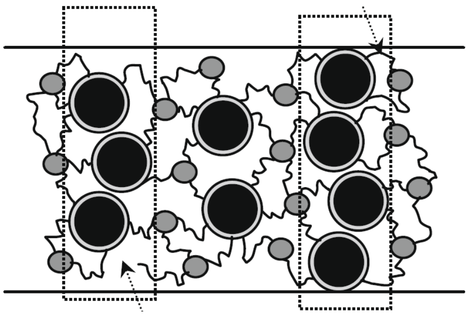

Figure 2.7: Local and effective conductive paths in a composite.

2.4.2 Challenges of conductive polymers

To bring conductive polymers into clinical practice, there are some major limitations, which should be properly addressed, including their processability, cytotoxicity, a considerable gap between in vitro and in vivo outcomes, and suboptimal mechanical and magnetic properties. Thanks to new technologies (e.g., nanotechnology and the 3D printing technique), some of the predetermined limitations (e.g., magnetic and mechanical properties) could be resolved to some extent. However, the major obstacle, which is the huge gap between in vitro and in vivo results needs to be addressed in the future.

As for drawbacks, conductive polymer based piezoresistive force sensors are behaving nonlinearly in response to hysteresis, signal drift and temperature sensitivity [12]. Henceforth, conductive polymer based piezoresistive force sensors have to be used in a steady temperature environment with thorough signal conditioning.

2.4.3 Materials used for conductive polymers

In general, flexible polymer substrates have been widely used in the development of tactile sensors. Thomas et al. reported a flexible tactile sensor with a large area of $100 \times 100\ mm^2$ [54]. Conducting adhesive printed with screen printing technology was used to pattern the resistive sensing array. Forces from different directions were successfully detected using the sensing array. Alternatively, Cheng et al. reported a resistive tactile sensor with great flexibility. Mixed conductive composites composed of carbon black, copper powder, silver powder and PDMS elastomer were printed on a spiral structure by ink-jet printing. The produced force sensor was capable of twisting up to 70° without damage [55].

Huang et al. [35] described a method of developing a conductive polymer based on silicone rubber and carbon black. This polymer reported a great amount of flexibility. Materials used by Huang et al. [35] are listed down in Table 2.4. Further, the researcher suggested and implemented a method of improving the conductivity using a nano modification. The customizability and the flexibility offered by this method shows promising signs for usage in biomedical applications.

Table 2.4: Raw materials used by Huang et al. for the polymer development.

Raw material	**Specification**
Silicon rubber	GD-401 Single component Room temperature Vulcanization (RTV)
Carbon black	ECP-CB-1 High conductive Resistivity $0.2 \sim 0.6\Omega cm$ Particle diameter $30 - 40nm$ Specific surface area $1000 - 1100m^2/g$
Nano-SiO_2	particle diameter $15 \sim 20nm$
Si-69	Density $650 \sim 750kg/m^3$

2.4.4 Fabrication processes

Huang et al. [35] conducted the polymer fabrication at normal temperature and pressure. The high-conductive carbon clack ECP-CB-1 was mixed with Si-69 silane coupling agent using FS-150 ultrasonic disposal equipment for $30 \sim 40$ minutes with ultrasonic dispersion method. Later for the nano modification, nano-SiO_2 was added and mixed for another 30 – 40 minutes. Finally, the liquid silicone rubber was added and prepared by ultrasonic dispersion for 20 – 30 minutes and injected the mixed solution into the prepared structural model of the tactile sensor and kept for 64 – 72 hours for curing.

2.5 Applications of Tactile Sensors

In many pragmatic situations, it is vital to obtain pressure distribution over an identified surface. Robotics, sports, biomedical, agriculture & food processing and consumer products fall under a few of those application domains of pressure/force sensors [44]. Key application areas of tactile sensors and design challenges in each application industry are listed down under the Table 2.5.

Table 2.5: Identified application industries of tactile sensors with key areas and challenges.

Application industry	**Key utility and application areas**	**Design challenges**
Robotics	Dexterous manipulation Tele-robotics Service robots Exploration robots Rescue robots	Arrayed sensors Discrimination & classification algorithms Repeatability & wear resistance Customization Characterized response over wide temperature range High frequency response
Sports	Posture analysis Sports training	Conformable & customizable sensors Wiring & power constraints Wireless interfaces

Sports	Posture analysis Sports training	Conformable & customizable sensors Durability Wiring & power constraints Wireless interfaces
Biomedical	MIS tools Tele-robotic operation Diagnostics tools Rehabilitation medicine Dentistry Gait analysis system	Bio-compatibility Rugged to withstand sterilization process Cost due to their disposable nature Characterization & classification algorithms Wireless interfaces Power consumption High frequency response Safety & reliability Ergonomics
Agriculture & food processing	Service robots	Adaptability to unstructured environments Toxin & allergin free construction Hygiene & cleanliness Dexterous movements Soft grippers Unexplored application area
Consumer products	Healthcare products Service robots for elderly Textile & clothing	User acceptance Wear resistance & reliability Cost for a wider application market Rugged to bear abuse

The tactile sensors essential in the aforementioned application areas have their special requirements. One of the vital aspects is its size. The required sensing areas can vary from $1m^2$ to $1mm^2$ or even less. Moreover, the number of sensing points (each usually termed tactel, taxtel, taxel or sensel analogy to a pixel (picture element) in an image sensing array) required for such a tiny sensing area is higher. These characteristics alone point to the requirement of implementing such tactile sensors as arrays of sensors manufactured using special techniques.

In one of the prior works and a motivation lead for this research in biomedical applications, a sensor embedded shoe was developed as a plantar pressure measurement system [56, 57]. This remote caretaking system that consists of a sensor embedded shoe and a waist belt allow monitoring gait patterns, activities and postures of patients remotely. A tactile sensor array of Flexiforce force sensitive resistors (FSR) [20], signal conditioning circuitry and communication modules were integrated into each shoe (Exploded view of a designed shoe is shown in Figure 2.8). Micro-controller development board based circuitry with an accelerometer, GPS location sensor, communication modules were incorporated into the waist belt of this system.

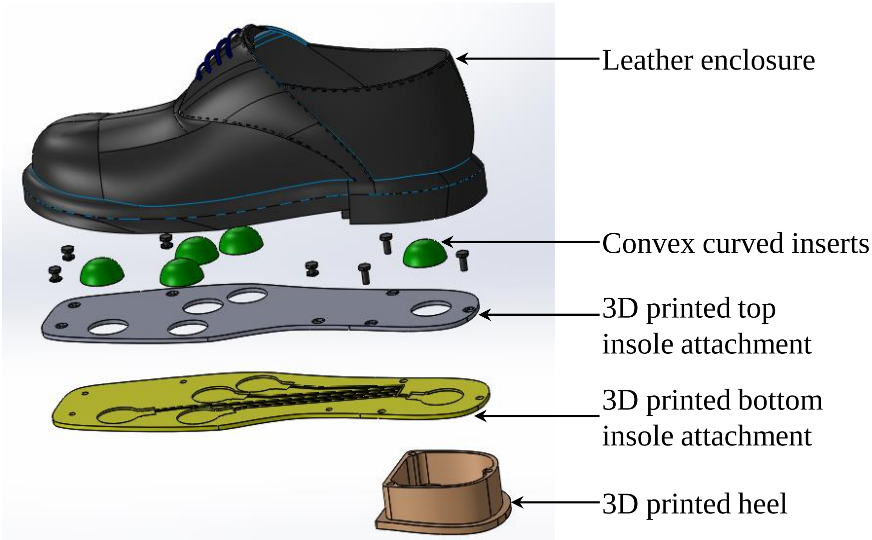

Figure 2.8: Tactile sensor embedded plantar pressure measurement system by De Silva et al. for remote patient monitoring.

In the design process of sensor embedded shoe, FSRs were aligned to vital plantar pressure points using three (03) 3D printed insole attachments [56, 57] (Figure 2.9 shows the arrangement of layers). Further, in the sensors embedded shoe by De Silva et al. [56, 57], convexly curved inserts made out of silicone rubber was used as a platform to capture plantar pressure data and transmit it towards the sensing element. Top and bottom insole attachments were used to provide protection and align sensors to those identified vital pressure points. The 3D printed heel was used as a compartment to the signal conditioning circuit.

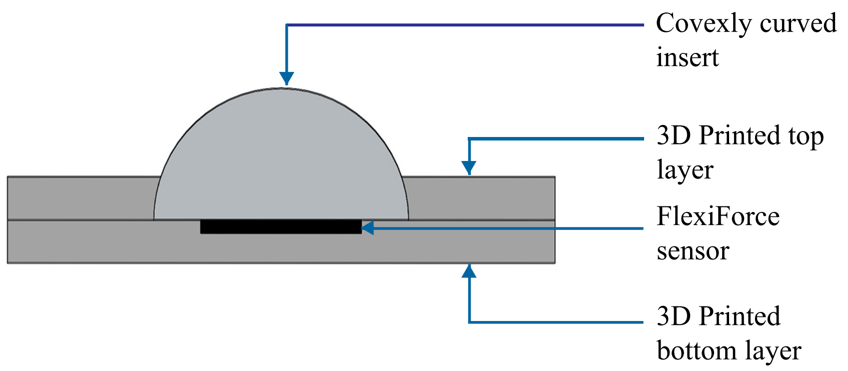

Figure 2.9: Assembly of layer and sensing element in De Silva et al. for remote patient monitoring.

2.6 Conclusion – Literature Review

Tactile sensing is one of the promising techniques used in wearables and existing tactile sensing techniques have their own advantages and disadvantages [44]. The use of tactile sensing technique and sensors should be identified by considering the performance required for the application. In this context, the sensitivity, response time, spatial resolution, range, geometry, stability, etc. should consider. In this literature survey, it was identified that a sensor/sensing technique that poses flexibility will open new paths for many technologies. In another way, it is necessary to develop novel tactile sensors with good performance to use with various biomedical applications.

With the recent advancements in tactile sensors, wearable biomedical devices with tactile sensors demonstrate capabilities noninvasive sensing, local controlling and processing, acquiring user feedback and communicating. Both real-time and post processing of those data captured using tactile sensors can be used for applications like vital signs and disease identification.

CHAPTER 3

DEVELOPMENT OF A CONDUCTIVE POLYMER BASED TACTILE SENSING MATERIAL

3.1 Introduction

According to the conclusion of the literature review conducted related to this research, it was identified that there is a requirement for a novel tactile sensor that posses flexibility in properties like geometry and force range, and which can be used with wearable devices. The development of a conductive polymer based tactile sensing element is discussed in this chapter while adopting existing such polymers.

3.2 Development of Tactile Sensing Material

3.2.1 Chemical composition of the sensing material

Promising aspects were shown in the nano-modified silicone rubber based conductive polymer developed by Huang et al. [35]. The fabrication process and materials (specifications are listed under Table 2.4) were closely monitored and chosen as a reference for the development of conductive polymer based sensing element of this research. Having identified the requirement of finding a type of highly conductive carbon black with the stated specifications, initially, three types of carbon black materials were used for the compound fabrication to identify their suitability. KETJENBLACK EC600JD, PRINTEX XE2-B and N330 are the there types of high conductive carbon black compositions studied in this fabrication process as their primary particle sizes fall within $30 - 40nm$ range. The average particle size is one of the distinguishing characteristics of a carbon black grade. Properties of those carbon black specimens are listed down under the Table 3.1.

Table 3.1: Carbon black types and their properties.

Property	Used by Huang et al. [35]	KETJENBLACK EC600JD	PRINTEX XE2-B	N330
DBP absorption ($cm^3/100g$)	–	495 (15g method)	420	100
BET surface area (m^2/g)	$1000 - 1200$	1270	1000	78±5
Resistivity (Ωcm)	$0.2 - 0.6$	$0.3 - 1$	–	$200 - 250$
pH	–	9.0	7.8	5-9
Ash content (%)	–	0.10	1.6	≤ 0.5
Primary particle size (nm)	$30 - 40$	34.0	30.0	31

3.2.2 Fabrication process of the conductive polymer based sensing material

The fabrication process of the conductive polymer based sensing element featured in this research consists of the chemical mixing stage and the moulding stage. Steps involved in chemical mixing stage and the identified fabrication steps needs to be discussed in this section under the chemical mixing stage. The development of a compression mould and steps followed during the moulding stage are also to be addressed in this section.

Adopting the method described by Huang et al. [35], a shear mixing process was used for polymer fabrication. The chemical compounds mixing was carried out in three steps as mentioned under the Figure 3.1.

As per the fabrication process described by Huang et al. [35], solution A was prepared at room temperature and atmospheric pressure for ∼30 minutes. Then SiO_2 was added to solution A and prepared for another ∼30 minutes. Both solution A and B were prepared using a shear mixing process and the shear mixing process is shown in

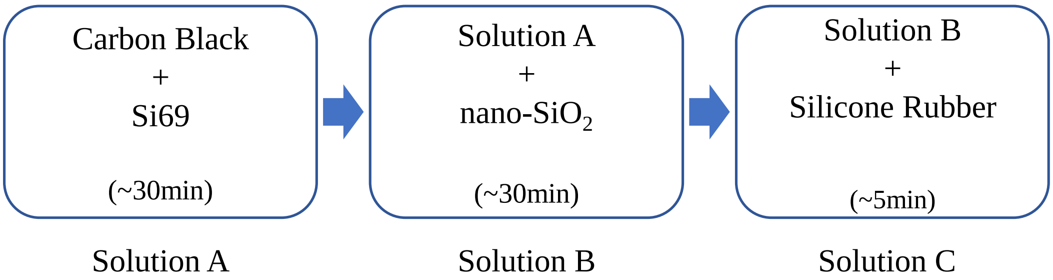

Figure 3.1: Chemical mixing procedure.

Figure 3.2. Later, Room Temperature Vulcanizing (RTV) Silicone rubber was added to solution B and prepared using a plasticoder that are used to compound rubber and plastic for ∼5 minutes. It was difficult to use shear mixing to prepare solution C due to its tendency to cure in a small period. The rotors of the plasticoder used to prepare solution C were shown in Figure 3.3.

Figure 3.2: A shear mixing process was used to prepare solution A and B.

Figure 3.3: The plasticoder was used to prepare the solution C.

Carbon black to RTV Silicone rubber and Nano-SiO_2 to RTV Silicone rubber weight ratios used by Huang et al. [35] were 8% and 3% respectively. Same weight ratios were practised in this research and their weights were mentioned in Table 3.2.

As mentioned earlier, the initial polymer development was carried out in three batches with carbon blacks of different conductivity levels described under Table 3.1.

Table 3.2: Compound weights used for polymer fabrication.

Compound	**Weight (%)**
Carbon black / RTV Silicone	8.0%
Nano-SiO_2 / RTV Silicone	3.0%
Si-69	Adequately

3.3 Development of the Conductive Polymer Based Tactile Sensing Element

3.3.1 Proposed design of the tactile sensing element

When deciding geometry and dimensions, the adaptiveness to most of the products should be considered. Therefore a cylindrical geometry can be identified as one of the potential geometry that can be easily incorporated into any design. Furthermore, cylindrical geometry with different sizes as shown in the Table 3.3 can be easily fabricated using a moulding process.

Table 3.3: Different sensing element sizes.

Geometry	**Diameter D (mm)**	**Thickness H (mm)**
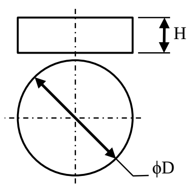	15	4, 7 and 10
	20	4, 7 and 10

3.3.2 Fabrication process of the conductive polymer based tactile sensing element

Compression or press moulding is one of the most frequently used moulding techniques in the plastic and rubber based industry where tightest tolerances and flawless finishes are not mandatory. Usually, in the compression moulding, uncured rubber is placed inside the mould and allows the rubber to get soften with the controlled temperature and pressure level until it fits the shape of the mould and gets cured [58]. The general process of the compression moulding is shown in the Figure 3.4.

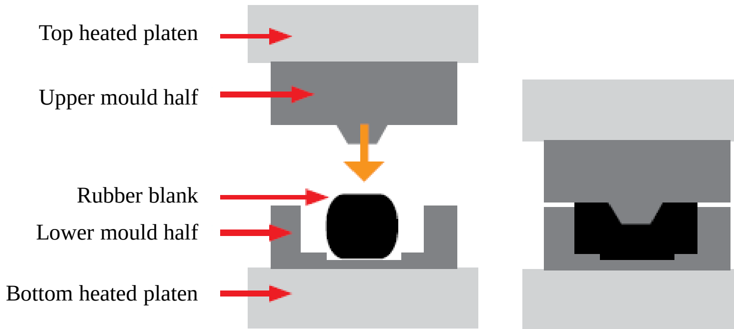

Figure 3.4: Compression moulding process.

A similar fabrication process is used for the production suggested by Huang et al. [35] that involves a moulding process carried out at room temperature and under atmospheric pressure. To prepare conductive polymer samples of different geometries and sizes in a batch fabrication process, a the development of a suitable mould is required for this research.

3.3.3 Development of the compression mould

Adopting the principles in compression moulding, a three (03) layered mould (shown in Figure 3.5) was developed with the capability to easily eject the polymer materials after curing. Initially, conductive polymer samples were designed into a cylindrical shape with different diameters and thickness levels as shown in Table 3.3.

Eight (08) number of nuts are used in the design to fasten three mould layers after adding uncured polymer materials into the mould (Figure 3.6). The top layer of the

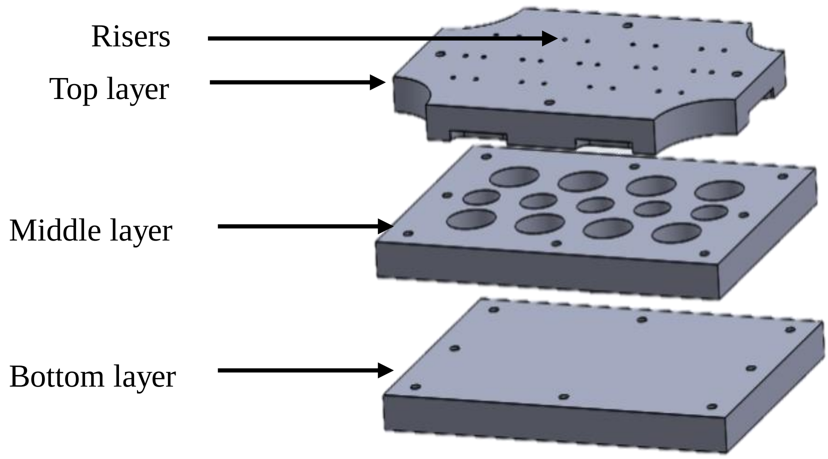

Figure 3.5: Chemical mixing: Exploded view of the mould design.

mould is equipped with risers which are extra voids created to discharge excessive polymer materials from cylindrical mould cavities.

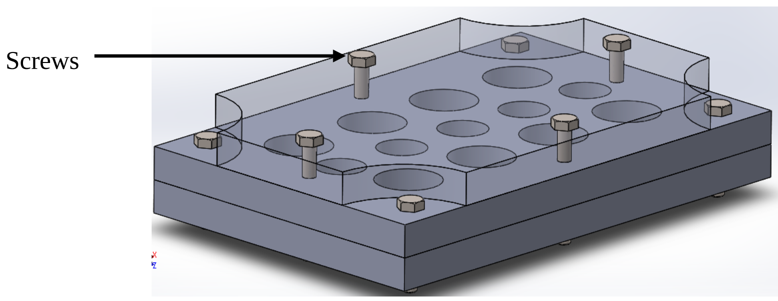

Figure 3.6: Assembled 3D design of the mould, screws are used to fasten the moulds.

The three-layered mould was fabricated using Aluminium with Computer Numerical Control (CNC) fabrication process. The top mould layer (Figure 3.7), middle mould layer (Figure 3.8) and bottom mould layer (Figure 3.9) are the three different mould layer and their production drawings are available as under the Appendix 8. Screws were used to fasten each mould layers and compress the polymer material appropriately as shown in Figure 3.10.

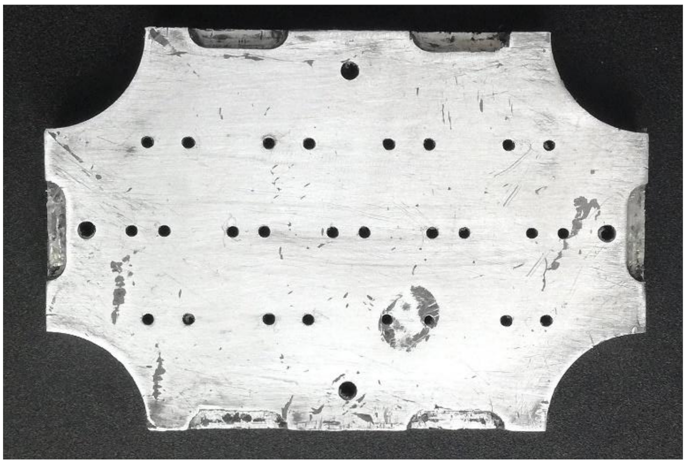

Figure 3.7: Parts of the Aluminium Mould: Top mould layer.

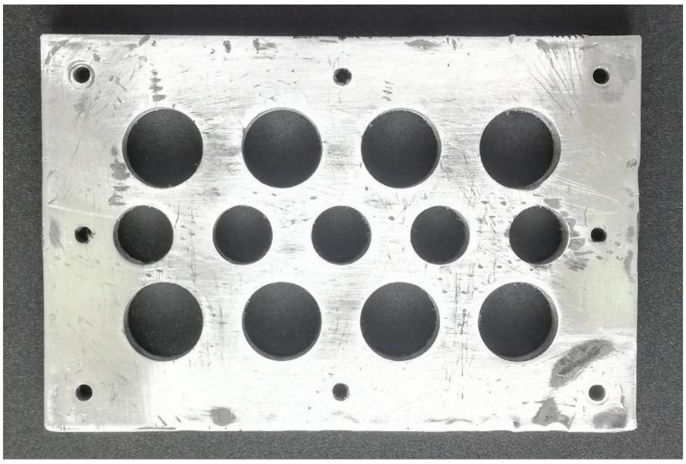

Figure 3.8: Parts of the Aluminium Mould: Middle mould layer.

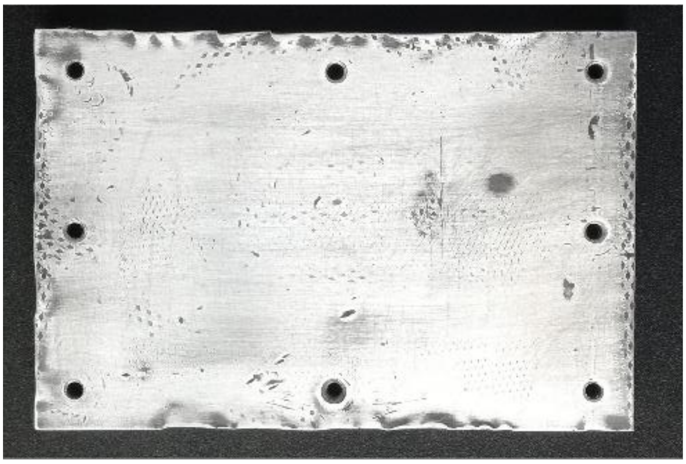

Figure 3.9: Parts of the Aluminium Mould: Bottom mould layer.

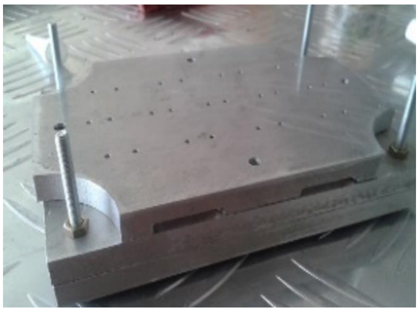

Figure 3.10: Assembled mould where screws were used to fasten three mould layers.

The thickness of conductive polymer samples could be adjusted by the spacers shown in Figure 3.11 and designed so that it could be inserted into the mould.

Figure 3.11: Spacers fabricated to adjust the thickness of conductive polymer samples.

3.3.4 Moulding and fabrication of conductive polymer

Before the moulding, a silicone based mould release spray was applied to all mould surfaces to ease the ejection process. Then the prepared solution C was moulded into the developed Aluminium mould and compressed using three Aluminium layers, nuts and bolts presented in the developed mould. The polymer was moulded at room temperature with a time of 64 $\sim$ 72 hours. Fabricated sensing elements are shown in Figure 3.12.

Figure 3.12: Fabricated sensing elements with different thicknesses.

CHAPTER 4

CHARACTERISATION OF THE CONDUCTIVE POLYMER BASED TACTILE SENSING MATERIAL AND ELEMENT

4.1 Introduction

The core component of a tactile sensor is the sensing element and the performance of tactile sensors mostly depend on the characteristics of the sensing element. In the scope of conductive polymers, conductivity is not the only property that governs the characteristics of the sensing element, but material and mechanical behaviours of the sensing element are required to be analysed to identify the performance of the tactile sensor. This chapter describes the characterisation of the developed conductive polymer based tactile sensing elements in terms of mechanical, electro-mechanical and material properties.

4.2 Mechanical Characterisation of the Developed Tactile Sensing Element

4.2.1 Piezoresistivity of the tactile sensing element

Conductive polymer samples prepared in three (03) batches as described in the Chapter 3 were initially tested for their piezoresistive response using a high precision multimeter. Two(02) Tin (Sn) metal plates were placed on both sides of sensing elements as sandwiched layers while applying a thin silver paste between the sensing element and metal plates. Force was applied to the sensing element as shown in the Figure 4.1.

During this initial test for conductivity and piezoresistivity, samples prepared using KETJENBLACK EC600JD and N330 only exhibited piezoresistive response (i.e.

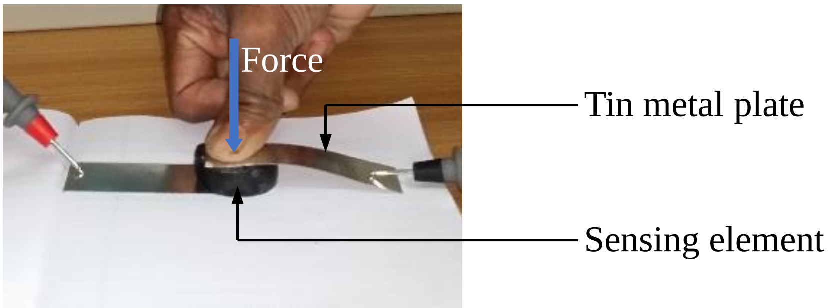

Figure 4.1: Inspected for piezoresistivity of sensing elements.

decrement in the resistivity when increasing the amount of applied force). Resistance variation in those two samples was in Ohm and mega-Ohm ranges respectively. Conductive polymer samples prepared using PRINTEX XE2-B were unable to test due to their ductile properties. Therefore, conductive polymer samples prepared using super-conductive carbon black, KETJENBLACK EC600JD was identified as a promising composition that posses piezoresistive properties, in the context of this research and its progress.

4.2.2 Development of a testing apparatus for mechanical characterisation

The conductive polymer based tactile sensing element fabricated using KETJEN-BLACK EC600JD was thoroughly inspected for its mechanical characteristics. When following the aforementioned technique, the losses that occurred at the contact between the metal plate and the tactile sensing element affect the performance of the element. Therefore, to inspect mechanical characteristics and minimise contact loses, a testing apparatus (as shown in Figure 4.2 and Figure 4.3) was developed with two electrode plates where one plate can move along guided pins. A bolt for each guide pin is used to provide the initial compression required for the conductive polymer sensing element to initiate conductive paths and make the element conductible. Further, a thin silver paste was applied in between the sensing element and two electrode plates to minimize transmission losses in the output signal and noises that can be generated at the contact points [59].

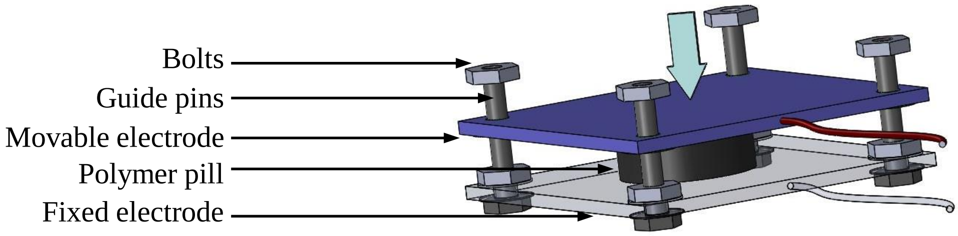

Figure 4.2: Conceptual design of the testing apparatus.

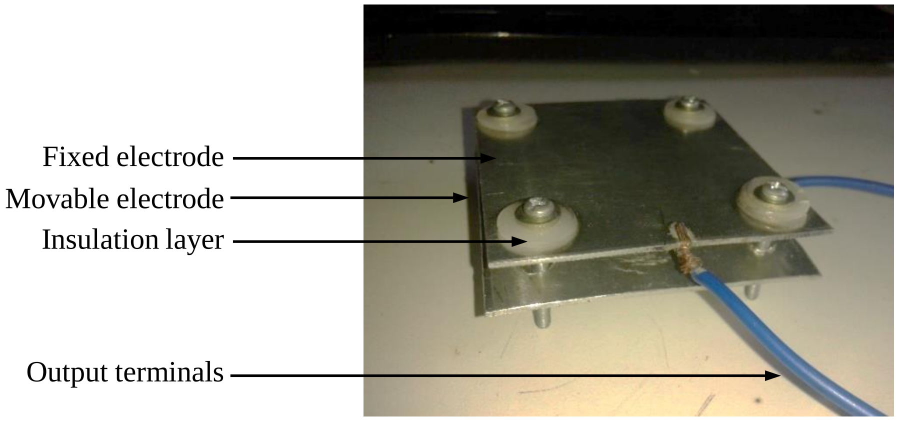

Figure 4.3: Developed testing apparatus for mechanical characterization in the conductive polymer pills.

4.2.3 Experiments for mechanically characterize the fabricated tactile sensing element

During this characterisation process, sensing elements were tested using a force indenter under different loading conditions to find out basic characteristics such as conductivity, elasticity, force range, hysteresis, non-linearity, and drift.

The elastic behaviour of the sensing element was tested using the force indenter with $10N$ step loadings. The elastic properties concerning the deformation under different loads are shown in Figure 4.4. This plot reveals that the sensing element posses a considerable amount of hysteresis in loading and unloading conditions and non-linear behaviour. Further, the conductive polymer based sensing element exhibited a maximum deformation of $2.5mm$ for a force range of $100N$.

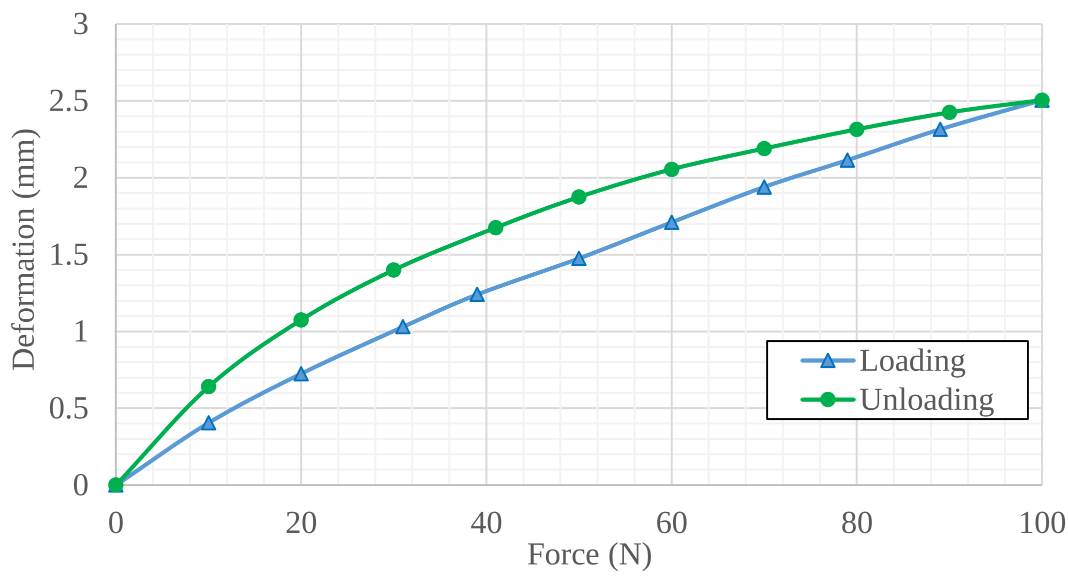

Figure 4.4: Experimental results: Deformation vs applied load plot for the sensing element.

4.3 Electro-Mechanical Characterisation of the Developed Tactile Sensing Element

The fabricated tactile sensing element was tested for its electro-mechanical properties as the sensor output characteristic is vital for the progress of this research. The tactile sensing element was tested with the same apparatus described under Figure 4.3 and the output characterisation results were obtained (Figure 4.5).

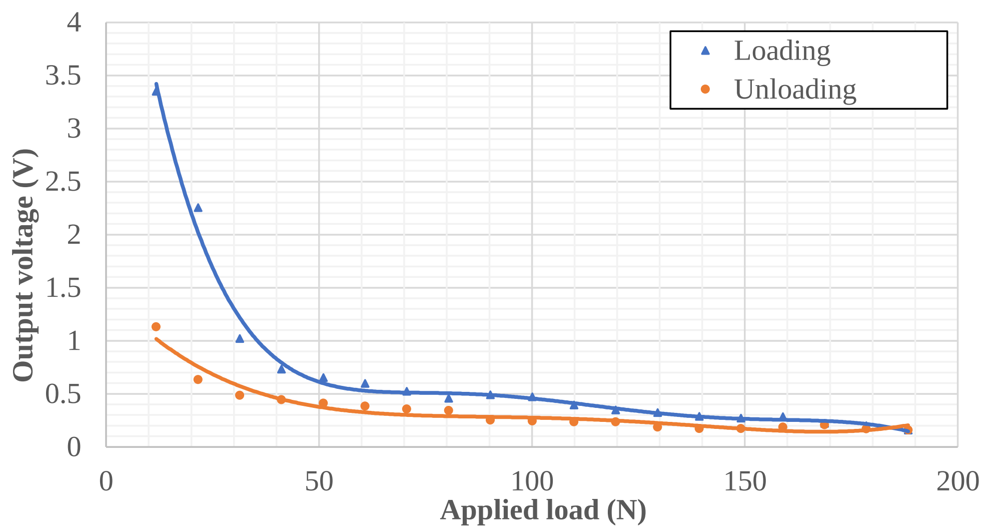

Figure 4.5: Experimental results: Output voltage vs applied load plot for the sensing element.

The drift (i.e. variation in the sensing element output) is also another important property that requires attention. The drift of the tactile sensing element was recorded for $10.2kg$ load for 35 minutes and plotted in Figure 4.6 where the resistance output of the element was measured using a high precision digital multimeter at $4Hz$ sampling frequency.

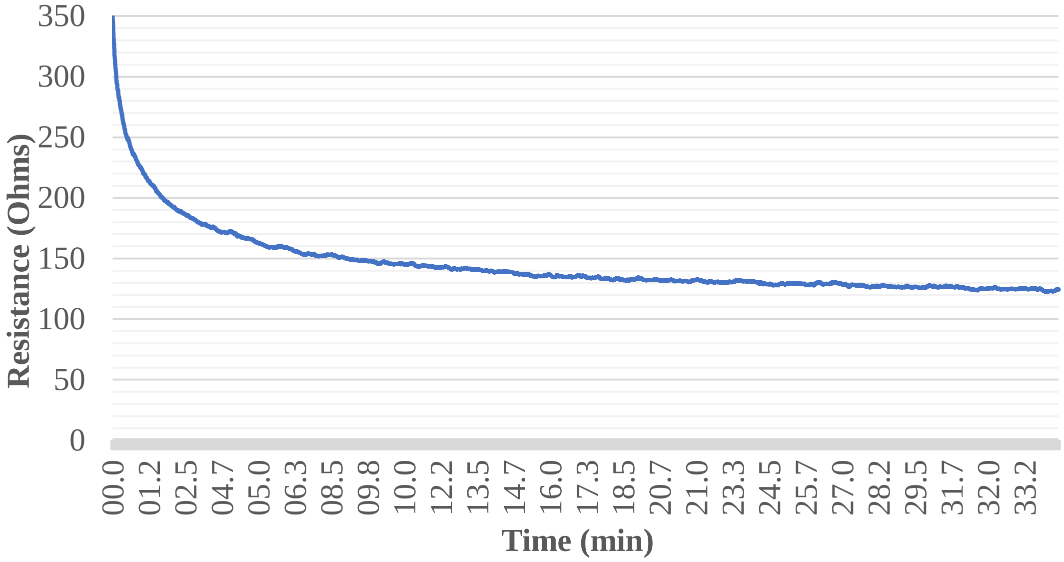

Figure 4.6: Experimental results: Drift of the sensing element.

4.4 Material Characterisation of the Developed Tactile Sensing Element

The material characterisation was inspected with the help of microscopic analysis and a particle/ composition analysis. The obtained data can be used as a reference for future researches and can be used to improve the mechanical, electrical and chemical properties of the sensing element.

4.4.1 Material morphology of the conductive polymer sample

Scanning electron microscope for the inspection of morphology

A maximum magnification of 1000X can be reached using the latest light microscopes. The resolution of a light microscope depends on the number of lenses and the quality of lenses. Furthermore, the resolution also relies on the wavelength of the light used for illumination. Accelerated electrons used in Scanning Electron Microscopes (SEM) a has a much shorter wavelength and it enables reaching higher resolutions.

A Scanning Electron Microscope (SEM) produces images of a sample by scanning the surface with a high energized beam of electrons. Secondary electrons, backscattered electrons and characteristic X-rays generate when the electrons bombard into the sample. Detectors are capable of collecting those signals and generating images.

Sample preparation for material characterisation

Preparation of the fabricated tactile sensing element was required before the microscopic analysis due to the limitations in the SEM and the geometry and size of fabricated tactile sensing elements. Sample preparation was conducted in two steps as shown in Figure 4.7.

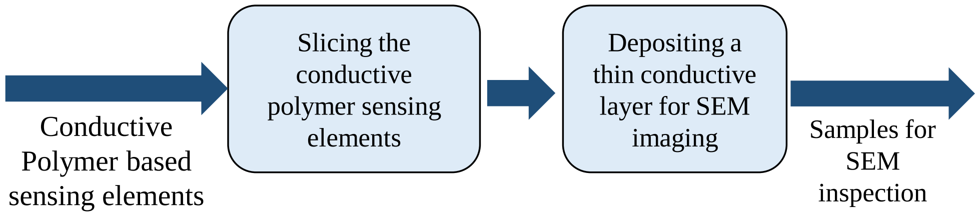

Figure 4.7: Preparation of conductive polymers samples for material characterisation.

To obtain detailed morphology of the developed conductive polymer sensing elements, transverse sections (see the Figure 4.8) of tactile sensing elements were inspected using the SEM instead of examining outer surfaces of the conductive polymer sensing elements. This allows the opportunity to analyse material properties inside the sensing element in a broader manner.

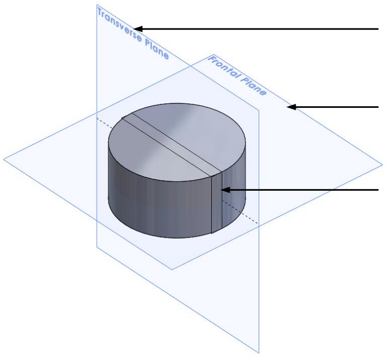

Figure 4.8: Transverse sectioning of conductive polymer based sensing elements.

The precision low speed saw that has a diamond blade that is shown in Figure 4.9 was used to slice conductive polymer sensing elements. Water was used as the cooling agent and $2-3mm$ thickness shown in Figure 4.10 were obtained from the slicing process.

Figure 4.9: Low speed saw with a diamond cutter was used.

Figure 4.10: Transversely sectioned conductive polymer samples.

The partial metalizing using gold sputtering was carried out before the SEM inspection. Using the sputter coater Figure 4.11, a thin gold layer of $10nm$ was applied to samples. This sputter coating prevents samples from being charged due to the growth in static electric fields. Further, this sputtering method could be used to escalate the number of detectable secondary electrons from the surface using the SEM and hence improves the signal to noise ratio. The prepared samples for the SEM inspection were placed on SEM studs for the SEM inspection (Figure 4.12).

(**a**) (**b**)

Figure 4.11: Sputter coater is used to deposit a thin layer of gold on conductive polymer samples: (**a**) Samples for spin coating; (**b**) Spin coater that was used.

Figure 4.12: Prepared samples were placed on SEM studs.

4.4.2 Morphological analysis using SEM

The morphology of the conductive polymer samples was inspected under the magnification levels of 100X, 250X, 500X and 1000X using the SEM and the microscopic images are shown in Figure 4.13. It can be confirmed that the prepared samples were porous, even though they were prepared using a mechanical compression moulding method. These porous areas have a significant effect on sensor drift and linearity.

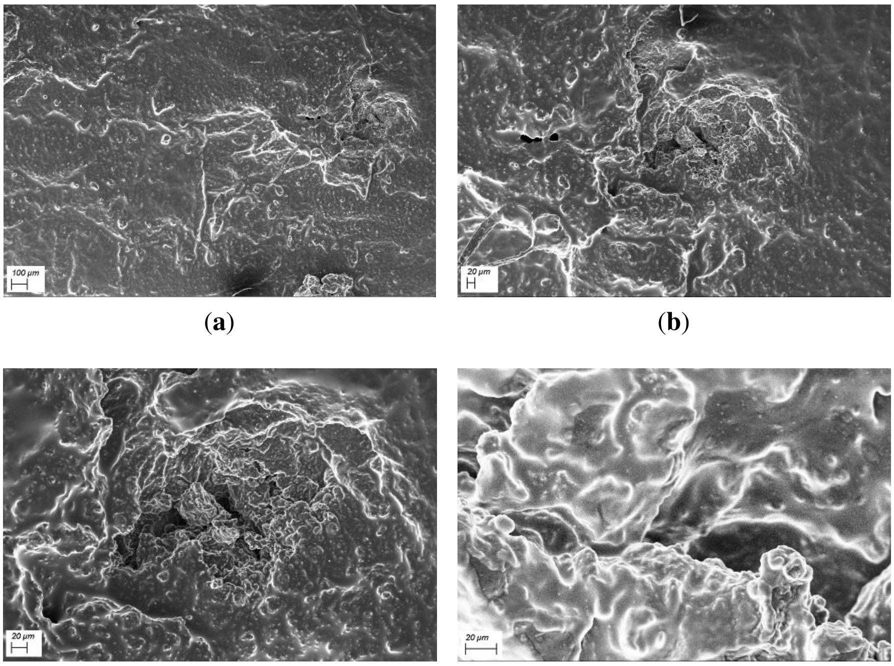

(**a**) (**b**)

(**c**) (**d**)

Figure 4.13: SEM images under different magnification levels: (**a**) 100X; (**a**) 250X; (**c**) 500X; (**d**) 1000X.

4.4.3 Elemental analysis of the conductive polymer samples

Energy-Dispersive X-ray technique for elemental analysis

The Energy-Dispersive X-ray (EDAX) technique is capable of detecting x-rays and measures the relative abundance of emitted x-rays versus their energy. The EDAX spectrum is used to characterize the elemental composition of prepared conductive polymer samples. When the sample is bombarded by the electron beam of the SEM, atoms on the surface and adjacent layers are ejecting electrons. The electrodes from higher states fill the void in atoms and x-rays are emitted to balance the energy between two states of electrons. The emitted x-rays are characteristics of the element from which it was emitted.

Conducting the elemental analysis using EDAX

The marked area - Full Area 1 shown under the Figure 4.14 was used to analysed with the EDAX. The Figure 4.15 illustrates EDAX spectrum of the marked Full Area 1 of prepared conductive polymer samples and Table 4.1 represents the EDS eZAF Smart Quant results of the analysed area.

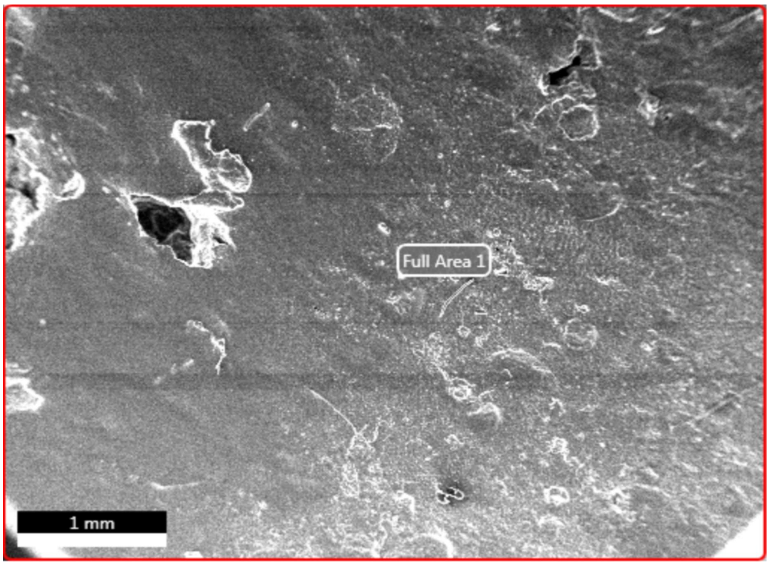

Figure 4.14: Sample area (marked as Full Area 1) inspected by EDX Analysis.

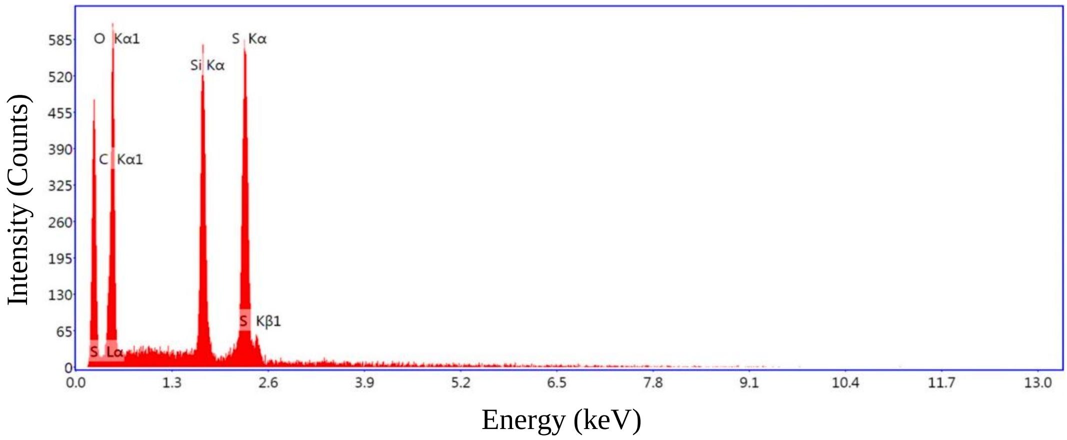

Figure 4.15: Material composition obtained by EDX Analysis: EDX spectrum of a polymer sample.

Table 4.1: EDS eZAF Smart Quant results of conductive polymer sample of the marked as Full Area 1.

Element	Weight %	Atomic %	Net Int.	Error %	K ratio	Z	R	A	F
C K	42.07	53.49	29.8	12.00	0.087	1.04	0.976	0.200	1.000
O K	38.44	36.69	44.6	11.21	0.071	0.99	0.996	0.186	1.000
Si K	8.14	4.42	48.0	4.57	0.063	0.90	1.039	0849	1.012
S K	11.35	5.40	57.0	3.85	0.091	0.88	1.050	0.906	1.006

During the conducted elemental analysis, Sulphur, Oxygen, Silicon and Carbon signals were recorded. These elements have been identified as major elements in the conductive samples prepared by Ying Huang et al. [35] that was adopted for the conductive polymer preparation in this research. The EDAX analysis shows the indirect evidence in presence of Nano-Silica (SiO_2) that was used to enhance the conductivity of the polymer.

4.5 Discussion

The developed conductive polymer based sensing element has promising aspects to use with many biomedical applications. Mainly the capability of producing sensing elements in different geometries opens a wide range of application to the developed sensing element without restricting to geometries or the range of commercially available sensors. The development of a sensing element that has flexibilities in the sensor range and geometry is another motivation of this research.

This conductive polymer based tactile sensor approach is capable of using for monitoring discrete point force/pressure and for monitoring force/pressure values in a whole and specific surface area [60]. In the point force/pressure measuring condition, an external structure is required to transmit applied force/pressure to the effective sensing area of the sensor as practised by De Silva et al. [56, 57]. Therefore, Chapter 5 is focused on the development of tactile sensors capable of measuring discrete point-based forces/pressures. Later the Chapter 6 is focused on improving the same concept to acquire force/pressure values over a whole and specific surface area as a sensor array.

On the other hands, to acquire the resistance variation in the tactile sensing element with the applied force/pressure placement of two distinct electrodes to the sensing element is required as practised by most of the researchers. Therefore, during the development of tactile sensors, special attention is required for the electrodes as well.

CHAPTER 5

DESIGN AND DEVELOPMENT OF A TACTILE SENSOR WITH A RIGID STRUCTURE DESIGN – I

5.1 Introduction

The span or the range of the sensor is a vital static characteristic of a sensor as it defines the minimum and maximum values that can be measured by the sensor. In the context of a force sensor, the term dynamic range closely relates to the application. To use the same sensing element for different applications, it is very much important to restrain the total deformation of the sensing element so that the desired range of the force sensor can be achieved.

One method to restrain the total deformation is to introduce an exterior structure. The structure also caters as a platform to transmit the applied force towards the sensing element while diminishing the amount of force applied to the sensor structure. A mechanical structure also protects the sensing element. In this section, the design and development of a novel external structure for the developed conductive polymer based tactile sensing element is discussed.

One of the identified configuration for a mechanical structure and a method to restrain the total deformation is to introduce an exterior spring system to the sensing element similar to the work done by Udayanga et al. [47, 48] and Tan et al. [45]. The process followed in the sensor development is shown under the Figure 5.1.

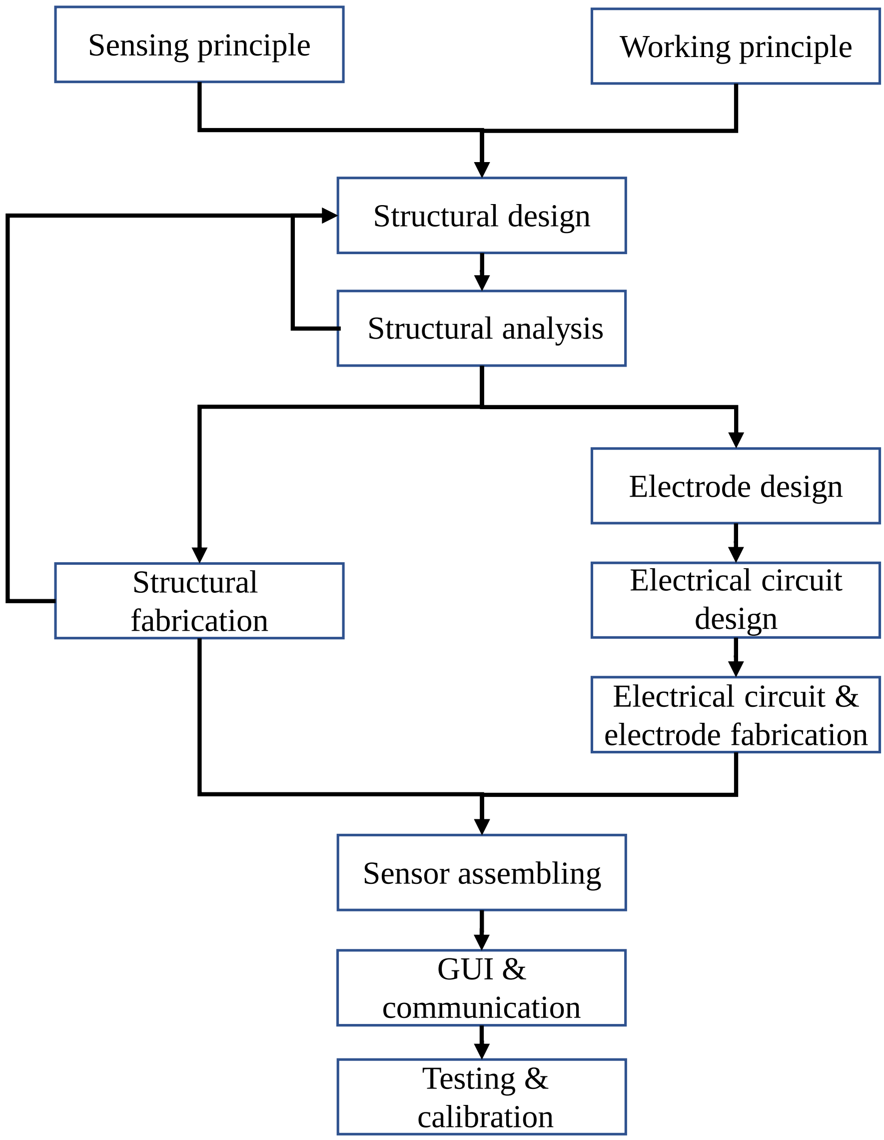

Figure 5.1: Tactile sensor development process.

5.2 Mechanical Structure of the Proposed Tactile Sensor – Design 01

A novel external cylindrical spring system (as shown in Figure 5.2) that inspired by a honeycomb structure was proposed as the mechanical structure of the sensor. This mechanical structure design posses a piston-cylinder mechanism. The cylindrical arch spring acts as the piston as well as the spring behaviour to the system while outer protection serves as the cylinder to the system. Force will be applied to the top face of the cylindrical arch spring.

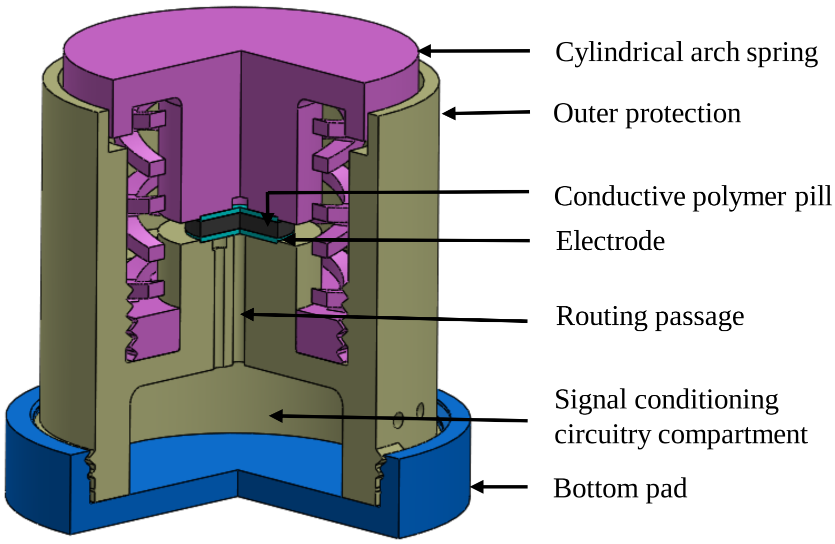

Figure 5.2: Half sectional view section of the proposed tactile force sensor design.

Listed below are some of the features of this design:

- Alignment problems won't occur at the assembling stage due to the minimum number of parts and the geometry of the parts.
- It is possible to give a pre-compression to the sensing element to initiate conductive paths, using the thread between the cylindrical arch spring and outer protection.
- Overload protection to the system can be applied using the vertical clearance kept between the cylindrical arch spring and the outer protection.

- A shear force that can be applied on the force acting platform of the structure would be mitigated by the minimal horizontal clearance kept between the cylindrical arch spring and the outer protection.
- Circuitry compartment allows locating its signal conditioning circuitry inside the sensor.

Arrangement of components of the proposed tactile sensor assembly is shown under Figure 5.3 while basic dimensions of the mechanical structure are mentioned in the Figure 5.4. Refer to Appendix 8 for detailed production drawings of the design.

Alterations in the arch spring arrangement and dimensions could enhance the output characteristics of the sensor. Due to the complexity of the spring structure, it was considered to adopt additive manufacturing methods like 3D printing for fabrication.

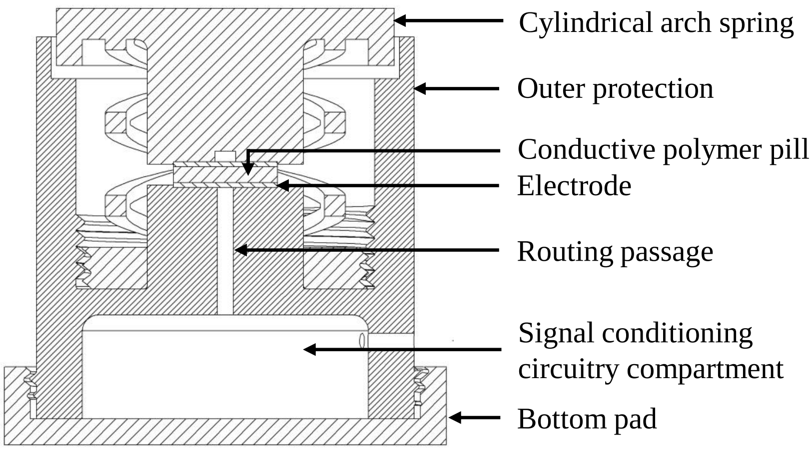

Figure 5.3: Component arrangement of the tactile sensor in the assembly.

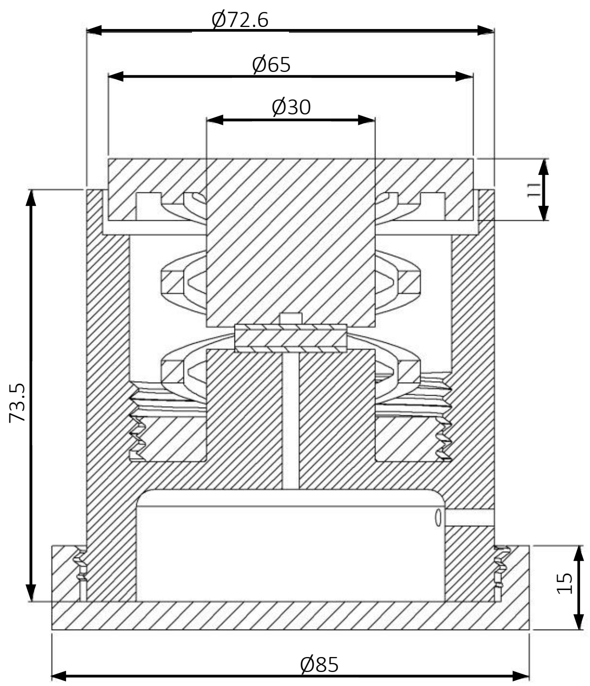

Figure 5.4: Basic dimensions of the proposed tactile sensor.

Extents of the piezoresistive elements described under Table 3.3 and the arrangement limitations of the universal testing equipment were taken into accounts when designing the cylindrical arch spring system. A three-point spline which has zero gradients at the apex and ends, was adopted for a single cylindrical arch design (as shown in Figure 5.5) to obtain the deformation that is necessary for the piezoresistive behaviour.

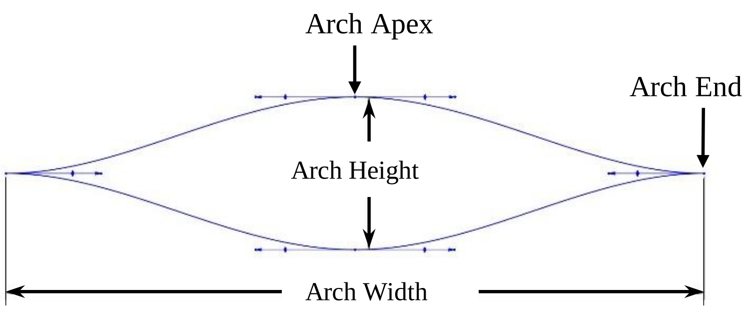

Figure 5.5: A single cylindrical arch design and the arch aspect ratio.

External diameter of spring system (ϕd_i), diameter of support layer (ϕd_e), total spring height (h) and fillet radius (r) shown under Figure 5.6 were considered as basic design dimensions of the proposed arch spring arrangement.

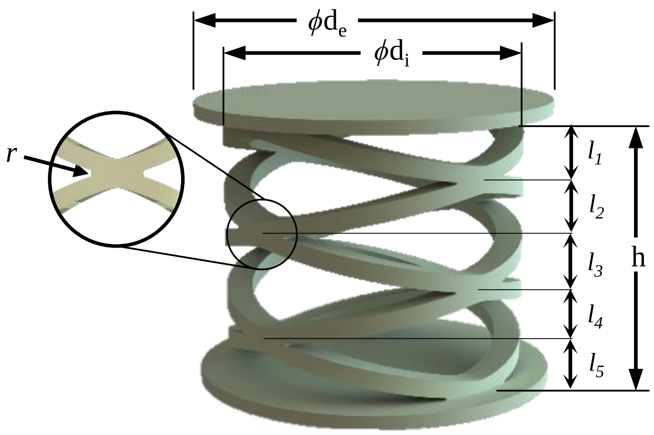

Figure 5.6: Cylindrical arch spring structure.

5.3 Working Principle of the Proposed Tactile Sensor – Design 01

Before the development of the mechanical structure design, it was identified the requirement of knowing the working principle of the sensor system combined with the sensing element and the mechanical structure, as it will act as a guide for the development. The free body diagram of the sensor is shown under the Figure 5.7. Consequences of the mechanical structure and the sensing elements were considered for this free body diagram and the behavioural changes (deformation - x) when subjected to loading (F) were considered.

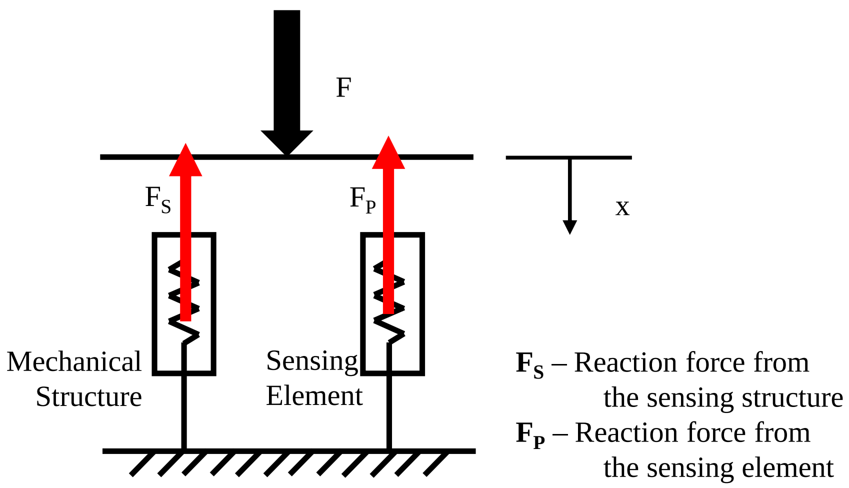

Figure 5.7: Free body diagram of the proposed sensor.

Considering the static balance of the free body diagram, load on the system (F) can be written as:

$$F = F_S + F_P \tag{5.1}$$

where the reaction forces from the mechanical structure and the sensing element are F_S and F_P respectively.

Equation 5.1 can be further simplified using basic stiffness equations. The mathematical relationship between the total deformation (x) of sensor and the applied load (F) can be expressed as:

$$x = \frac{F}{k_S + k_P} \tag{5.2}$$

where the stiffnesses of the sensing structure and the sensing element are k_S and k_P respectively.

5.4 Analytical Calculations and Numerical Simulations of the Proposed Design

To observe the behaviour of the tactile sensor under different loading conditions, it was required to conduct a Finite Element Analysis (FEA) for the proposed design. The developed design was carefully analysed with $COMSOL\ Multiphysics$ and its FEA tools. The design of the cylindrical arch spring structure was simplified (as shown in Figure 5.8) and was used for the FEA.

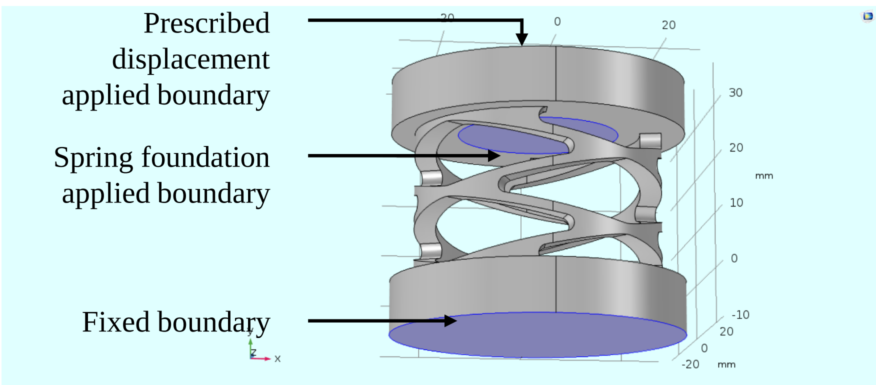

Figure 5.8: Simplified cylindrical arch spring structure and boundary conditions.

During the Finite Element Analysis (FEA), the sensing pill inside the structure was modelled and simulated as a virtual spring with stiffness of $40,083N/m$. Then, the combined system was analysed using FEA tools by applying a prescribed displacement of $2.5mm$ for the sensing element (virtual spring) along the centre axis. It was inspected during the static load test that the sensing elements exhibit an average stiffness of $40,083N/m$ and a maximum of $2.5mm$ displacement at the expansion of its range.

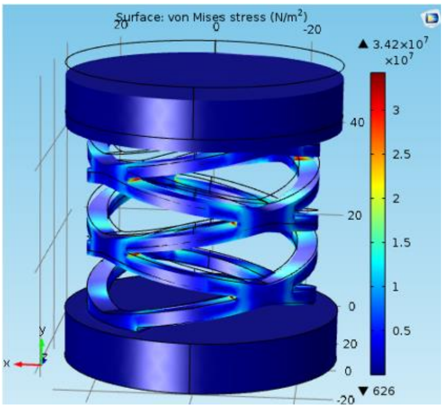

Figure 5.9: Structural simulation of arch spring structure.

Structural simulation results for the cylindrical arch spring structure is shown in Figure 5.9. Analysed maximum von-Mises stress, ($3.42 \times 10^7\ N/m^2$) was well within the maximum tensile strength of ABSplus ($3.6 \times 10^7\ N/m^2$) [61], which was used for the 3D printing fabrication process of the structure.

The arch spring structure was simplified to a parallel and series spring system and used to introduce further modifications to the spring structure. The simplified analytical model is shown in the Figure 5.10 and it is equivalent to the proposed design as seen in Figure 5.2. The number of arch spring layers are represented as "n" (which have been depicted as l_1, l_2, ... and l_5 in Figure 5.6 for the proposed structure). The number of parallel springs between two boundaries (shown in Figure 5.10) of the spring layer are indicated as "m". Equation (5.3) would give the representation for the axial spring constant of the spring structure:

$$k_s = m \times \frac{k_a}{n} \tag{5.3}$$

where the stiffness of the arch spring structure and the stiffness of a single arch are represented by k_s and k_a, respectively.

The FEA study was carried out using the $COMSOL\ Multiphysics$ to justify the analytical model for the same model used for the structural simulation (as shown in Figure 5.8). In the analysis conducted for the single cylindrical arch spring Figure 5.11, a force component is given to the top-most surface of the spring to calculate the maximum deformation. Stiffness for a single cylindrical arch and the entire spring structure (without the consequence of the sensing element) were derived as $25,673N/m$ and $10,888N/m$, respectively. Equation (5.3) could be verified by the above results with an error percentage of 6.02%. whose causes could be the assumptions of the equations and the round-off errors in the FEA study.

In order to determine the necessary stiffness of the single cylindrical arch spring portion which is to be implemented for Force Range (FR) increment per given deformation, Equation (5.4) could be used, which was derived via the basic equation for spring stiffness:

$$FR_{extended} = \frac{k_p + \frac{m}{n}k_a}{k_p} \times FR_{sensor\ pill} \tag{5.4}$$

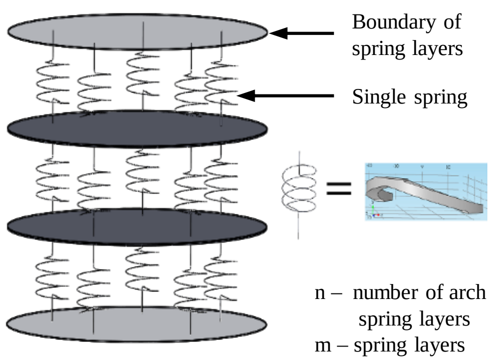

Figure 5.10: Cylindrical arch spring structure was analytically modelled for further modifications.

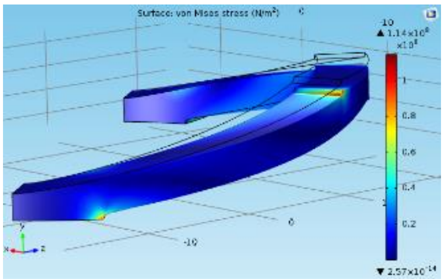

Figure 5.11: FEA study for a single cylindrical arch where the apex boundary is subjected to a force component.

where k_p is stiffness of the sensor pill which is mounted according to Figure 5.2.

The nonlinearity of the sensing element and the spring structure should have to be eliminated at the manufacturing stage by enhancing the material composition of the sensor pill and by adjusting the 3D printing parameters, respectively.

The arch spring structure was prototyped (the fabrication stage will be discussed under the next section) according to the fail-safe verifications that were obtained from the FEA study, where the prototyped sensor had five layers of arch springs and two arch springs in parallel in each layer. To attain a desired force sensor range, the prime aspect would be to design a single arch with a specific stiffness by considering its width, height (shown in Figure 5.5), beam thickness and height (shown in Figure 5.12). In each arc, beam width, beam height, arch width and arch height are $4mm,\ 2mm,\ 55mm$ and $12mm$, respectively, following the terms that were referenced in Figure 5.5 and Figure 5.12.

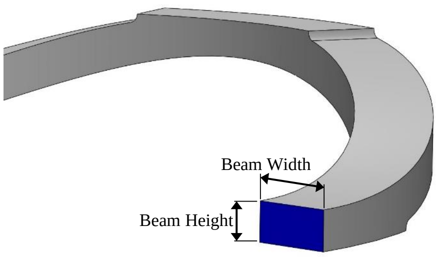

Figure 5.12: Beam aspect ratio.

Considering the Arch Aspect Ratio (=arch width/arch height) and the Beam Aspect

Ratio (=beam width/beam height), which are two major design parameters, a parametric study was conducted with adaptive mesh refinements for each parametric step. Figure 5.13 and Figure 5.14 depict the results of the parametric study and status of the prototyped cylindrical arch spring structure.

Hence, this parametric design methodology (the results of the parametric study) could be adhered by a sensor designer to obtain the desired characteristics out of a sensor by altering the structural parameters. The dimensions of the sensor packaging and the application of specific constraints must also be considered. Despite the validated single arch spring, the entire cylindrical arch spring structure should be thoroughly validated by simulations to be fail-safe before the fabrication, as the arch crevices are the areas with the highest stress concentration.

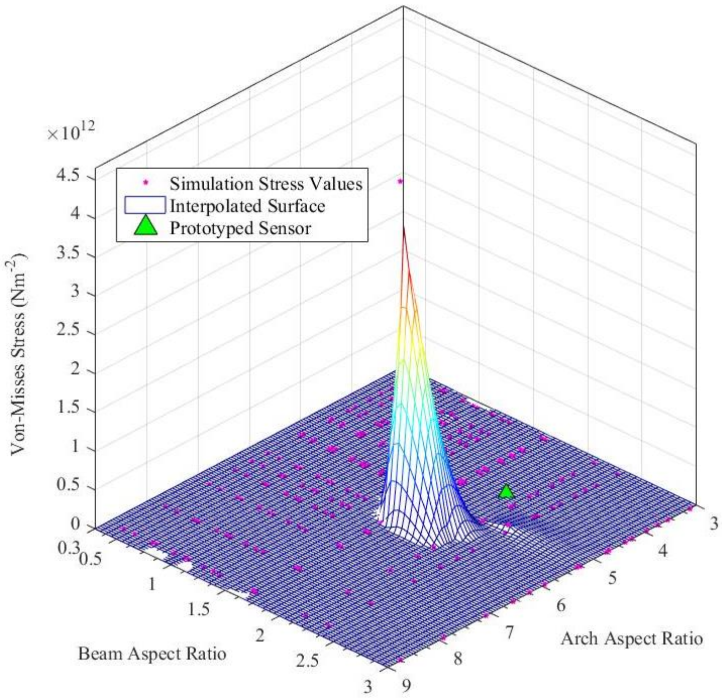

Figure 5.13: Von-Mises stress vs. structural design parameter study for the cylindrical arch spring.

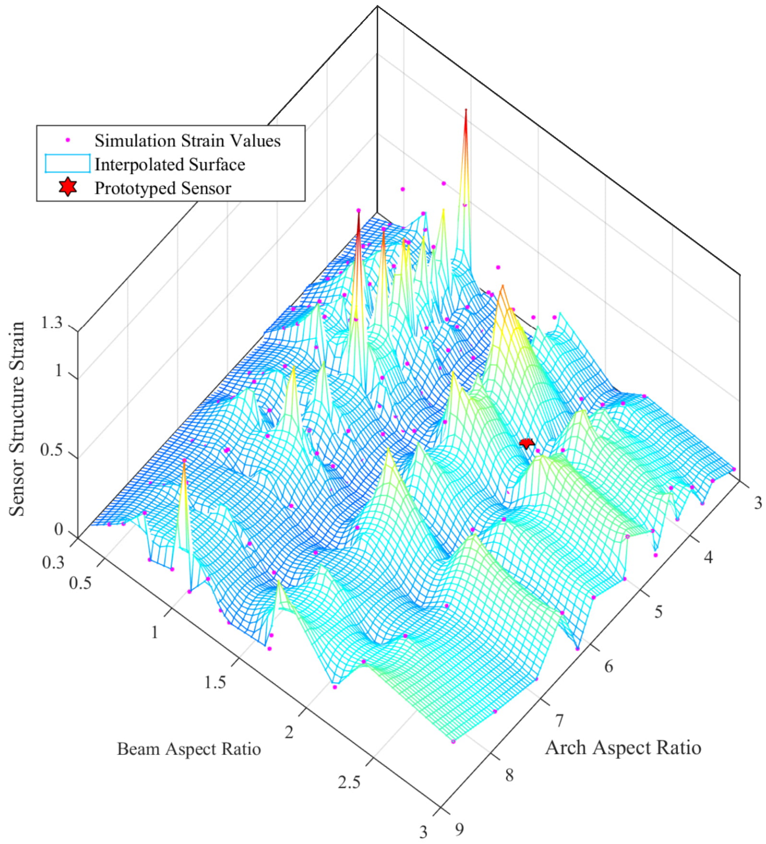

Figure 5.14: Sensor strain vs. structural design parameter study for the cylindrical arch spring.

5.5 Fabrication of the Cylindrical Arch Spring Structure

5.5.1 Conventional manufacturing and additive manufacturing methods

Additive manufacturing is a technique of building products by adding materials and laying down successive layers of material until the object is created. But in a conventional manufacturing process, excess materials are subtracting/removing from a larger workpiece. 3D printing is one of the famous techniques used in Additive Manufacturing. A 3D printing facility would be capable of producing a vast range of products without retooling while allowing the capability for customizing without extra cost. The 3D printing over conventional manufacturing methods can be contrasted as follows:

- Complexity of parts have been increased and complex geometries can be achievable.
- Digital design and manufacturing allows making modifications to products within a lesser time frame.
- Retooling is not required and only a single tool can handle the fabrication. Also reduces the time required for retooling depending on the material removal process in conventional fabrications.
- Allows the selectively for placing material only where it is needed, which reduces the wastage amount.

5.5.2 3D printing for fabricating the cylindrical arch spring structure

After considering the complexity of the design and the strength of the cylindrical arch spring structure, it was decided to choose 3D printing technology for the fabrication of the cylindrical arch spring structure.

When considering the tensile moduli of 3D printing materials, ABSplus [61], ABS [62] and PLA [63] possess tensile moduli of $2.265\ GPa$, $2.3\ GPa$ and $2.76\ GPa$, respectively. The failure stresses of the ABSplus, ABS and PLA are $36.0\ MPa$, $22.0\ MPa$ and $26\ MPa$, respectively. Details are summarise in the Table 5.1. Thereupon, ABSplus was selected as it possesses the minimum failure stress to tensile modulus index value since the sensor structure manipulates the stiffness by the geometry and the strength should be safeguarded by the material itself.

ABSplus production-grade thermoplastic is a material for prototyping through direct digital manufacturing, which possesses $36.0MPa$ of the tensile strength (refer Appendix 8 for material specifications). ABSplus can 3D print components directly from digital files which are stronger and smoother in finish and with more feature details. Moreover, ABSplus has a higher adhesion between 3D printed layers [64]. In practice, ABSplus is known for its resilience to warping after fabrication, where the misalignments and assembly misfits could be minimised.

Table 5.1: Commonly used materials for 3D printing and their properties.

Material	**Tensile Modulus (GPa)**	**Ultimate tensile strength (MPa)**	$\frac{\textbf{Tensile modulus}}{\textbf{Tensile stress}}$
ABSplus	2.200	33	66.67
ABS	2.180	28	77.86
PLA	2.539	26	97.65

ABSplus [61] with 3D printing technology was used to fabricate structural parts of the sensor (Figure 5.15). The outer protection (Figure 5.15(b)) and the bottom pad (Figure 5.15(c)) were fabricated using the Flashforge Dreamer 3D printer. The other part(Figure 5.15(a)) was fabricated using the Stratasys Uprint SE 3D printer.

The infill ratio is one of the factors that decide the strength, weight and printing duration of the 3D printing part. This term refers to the amount of materials printing inside the object. The cylindrical arch spring was 3D printed with an infill ratio of 100% and a layer thickness value of $0.254\ mm$ as it is vital to bear high stresses as much as $3.42 \times 10^7\ N/m^2$.

Table 5.2: External structure parts were 3D printed.

Part(s)	**3D printer**	**In-fill ratio**	**In-fill pattern**	**layer thickness**
Cylindrical arch spring	Stratasys Uprint SE	100%	Diagonal	0.254 mm
Outer protection & Bottom pad	Flashforge Dreamer	80%	Diagonal	0.3 mm

(a) (b) (c)

Figure 5.15: 3D printed parts of the force sensor: (**a**) cylindrical arch spring; (**b**) outer protection; (**c**) bottom pad.

5.6 Development of Electrical Circuit Design 1-DOF Tactile Sensor

5.6.1 Development of electrodes the tactile sensing element

Novel electrode design

Electrode design was carried out by adopting the full electrode configuration where it uses two electrode layers at both sides of the sensing element. This novel wire piercing design (as shown in Figure 5.16) method has significantly eased the routing provisions inside the sensor packaging, thus simplifying the packaging of the structure. Two copper-clad foils were used as electrodes.

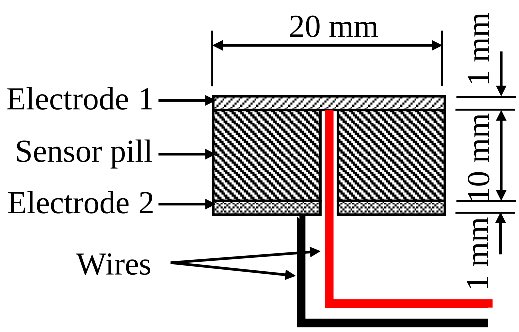

Figure 5.16: Electrode design for the conductive polymer based tactile sensing element.

Fabrication of electrodes for the sensing element

Transmission losses in the output signal and noise can be generated at the contact points between the sensing element and electrodes. A layer of silver paste layer [59] is used in between the conductive polymer based sensing element and the electrodes to minimise the above-mentioned phenomena. Electrodes embedded sensing element is shown in Figure 5.17.

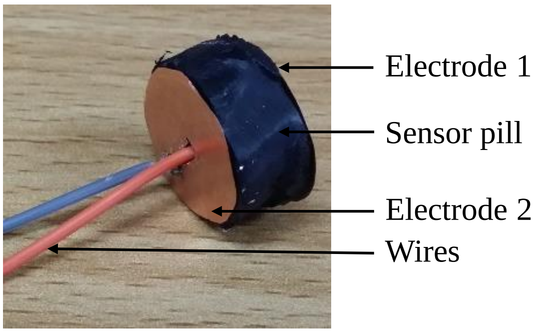

Figure 5.17: Fabricated electrodes with the wire piercing design.

5.6.2 Data acquisition, signal conditioning and communication

System layout of controller

When developing the system layout described under the Figure 5.18 for the proposed controller and the user interface, the following aspects were considered.

- Data Acquisition.
- Signal Conditioning.
- Data Processing.

In this proposed layout, the hardware interface that contains the sensor and the micro-controller based development board acts as the DAQ system while the LabVIEW based software interface provides both signal conditioning and data processing platforms.

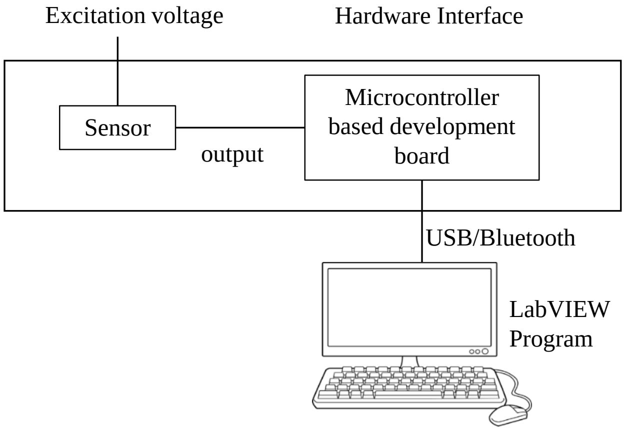

Figure 5.18: The proposed circuitry and system layout.

Development of the microcontroller based interface

The developed microcontroller based interface circuitry (Figure 5.19, R_v denotes the sensing element) uses a microcontroller based development board ($Arduino\ nano$) equipped with a ATmega 328p, for data acquisition and basic signal conditioning part. Technical specifications of $Arduino\ nano$ development board is presented in Table 5.3.

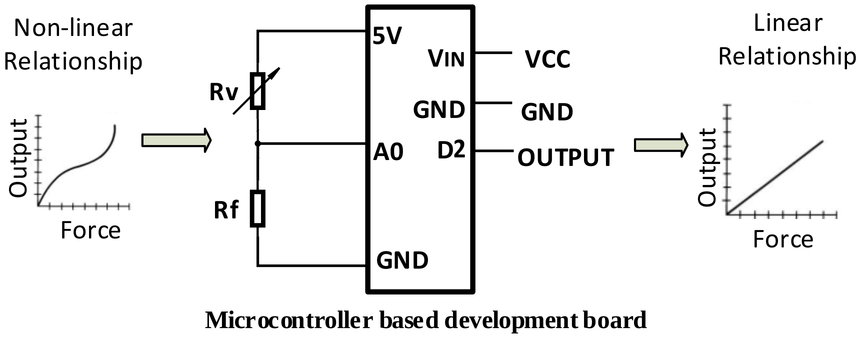

Figure 5.19: Developed microcontroller based interface circuitry.

Analogue to Digital Conversion (ADC) of a 10-bit resolution was used to acquire a voltage sensitivity of $0.0048\ V$. Deriving linear relation from nonlinear outputs taken from sensing element considering loading condition and hysteresis errors were implemented in the system using a microcontroller based development board. The circuitry used for data acquisition is shown in Figure 5.19. Another method used to mitigate the nonlinearity of the sensor was the Look-up-table method. It was generated based on experimentally obtained tactile force sensor values.

Table 5.3: Specifications of Arduino nano development board.

Micro controller	ATmega2560
Operating voltage	$5V$
Input voltage (recommended)	$7-12\ V$
Digital I/O pins	22 (6 of which are PWM)
Analogue input pins	8
DC current per I/O pin	40 mA
Flash memory	32 KB of which 2 KB used by bootloader
SRAM	$2KB$
EEPROM	$1KB$
Clock speed	$16MHz$

Implementation of data communication method

The developed interconnectivity circuitry of the tactile force sensor uses two modes of communication methods to transmit initially process data for signal filtering and post-processing. It consists of both wireless data transmission using Bluetooth and wired communication via Universal Serial Bus (USB) as shown in the Figure 5.20. To facilitate wireless communication, a HC-05 Bluetooth module was incorporated into the tactile sensor.

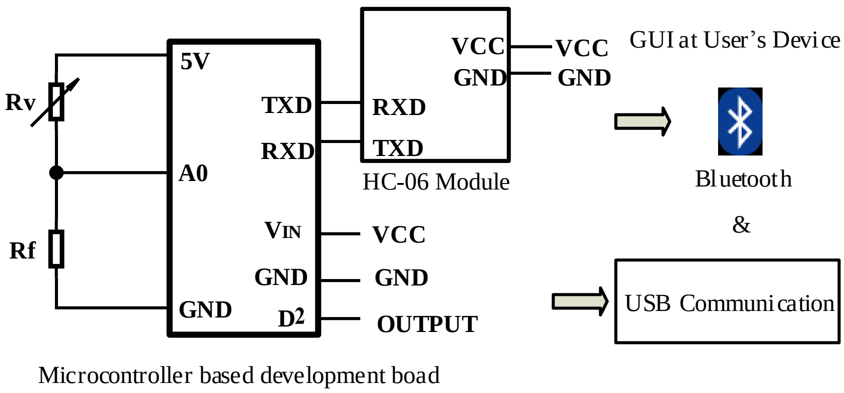

Figure 5.20: Communication methods used for the tactile sensor.

5.7 Assembling and Packaging the 1-DOF Tactile Sensor

As shown in Figure 5.15, the 3D printed parts of the force/tactile sensor, electrode embedded sensing element and interconnection circuitry were assembled (Figure 5.21a). Later, the assembled 1-Degree of Freedom (DoF) tactile sensor, “$Tac - ME''$ (Figure 5.21b) was further tested to identify its mechanical behaviour and its performance. The developed interconnection circuitry was inserted into the circuitry compartment at the bottom pad.

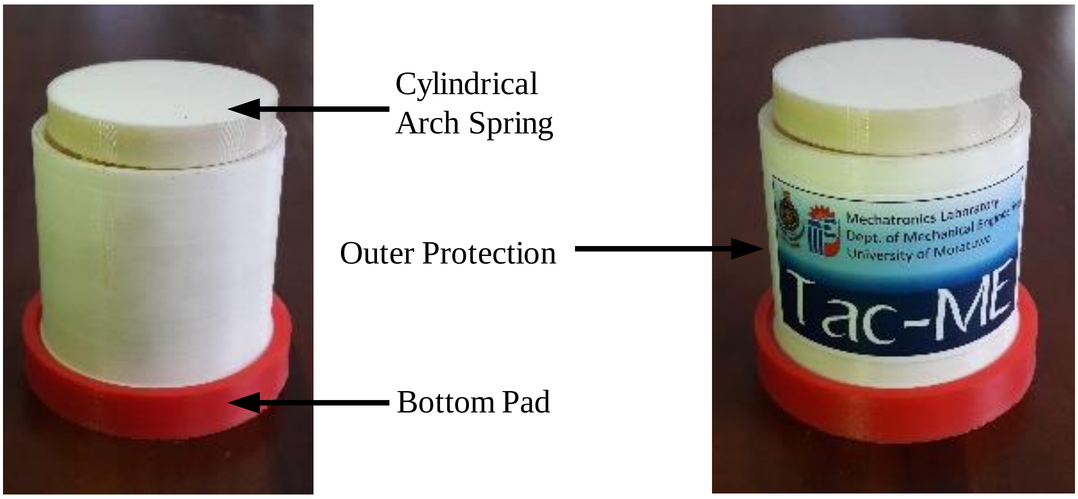

(a) (b)

Figure 5.21: Assembling the tactile sensor: (**a**) Assembled 3D printed sensing structure; (**b**) “Tac-ME”: a 1-DoF Tactile sensor with the insertion of conductive polymer based sensing elements.

5.8 Testing and Characterization of 1-DOF Tactile Sensor

It was required to characterise the developed mechanical structure as well as the assembled tactile sensor to get an idea of how the sensor behaves for external forces. To characterise the sensor, universal testing machine (force indenter) was used with an external data acquisition system connected to it. Force was applied to the force applying surface of the sensor as a distributed load during increasing and decreasing stages.

The Figure 5.22 shows the layout of the system and the Figure 5.23 shows the experimental setup.

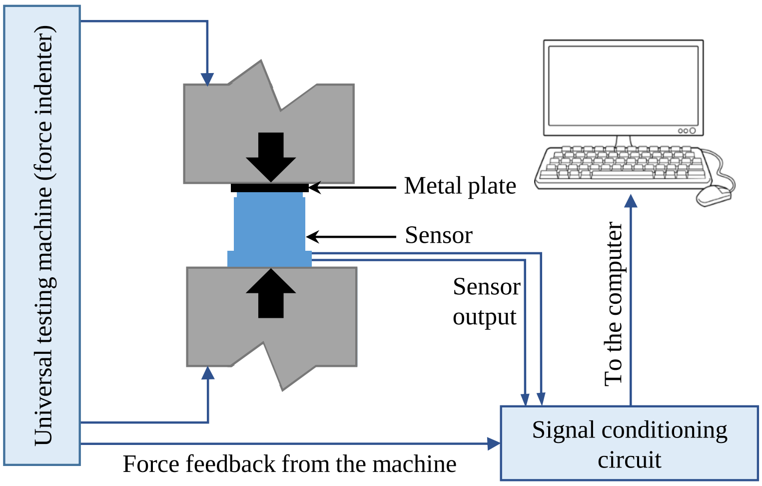

Figure 5.22: Layout of the experimental setup.

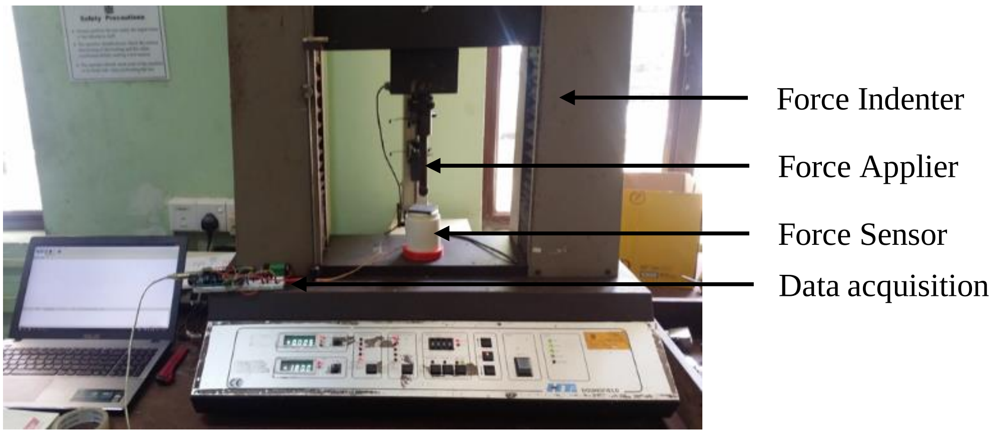

Figure 5.23: Force indenter was used to conduct experiments.

The spring effect of the cylindrical arch spring structure is vital for controlling the force range of the tactile sensor. Therefore, in the beginning, the force indenter was used to observe the spring behaviour of the entire spring structure (without the sensor pill insertion). The obtained experimental results for ten (10) loading and unloading cycles are shown in Table 5.4 and plotted in Figure 5.24. The maximum standard deviation of $0.117mm$ was recorded for a deformation that occurred due to the given forces.

Table 5.4: Experimental results: Force and structure deformation values of the spring structure (only) obtained in ten consecutive cycles.

Load (N)	Cycle 1 (mm)	Cycle 2 (mm)	Cycle 3 (mm)	Cycle 4 (mm)	Cycle 5 (mm)	Cycle 6 (mm)	Cycle 7 (mm)	Cycle 8 (mm)	Cycle 9 (mm)	Cycle 10 (mm)	Std. deviation
5	0.94	0.83	0.86	0.82	0.93	0.71	0.95	0.91	0.90	0.79	0.077
10	1.29	1.19	1.21	1.23	1.33	1.13	1.25	1.23	1.27	1.17	0.060
15	1.69	1.60	1.56	1.54	1.63	1.45	1.75	1.66	1.60	1.51	0.089
20	2.10	2.04	1.95	1.99	2.05	1.93	2.14	2.04	2.00	1.94	0.068
25	3.05	2.93	2.98	2.94	3.06	2.83	3.04	3.01	3.02	2.90	0.076
30	3.79	3.62	3.68	3.61	3.78	3.44	3.79	3.74	3.73	3.56	0.117
35	4.65	4.57	4.54	4.52	4.59	4.44	4.71	4.62	4.56	4.49	0.077
40	5.52	5.45	5.38	5.43	5.50	5.36	5.53	5.46	5.44	5.37	0.061

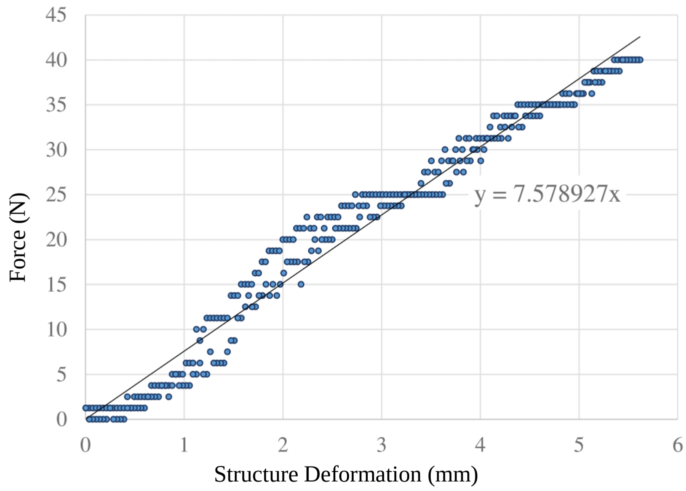

Figure 5.24: Experiment results: force vs. deformation of the structure (only) obtained in ten consecutive experimental cycles.

The average stiffness for the structure was recorded as $7701.12N/m$ with a standard deviation of $196.77N/m$. The experimental results for the stiffness had a deviation of 29.27% compared with the simulation results.

The layering technique of 3D printing might be a major reason, whereas the 90° diagonal material layering has negative and adverse concerns over the structural simulation assumption of solid and consistent ABSplus material in the sensor structure.

Due to the fact of homogeneous characteristics of the structure is enhanced, the parallel material layering in 3D printing would diminish the deviation between the simulated results and the actual results.

Then, the assembled tactile force sensor "$Tac - ME''$ (Figure 5.21b) was tested with several experiments to find out basic characteristics like conductivity, dynamic force range, hysteresis, non-linearity and drift of the sensor. The apparatus described under the Figure 5.23 was used for these experiments that were conducted using the force indenter.

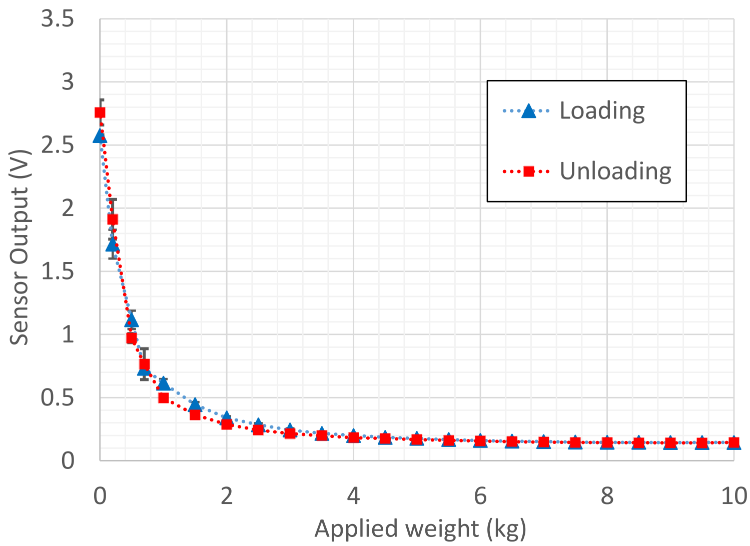

Figure 5.25: Experiment results: sensor output voltage vs. applied weight plot obtained using dead-weight testing with error bars based on standard deviation.

For the sensor output characterisation (or sensor calibration), the sensor output voltage was measured against the applied load for four consecutive cycles and plotted in the Figure 5.25 with the standard deviation of its variation. Experiment results revealed that the tactile force sensor assembly, "$Tac - ME''$ exhibits a slight hysteresis error and shows noteworthy repeatability as the error bars - standard deviation of output values are small. This characteristic is a promising aspect for different applications. Furthermore, the force measurements using the "$Tac - ME''$ was carried out using a comparison of the output voltage with look-up table values (Figure 5.25) obtained for each $10N$ force interval.

Later, the variation in deformation of both developed mechanical structure and compound tactile force sensor was tested separately. Results are shown in Figure 5.26 and a particular amount of hysteresis was featured in between loading and unloading plots.

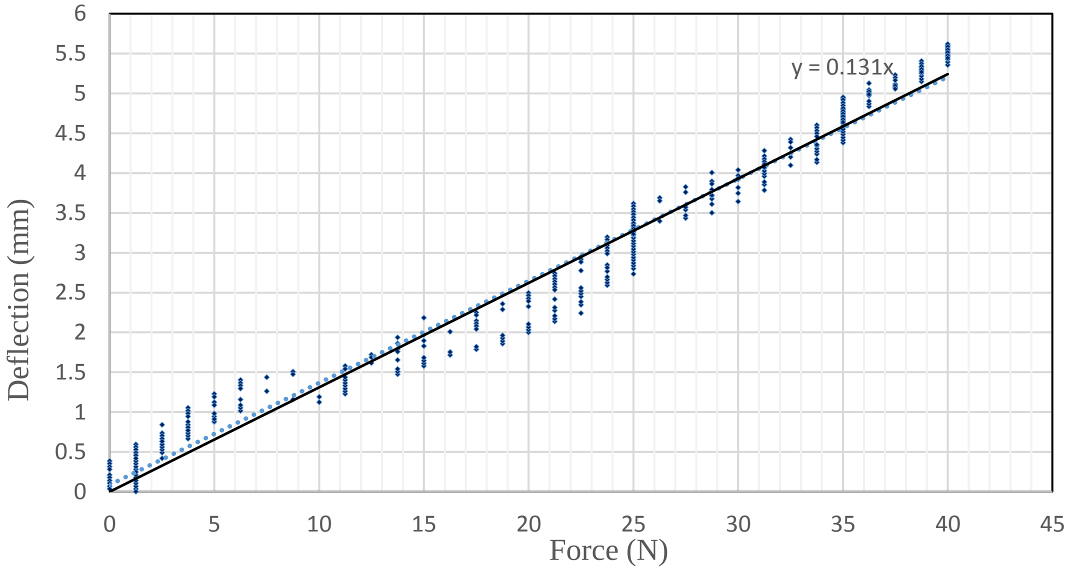

(a)

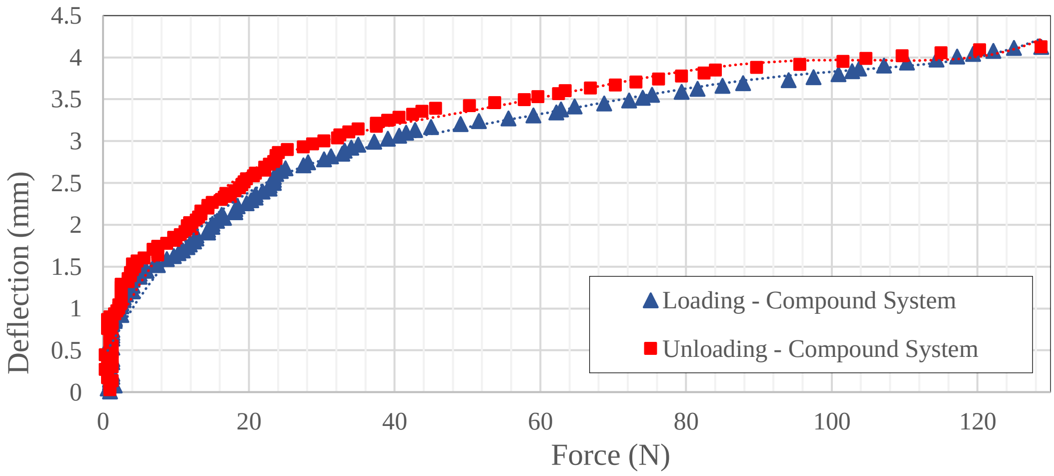

(b)

Figure 5.26: Experiment results using force indenter: deformation vs. applied force plots (**a**) structure only; (**b**) compound system.

The variation in the sensor response over the time is a vital characteristic for a sensor and sensing element. Therefore, the Figure 5.27 represents the drift posses by the sensor for 27 minutes. These results were obtained using the static load test for two steady loads (i.e. $5kg$ and $10kg$) and plots became steady after some time. A high precision digital multimeter was used to record resistance change.

The drift of tactile sensing materials mainly caused by the porosities that occur at material preparation. There won't be any further transient imperfections after diminishing the porous pockets due to the load and time. A significant modification to the conductive polymer moulding (by considering the viscous fluid flow inside the press mould) could mitigate the drift by eradicating porosity creation.

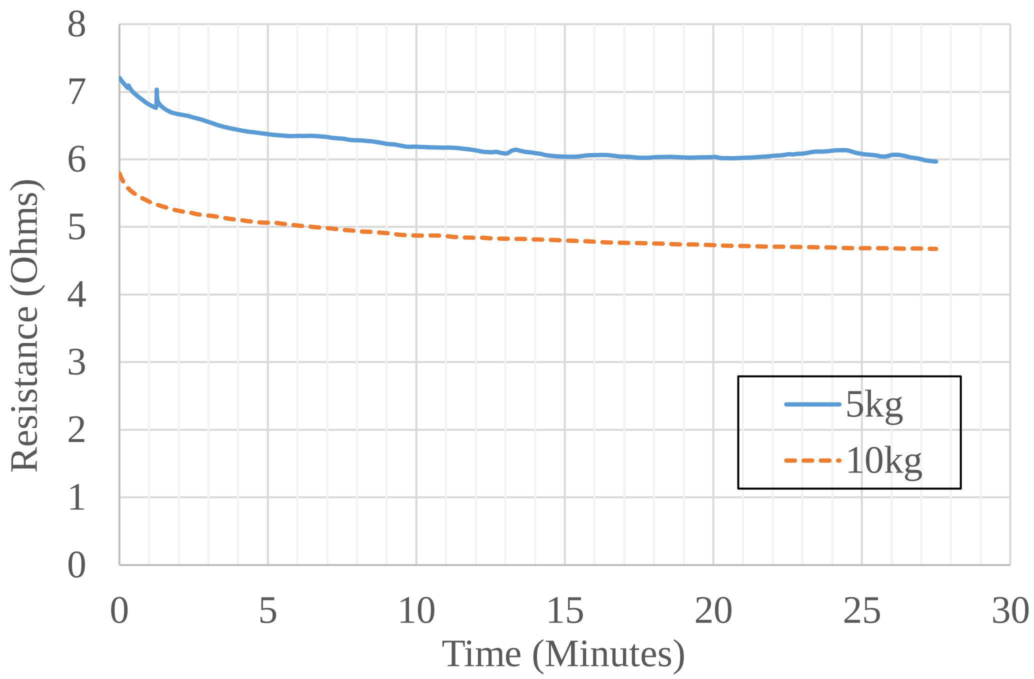

Figure 5.27: Experiment results: sensor drift plot—resistance change over the time.

5.9 Design and Development of Graphical User Interface for Tactile Sensor

The main motive of developing a graphical user interface for the developed tactile sensor is to assist the users to visualize the output of the developed sensor graphically. The developed Graphical User Interface is based on LabVIEW (shown in Figure 5.28) and was used to record, visualize and monitor the behaviour of testing data captured using microcontroller based data acquisition (DAQ) system.

NI-VISA software library available in LabVIEW was used to interface USB and Serial data transmitted by the sensor system. The Virtual Instrument Software Architecture (VISA) is a standard for configuring, programming, and troubleshooting instrumentation systems comprising GPIB, VXI, PXI, Serial, Ethernet, and/or USB interfaces. NI-VISA is the National Instruments implementation of the VISA I/O standard. Further, this GUI was built as a stand-alone application which is an executable file so that it can be run on any PC that is equipped with the LabVIEW run-time engine.

The output voltages from the DAQ w.r.t. exerted force was most difficult to differentiate in the interval of $90N$ to $100N$. Therefore, a margin of $23mV$ was evident with a maximum standard deviation of 0.01. Due to the $5mV$ resolution of the DAQ of the sensor, identification of this $23mV$ should have to be reliable, and therefore a force scale of $10N$ was chosen and visualized on the GUI. The force scaling was carried out based on a comparison between the voltage value and a list of look-up table values obtained for each force interval during the force indenter testing, and force sensor data values were visualized using a colour band.

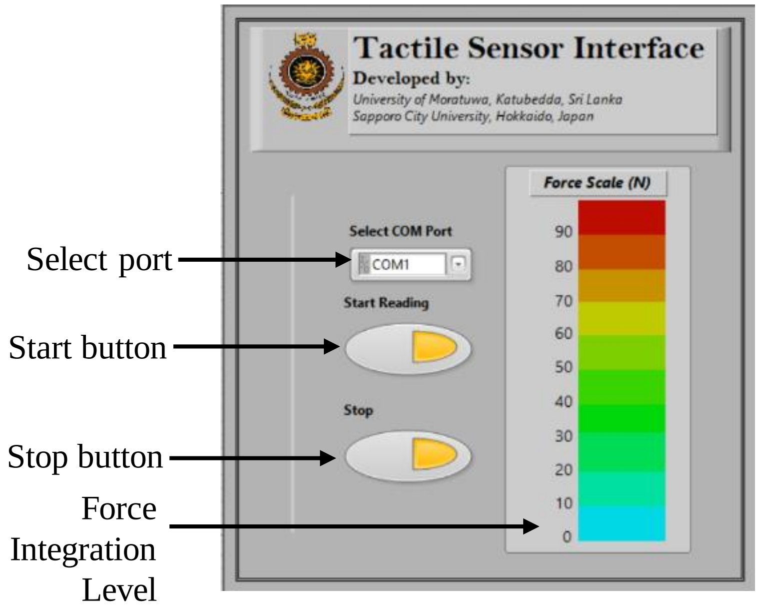

Front Panel

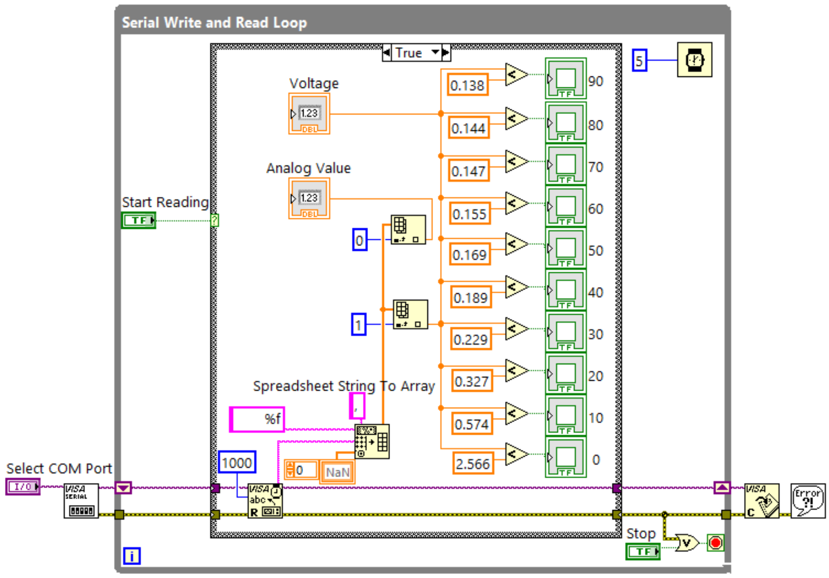

Block Diagram

Figure 5.28: The front panel and the block diagram of the GUI developed using LabVIEW.

5.10 Strength and Weakness in Using the Developed 1-DOF Tactile Sensor as a Biomedical Device

This customizable 3D printed sensor fabrication approach allows to develop of products and easily make changes to the design at a comparably low cost as only the designing/analysis stages require to undergo modifications. Therefore, utilizing an additive manufacturing method gives flexibility to the manufacturing process. In addition to that, the customizable geometry allows to vary its dimensions according to the desired application.

An array arrangement of sensors is required in biomedical applications like tactile imaging which uses an array of tactile sensors for medical diagnosing and plantar pressure measurement systems which measures the variation in foot pressure at vital pressure points. In the context of the developed 1-DOF tactile sensor, it can be utilised into an array in two ways as such, by assembling separately 3D printed sensors into an array or directly 3D printing the sensor array in the desired base fixture shape.

5.10.1 Assembling separately 3D printed sensors into an array

In this method, separately fabricated and assembled "$Tac - ME''$ can be closely arranged to create an array of sensors as shown in Figure 5.29. In literature, it was identified that the tactile sensing element density per unit area is an important feature for an application like tactile imaging. When considering the "$Area - A''$, an area of $14,450mm^2$ bounded by dashed lines in Figure 5.29 of closely arranged "$Tac - ME''$ effective sensing area (area covered by sensing elements) is $1,413.72mm^2$ and a 90.22% area percentage is belongs to void spaces.

Therefore, when using the developed "$Tac - ME''$ for an application that requires the sensing element density, the spring structure needs to be modified to meet the required density.

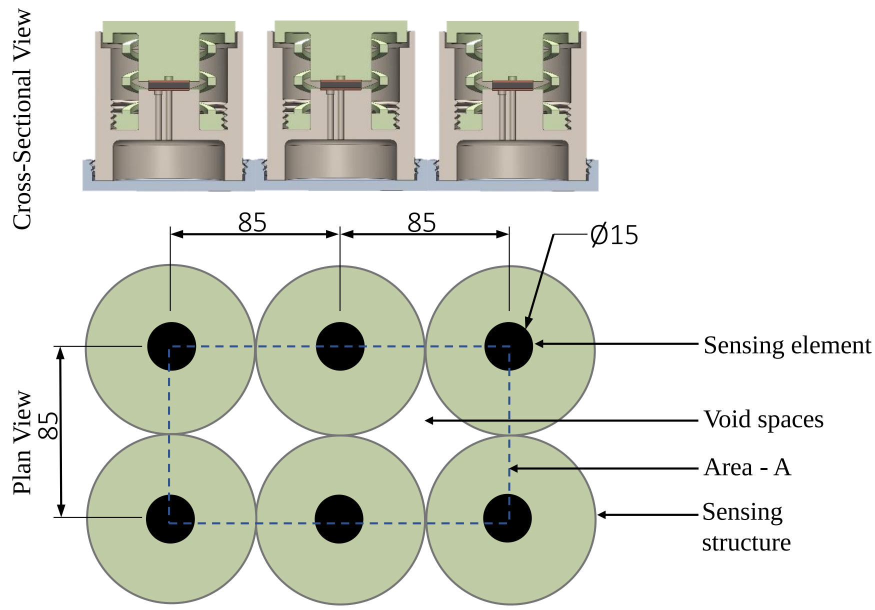

Figure 5.29: Arranging the 1-DOF tactile sensor with cylindrical arch spring structure to a sensor array.

5.10.2 3D printing sensor array in the desired base fixture shape

Having using 3D printed three parts for the development of 1-DOF tactile sensing structure fabricated using 3D printing, this design could be adopted and applied for the sensor embedded shoe described in [56,57] using a miniaturised model. The Figure 5.30 shows how these two designs can be mapped to each other.

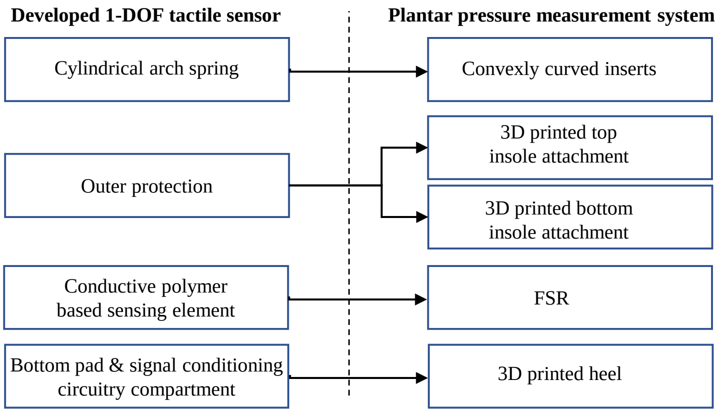

Figure 5.30: Adopting the 1-DOF 3D printed sensor structure to the sensors embedded shoe.

CHAPTER 6

DESIGN AND DEVELOPMENT OF A TACTILE SENSOR WITH A RIGID STRUCTURE DESIGN – II

6.1 Improvements to the Tactile Sensor Structure Design – i

The 1-DOF tactile sensor discussed under the Chapter 5 exhibits its potential in introducing applications that involve point based load measurement. But having identified the limitations in acquiring forces applied over surface based load measurements using an array of sensors, this chapter focuses on the development of another tactile sensor with improved tactile sensing element density per unit area.

6.2 Mechanical Structure of the Proposed Tactile Sensor – Design ii

The sensing structure discussed under the Chapter 5 was adopted to develop a sensing structure with cuboid geometry. The structure is designed to facilitate a 2×2 array of sensing elements.

The sensing structure was designed to a cuboid shape with a square type spring structure. The quarter sectioned view of the proposed sensor is shown in Figure6.1. The overall outer dimensions of the proposed sensor is $50 \times 50 \times 54\ mm$. The other basic dimensions are shown in Figure6.2

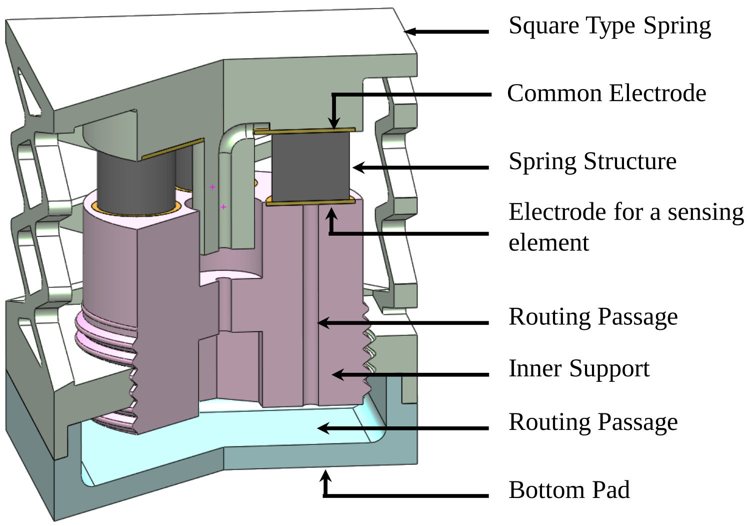

Figure 6.1: Quartered sectional view of the proposed design for the 3-DOF tactile sensor.

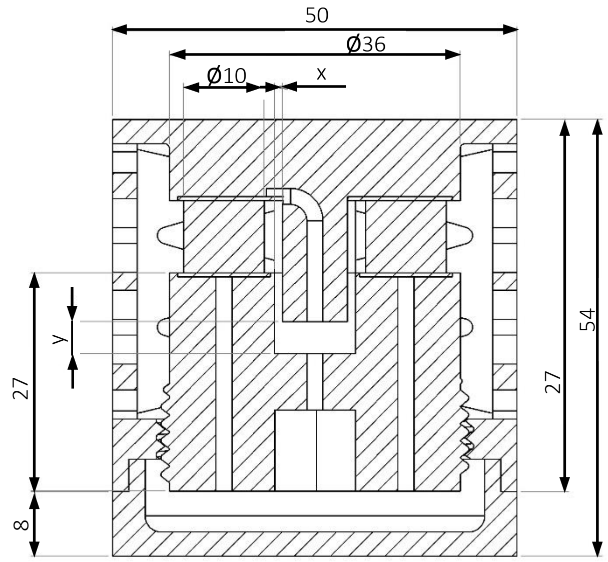

Figure 6.2: Basic dimensions of the proposed tactile sensor.

Furthermore, the following design features were considered in the development process.

- 3-Degrees of Freedom due to the inclusion of 2×2 sensor array.
- The initial compression for sensing elements to initiate conductive paths, screw thread type mechanical fastening between the spring and inner support is used.

- An overload protection to the sensor structure is given by the horizontal and vertical clearance (x and y respectively) between guide pin and the inner support.
- Structure facilitates electrodes, routing for wires and a compartment for internal circuitry.

6.3 Working Principle of the Proposed Tactile Sensor – Design 02

The working principle is similar to the principle described for 1-DOF tactile sensor under the Chapter 5. The free body diagram of the sensor is the same as Figure 5.7 where the term F_p represents combined reaction forces applied from all sensing elements. Using the Hook's law for parallel springs, the equation 5.2 can be modified as:

$$x = \frac{F}{k_S + k_P/4} \tag{6.1}$$

6.4 Analytical Calculations and Numerical Simulations of the Proposed Design

A similar spring design to the cylindrical arch spring structure was used for this proposed sensor design that featured a two-layered saw tooth shaped (Figure 6.3(a)) single square type spring. A fillet radius of R (shown in Figure 6.3(b)) was introduced to enhance mechanical strength of the structure.

A FEA was performed using $COMSOL\ Multiphysics$ for the simplified structure shown in (Figure 6.4(a)). The same governing physics of compressing the combination of spring structure was used as in the Chapter 5. In the simulation, the force on the system was applied using a compression that involved a compression to the spring structure and sensing elements (simulated as a virtual spring) along the centre axis by $2mm$ prescribed displacement.

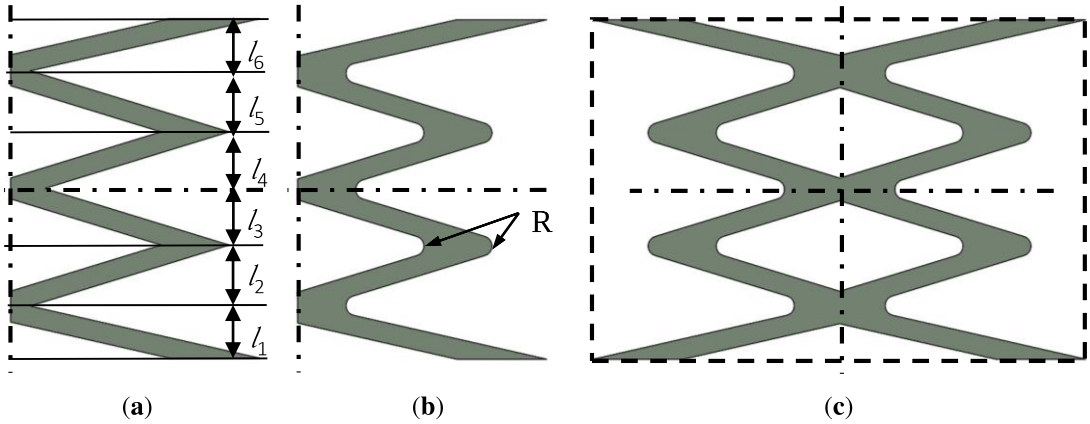

Figure 6.3: Development of the square type spring structure: (**a**) A two-layered saw tooth shape is used; (**b**) Fillet is to enhance the mechanical strength ; (**c**) Single spring.

Stratasys ABSplus that has a maximum tensile strength of $3.6 \times 10^7\ N/m^2$ is used as the material for the simulation and in the analysed results it was shown with maximum von-Misses stress of $2.79 \times 10^7\ N/m^2$ (Figure 6.4(b)).

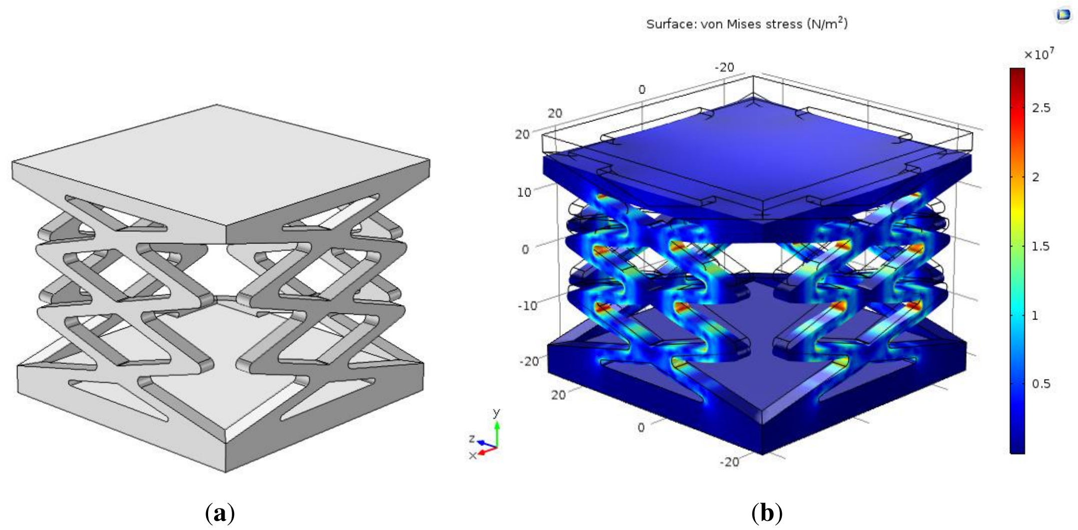

Figure 6.4: Structural Analysis: (**a**) Simplified model of the spring structure; (**b**) Structural analysis carried out using COMSOL Multiphysics.

During the design process, the clearance between the guide pin and inner support also derived using Figure 6.5 that obtained using a tilt angle of θ for a force applied on the force acting surface which reached the maximum allowable deflection of the guided pin.

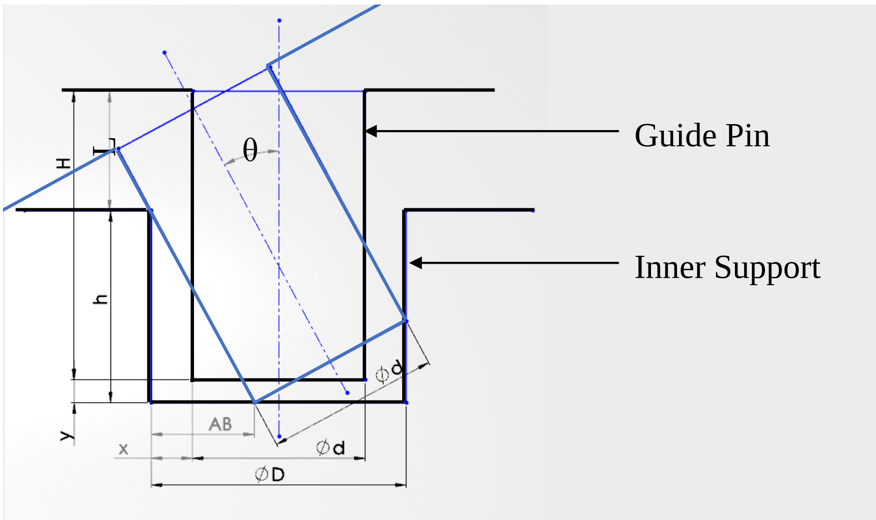

Figure 6.5: Deciding the clearance between the inner support and the guide pin.

Using the geometric relationships, equation 6.2, 6.3 and 6.4 were derived in order to find an expression for vertical clearance - y and horizontal clearance - x.

Consider distance AB,

$$h = \frac{(D - dcos\theta)}{tan\theta} \tag{6.2}$$

Vertical clearance y given by,

$$h = L - H + \frac{(D - dcos\theta)}{tan\theta} \tag{6.3}$$

Horizontal clearance x given by,

$$h = \frac{(D - d)}{2} \tag{6.4}$$

6.5 Fabrication of the Square Type Spring Structure

Considering the fabrication process of the 1-DOF tactile sensor with cylindrical arch spring structure that discussed in Chapter 5, three parts as shown under the Figure 6.6 were fabricated using 3D printing technology as it eases the fabrication process of complex geometries. Square type spring structure (Figure 6.4(c)) was fabricated using ABSplus with 100% infill ratio as the structure should endure higher strength levels. Polylactic acid (PLA) with 75% infill ratio was used for the remaining two parts.

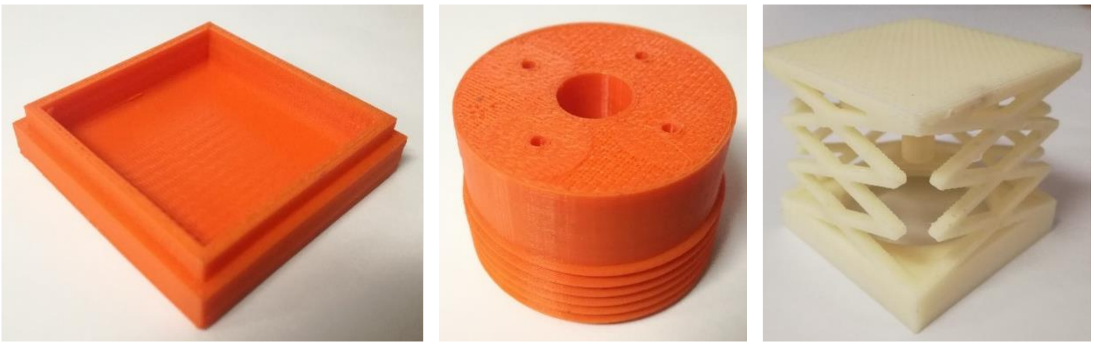

(**a**) (**b**) (**c**)

Figure 6.6: 3D Printed sensor parts: (**a**) Bottom pad; (**b**) Inner support; (**c**) Square type spring structure.

6.6 Development of Electrical Circuit Design for the 3-DOF Tactile Sensor

6.6.1 Development of electrodes for the tactile sensing element

Electrode design was carried out by improving the previously discussed design in Chapter 5. In this full electrode configuration, a copper clad foil was maintained as a common electrode to all the four sensing elements while each sensing element has another copper clad foil to make two electrode layers at both sides of the sensing element. The electrode configuration is shown in Figure 6.7.

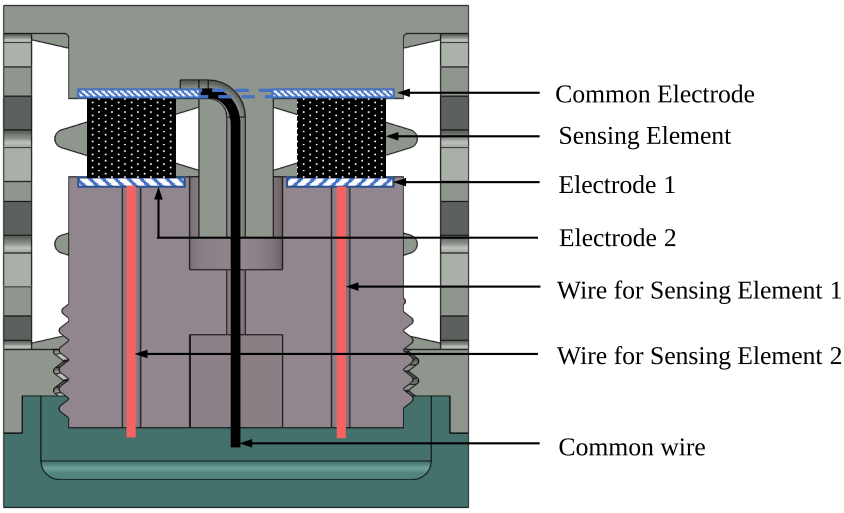

Figure 6.7: Development of the electrode design for the 3-DOF tactile sensor.

6.6.2 Data acquisition, signal conditioning and communication

Data acquisition and signal conditioning of the system was carried out using a ATmega328p development board while maintaining a voltage divider circuit for each sensing element. A bluetooth module was implemented to the circuit for the communication between the sensor and GUI that was developed based on the LabVIEW. The schematic diagram of the circuit is shown under the Figure 6.8. This front panel of the LabVIEW based user interface is shown in Figure 6.11.

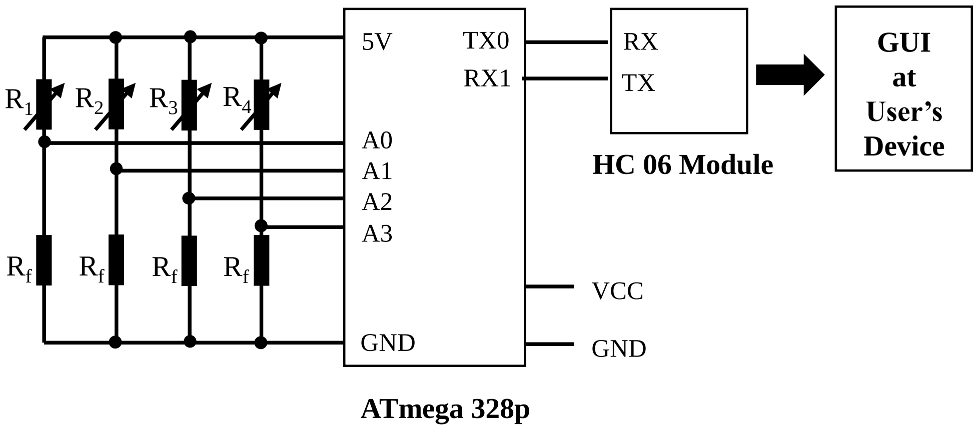

Figure 6.8: Proposed design for the 3-DOF tactile sensor.

6.7 Assembling and Packaging the 3-DOF Tactile Sensor

The assembled sensor using the three 3D-printed structure parts, sensing elements & fabricated electrodes and developed circuitry that was inserted into the circuitry compartment is shown in Figure 6.11. The inner support was inserted and tightened in the assembly so that conductive paths are activated in each sensing element due to the initial compression.

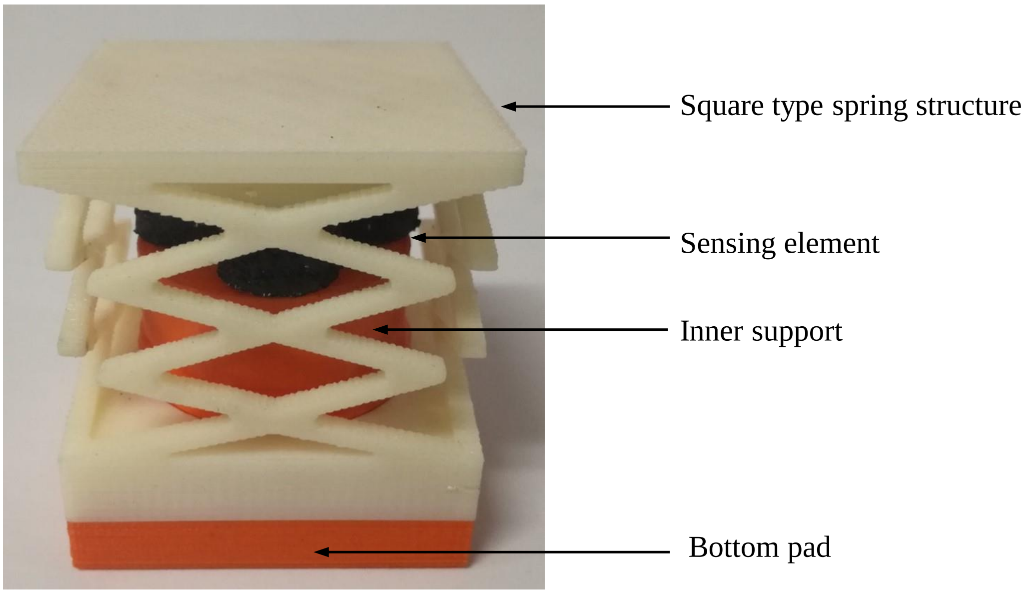

Figure 6.9: Assembled 3-DOF tactile sensor with square type spring structure.

6.8 Testing and Characterization of the 3-DOF Tactile Sensor

Later the assembled sensor was checked with the force indenter and static load testing for its performance. The output obtained from a single sensing element under an axial loading condition is shown under the Figure 6.10.

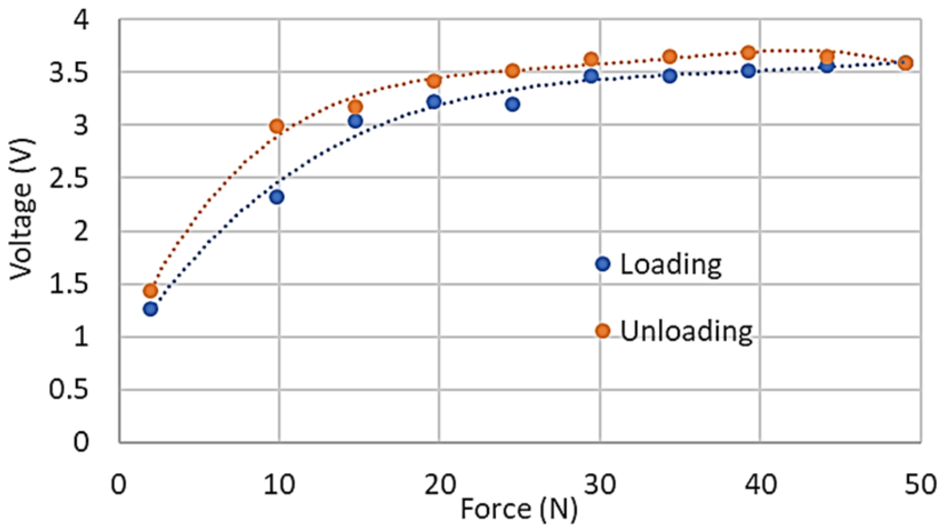

Figure 6.10: Output characteristic of the 3-DOF tactile sensor.

6.9 Design and Development of a Graphical User Interface for the Tactile Sensor

The Graphical User Interface developed (Figure 5.28) under the Chapter 06 was upgraded for four channels to use with this design of the tactile sensor structure.

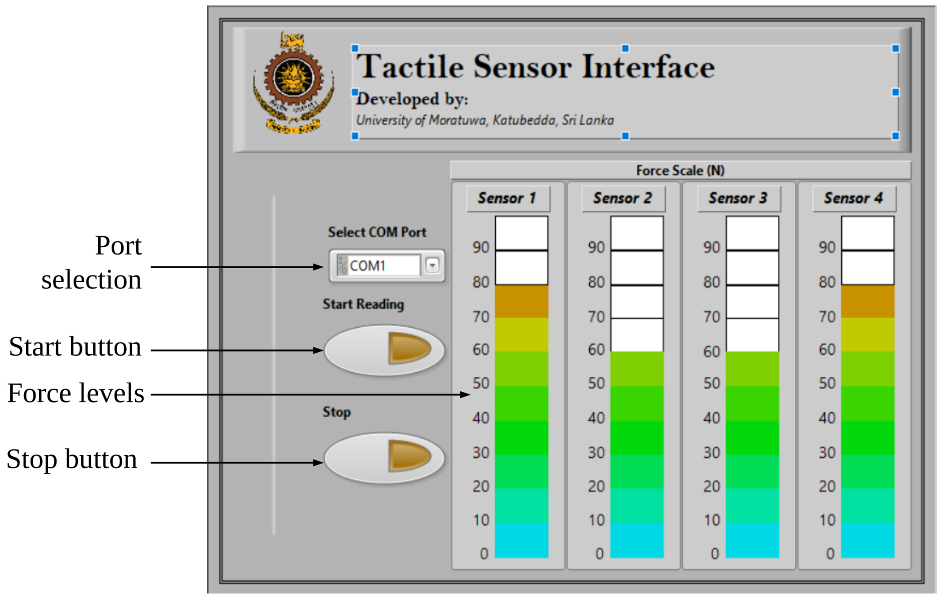

Figure 6.11: The LabVIEW front panel of the modified GUI.

6.10 Discussion

When considering the "$Area - B$", an area of $5,000mm^2$ bounded by dashed lines in Figure 6.12 of the closely arranged sensor array and effective sensing area (area covered by sensing elements) is $1,413.72mm^2$ and a 71.73% area percentage belongs to void spaces. In comparison to the 90.22% void percentage obtained with the sensor arrangement discussed in Chapter 5, using this design the effective tactile sensing density can be improved.

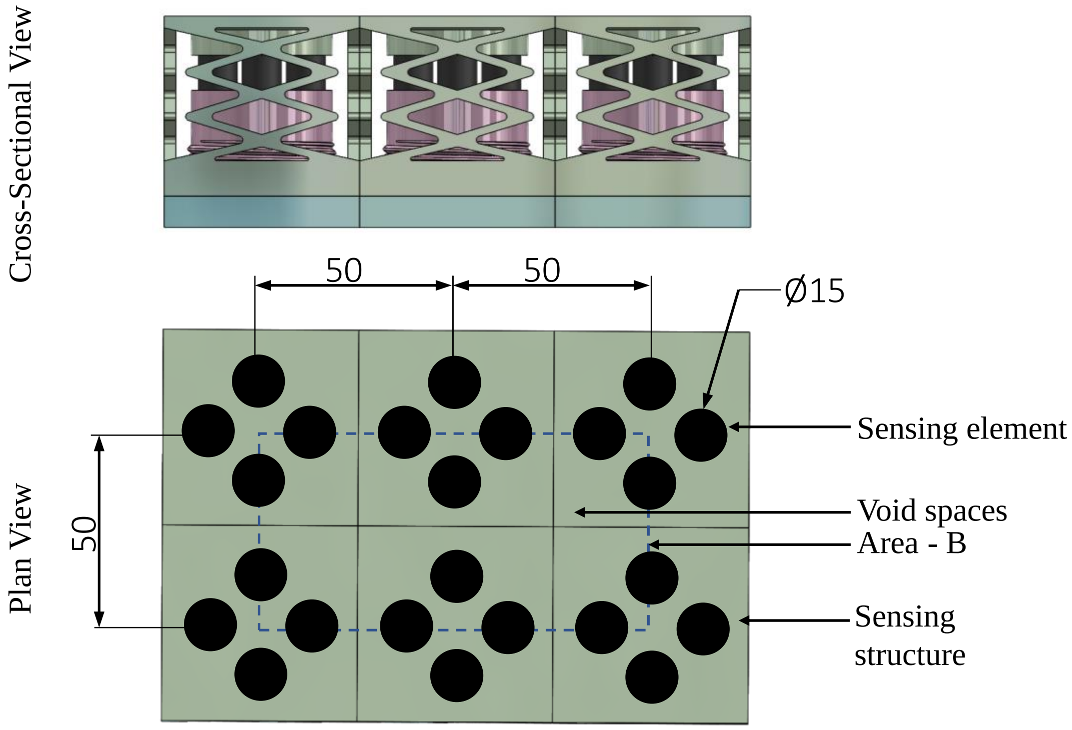

Figure 6.12: Arranging the 3-DOF tactile sensor with square type spring structure to a sensor array.

CHAPTER 7

DESIGN AND DEVELOPMENT OF A SOFT TACTILE SENSOR FOR BIOMEDICAL APPLICATIONS

7.1 Introduction

During the sensing element preparation stage of this research, the possibility of the sensing material to gain flexible behaviour was observed. In this chapter, the focus is to develop a flexible sensing element that will lead to many biomedical applications.

The importance of identifying and monitoring human activity or behavioural changes were identified during the literature review and a lot of researches were conducted related to it and they revealed important aspects of using wearable knee supports or braces as biomedical devices.

The development of a flexible tactile sensing element using conductive polymers and integrate it into a knee brace to monitor and recognize activities will be discussed in this chapter.

7.2 Soft Tactile Sensors for Bio-medical Applications

The previously design tactile sensors in this research and the commercially available conventional tactile sensors are typically rigid. They might restrict and affect various natural body movements when used. These sensors might also be subjected to plastic deformation and failure when pressure is exerted, resulting in compromises in conformability, durability and overall robustness. Therefore, a soft material for the tactile sensor would open several potential paths in the medical applications.

7.3 Proposed Wearable Sensor System

With the advancements in the healthcare industry, a lot of attention was paid towards real-time human monitoring or tracking services. Activity recognition or monitoring devices are mostly used in medical application, home monitoring & assisted living application and sports & leisure applications [65]. Different usages of activity monitoring and recognition in the aforementioned fields are listed in the Figure 7.1.

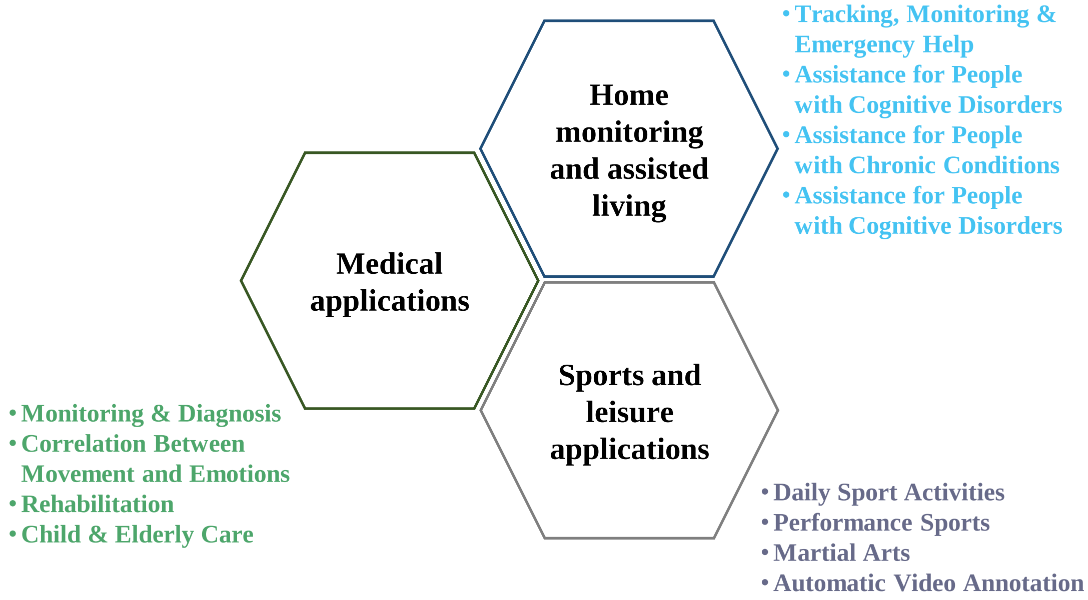

Figure 7.1: Different usages of activity monitoring and identifying devices.

Different types of sensors including vision sensors and inertial sensors are used with human activity monitoring and recognizing. Even though inertial sensors are the most common in the field, effects from human behaviour, sensor inaccuracy and placement difficulties are a few of those limitations associated with inertial sensors when using with activity monitoring and recognizing devices. Image processing is used in vision based sensors, but there might be privacy related concerns with that. Therefore, wearable device consists of flexible tactile sensors, has a potential of addressing most of those mentioned concerns [65].

The proposed knee brace is developed so it could be able to reveal real-time monitoring data as well as storing those data for post processing. The proposed knee brace consists of a flexible sensing element that was aligned to the patella using a knee brace. A micro-controller based controller of the system is capable of acquiring useful data through sensors and processing them. The proposed system layout for the flexible tactile sensor integrated knee brace is shown in Figure 7.2.

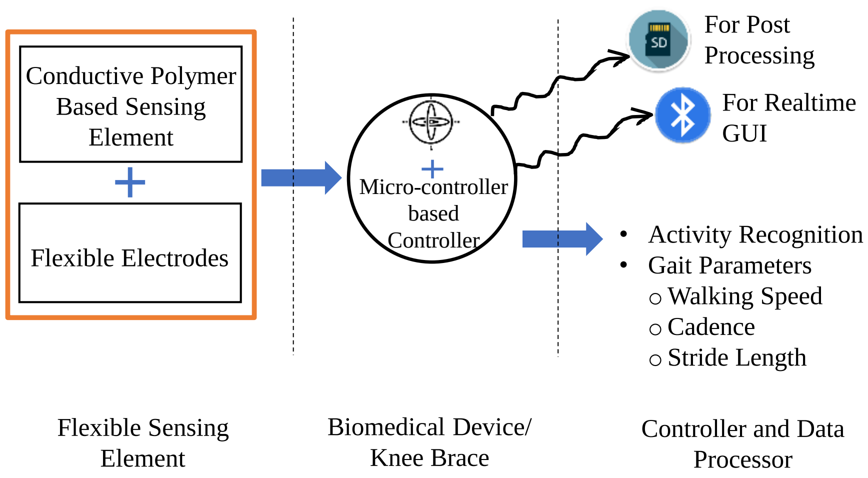

Figure 7.2: System layout of the proposed flexible tactile sensors integrated wearable knee brace.

7.4 Development of the Flexible Electrode

In comparison to commercially available electrodes, it should be easily deformable. Electrodes should be capable of adapting to curvature changes in human skin. Therefore, flexibility and stretchable qualities would be the parameters that should concern during the material selection for base substrate and electrodes.

In order to develop flexible electrodes for the proposed biomedical device, selection of a suitable substrate, a material and a structure design is needed to be carried out by considering prior works in the same field.

7.4.1 Selection of the substrate

According to the literature, the substrate material should pose a near-non-stretchable behaviour when subjected to forces applied by the knee, during human activities. Further, near-non-stretchable quality is required from the substrate to support electrodes without losing its geometry [66] and transferring a maximum amount of pressure or force to the sensing element. More importantly, the substrate material should be comfortable enough for the user as there are contact regions between the fabric and human skin. Table 7.1 summarises different substrate materials and conductive components used in literatures.

Table 7.1: Materials used for textile electrodes.

Researchers	**Ref.**	**Substrate material**	**Conductive component and method**
M. Ishijima	[67]	Nylon fiber filament	Silver plating
Paradiso et al.	[68]	Viscose yarn	30% Stainless steel core-spun
Choi and Jiang	[69]	Conductive fabric	Copper coating
Lobozinski and Laks	[70]	Acrylic fiber filament	Ag/AgCl coating
Zheng et al.	[71]	Cotton, lycra	Stainless steel thread
Jang et al.	[72]	Nylon fabric	Cu sputtering
Rattfalt et al.	[72]	Cotton, polyester staple	Stainless steel mixed spun
Mestrovic et al.	[73]	Nylon mono filament, copper filament	Silver coating Stainless steel
Scilingo et al.	[74]	Continuous viscose yarn	Stainless steel twisting
Shen et al.	[75]	Conductive fiber	Silver coating

Going through the above researches and the availability of substrate materials, cotton linen was chosen as the substrate in order to develop the flexible electrode.

7.4.2 Selection of the electrode material

Materials used as electrodes in textiles should pose several characteristics. Usually, those materials should be in the fibre format as it allows to fabricate electrodes into flexible textile structures [66]. Further, those materials should be strong enough to endure stretching, bending, twisting, etc. More importantly, electrode materials should exhibit characteristics such as non-polarizability, electrochemical stability and mechanical robustness. The Table 7.2 represents materials used as textile electrodes in biomedical applications.

Table 7.2: Commonly used textile electrode materials in biomedical applications.

Application	Metal	Properties
Skin surface ECG, EMG	Silver-silver chloride	Non-biocompatibility, Stable DC reference, low DC polarization
	Carbon	X-ray translucent
Skin surface	Polymers	Special consideration must be taken for the ionic contact medium
	Nickel	Thin flexible plates, skin allergic reactions
Needles	Stainless steel	Mechanically strong, non-corrosive, alloy dependent

It was identified that the conductive yarns might be useful in the context of this research as they ease the amount of difficulty associated with the fabrication process of electrodes. Sewing methods can be incorporated into the electrode fabrications of complex geometries. Further, commercially available conductive yarns took the attention as they were used for several wearable/e-textile projects and can be sew-able by hand with a medium-eye needle or by a sewing machine that can handle heavy thread.

Other than material properties mentioned in Table 7.1 and Table 7.2, yarn structure and the fabric structure are vital when designing textile electrodes.

In the context of conductive yarns, mainly three (03) types of yarns were identified in the literature. Yarn structures used with textile electrodes can be in the form of conductive or non-conductive. Spinning metal wires (Figure 7.3.(a)) and a combination of metal wires and non-conductive fibers (Figure 7.3.(b)) are often used. There is another yarn structure that produced using a twist conductive and non-conductive to a plied yarn (Figure 7.3.(c)).

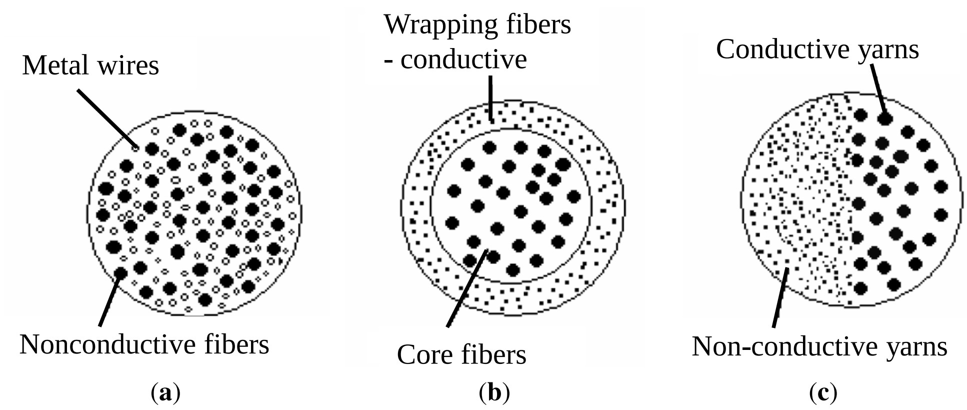

Figure 7.3: Conductive yarn structures are usually a mixture of conductive and non-conductive fibers. They are mixed using: (**a**) blending; (**b**) core-spinning; (**c**) twisting.

Mechanically strong and non-corrosive, Stainless medium conductive thread available at the Adafruit store [76] was identified as a potential type of yarn to use in the research due to its specifications listed under the Table 7.3.

Table 7.3: Specifications of the conductive yarn.

Material	**Details**
Material	316L stainless steel
Number of plys	3 ply tread
Thickness	$0.25mm$
Resistivity	$0.83\Omega/in$
Available at	Adafruit store

7.4.3 Electrode structure designing

The next important design feature is the structure of the flexible electrode. Incorporation of two-electrodes configuration with cylindrical parallel plate method described under the Chapter 5 would produce several design limitations to the system as it requires an electrode layer at each side of the sensing element.

The interdigit method used in a two-electrodes configuration that uses two combs faced to each other creating interdigitated geometry used in gas sensors, humidity sensors, etc. would be a compatible electrode configuration. The electrode arrangement is in one side of the sensing element makes it a potential configuration to use with the proposed flexible tactile sensor arrangement.

The Figure 7.4 represents the proposed interdigitated electrode design where the electrodes are in a comb shape geometry and serpentine area (the area between two electrodes) shown in grey colour is the sensing area. In this configuration, the sensing material is mostly deposited on top of electrodes. But, when the sensor is used as a resistive sensor, only the material deposited in the sensing area is responding to the stimuli [77].

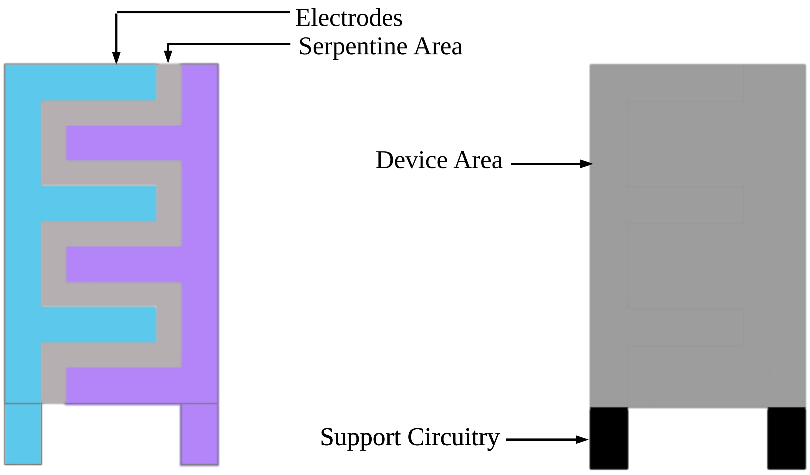

Figure 7.4: The proposed interdigitated electrode configuration.

7.4.4 Validation of the flexible electrode design

An analytical model for interdigitated electrodes was developed by W.H. Grover [77] in one of his studies. When using an interdigitated electrode configuration with a resistive sensing element, current flow only occurs in the serpentine area shown in Figure 7.4. No current passes through the area directly on top of the electrodes.

When analysing further, it can be identified that the gap of the serpentine area varies from (G) to $\sqrt{2} \times G$ when considering parallel portion and diagonal portions (as described in Figure 7.5). A higher amount of current will flow through the low resistive parallel portions (effective sensing area). In the diagonal area (un-optimized area), the amount of current flow will be lesser [77].

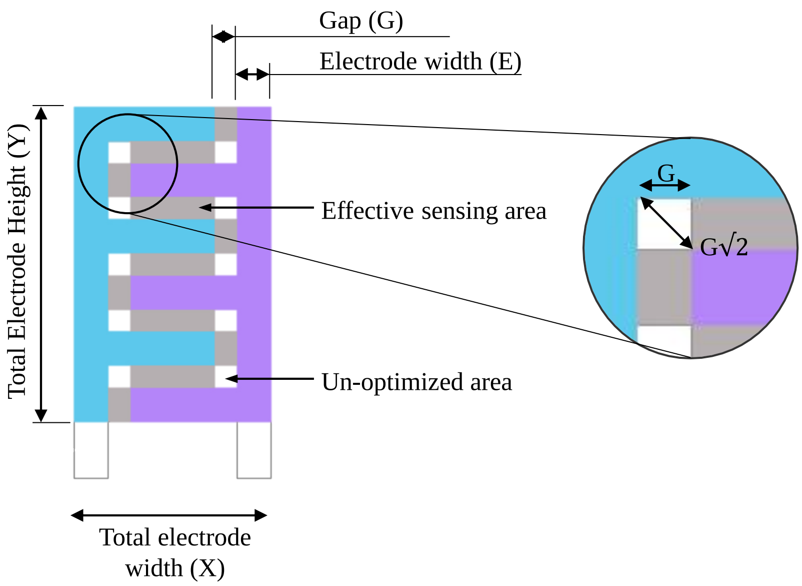

Figure 7.5: Optimized and un-optimized area in the proposed interdigitated electrode design.

Considering the above fact, the efficiency of an interdigitated electrode can be written as follows:

$$\varepsilon = \frac{Sensing\ Area\ (A)}{Total\ Device\ Area\ (A')} \tag{7.1}$$

Table 7.4 shows an analytical comparison of efficiency between interdigitated electrodes and parallel electrodes. For the same device area, an interdigitated electrode configuration exhibits a higher amount of efficiency. Therefore, the effectiveness of the interdigitated electrode design is relatively higher.

Table 7.4: Different sensing element sizes.

	Interdigitated Electrode Design	**Parallel Electrode Design**
Electrode design	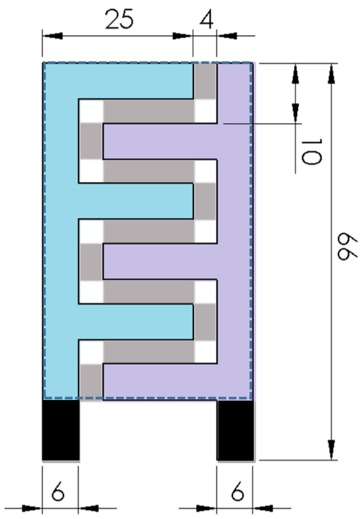	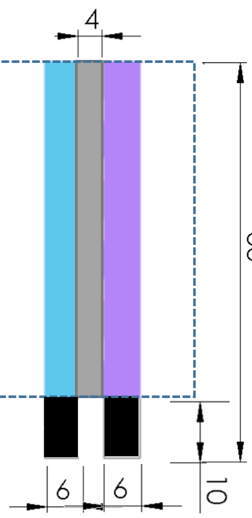
Effective sensing area (A)	444	224
Total device area (A') *	1960	1960
Efficiency (ε)	0.2265	0.1143

* Boundary of the total device area is indicated in dotted lines

7.4.5 Fabrication of the flexible electrodes

Different techniques to fabricate textile electrodes

According to Xu et al. [66], weaving, knitting, embroidering and sewing are the methods that can be used for the fabrication of textile based electrodes. The Figure 7.6 represents different fabrication methods that can be associated with textile electrodes [78]. The electrode fabrication using sewing only associated with lesser skills in sewing and no involvement in machinery equipment. Therefore, sewing can be identified as one of the simplest methods to develop textile based electrodes.

(a) (b) (c) (d)

Figure 7.6: Different methods are available to fabricate textile based electrodes: (**a**) Weaved: Conductive yarns were following the weft; (**b**) Weaved: Conductive yarns were along with the weft; (**c**) Knitted: Conductive yarns were crossing at an angle on the fabric; (**d**) Embroidery: Conductive yarns in a random pattern on a fabric with a sewing machine.

Sewing the flexible electrode

After the selection of fabric and yarn, electrodes were sewn by hand using a medium-eye needle. Cross-stitches were used and the flexible electrodes that were sewn by hand are shown under Figure 7.7. Further, sewed electrodes were checked for continuity using a multimeter and confirmed that the continuity stayed in the same electrode.

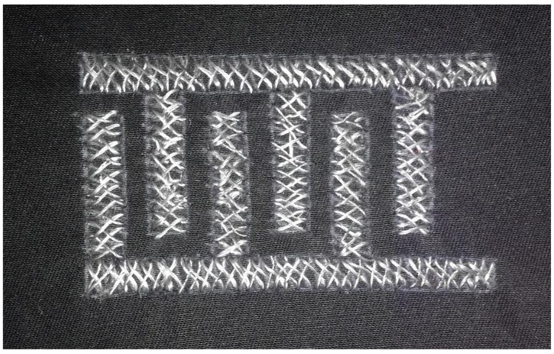

Figure 7.7: Electrodes were sewn by hand using cross-stitches.

7.5 Development of Flexible Tactile Sensing Element

After the design, development and fabrication process of flexible electrodes, the development stage of the conductive polymer based flexible tactile sensing element was the next-in-line stage.

7.5.1 Sensing element design

With the intentions of covering the patella of the knee, the polymer component was designed with dimensions of $72mm \times 60mm \times 3mm$ in length, width and thickness respectively and a fillet of $10mm$ radius at each corner of the rectangular design. Also, it was designed so that both centres of flexible electrode design and the polymer are aligned to each other. The proposed design is shown under Figure 7.8.

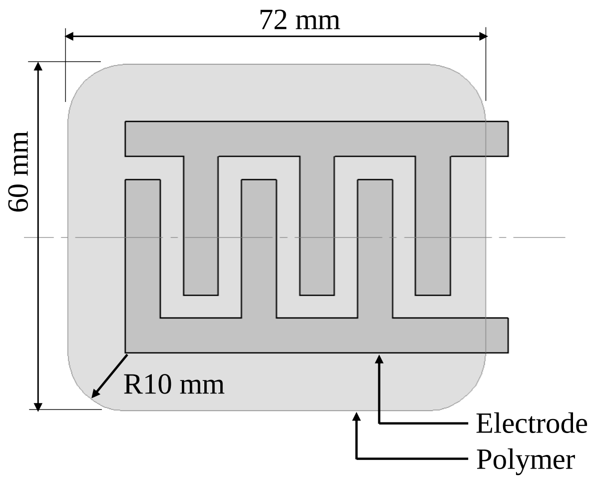

Figure 7.8: Conductive polymer based tactile sensing element design for the knee brace.

7.5.2 Designing the mould for the polymer fabrication

Adopting the moulding method described under the Chapter 3, another three-layered mould was designed in order to fabricate the flexible tactile sensing element and to easily eject the polymer from the mould. Three mould layers were designed using different thickness layers in order to give a $3mm$ thickness to the polymer layer and to support it from the top and bottom (shown in Figure 7.9). An array of risers was included in the top-mould layer to remove extra polymer materials through “Risers” during the compression stage. The proposed mould design is shown in Figure 7.10.

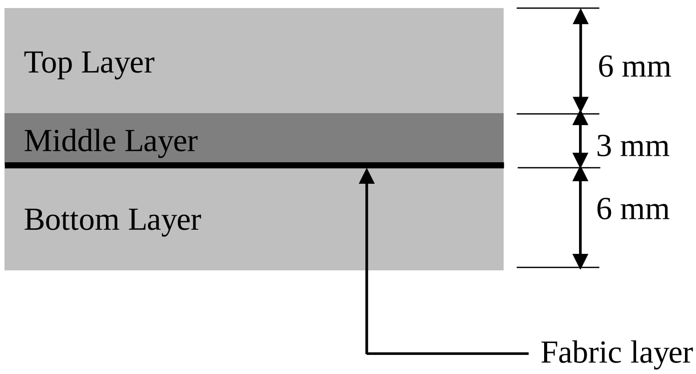

Figure 7.9: Mould design: Layers with different thickness were used.

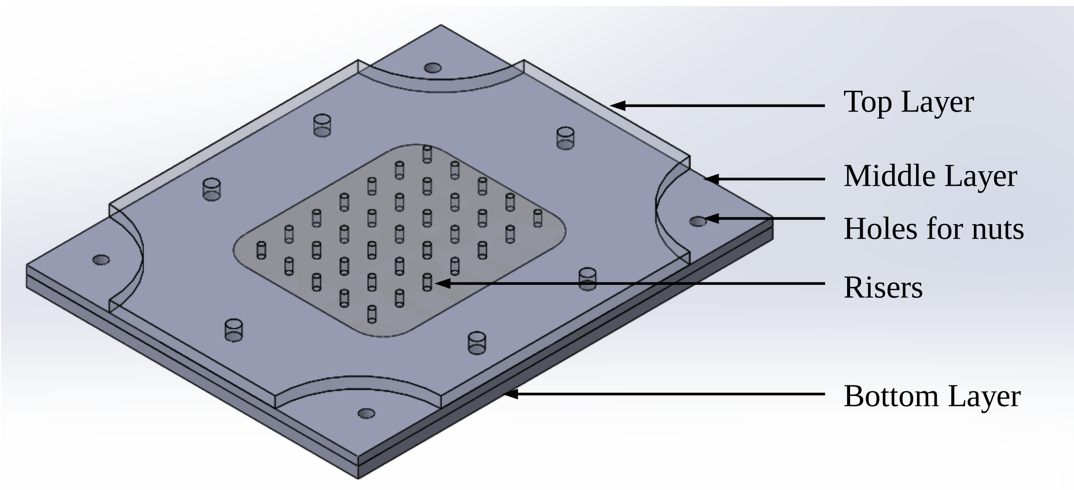

Figure 7.10: Mould design: 3D model of the mould.

Poly(methyl methacrylate) or commercially known as perspex was used as the material for the mould as laser cutting can be interoperated to the fabrication to ease the process to minimise the cost component. Fabricated three layers of the perspex mould is shown under the Figure 7.11.

(**a**) (**b**) (**c**)

Figure 7.11: Mould fabricated using perspex: (**a**) Bottom layer; (**b**) Middle layer; (**c**) Top layer.

7.5.3 Flexible tactile sensing element fabrication

Alignment and placement of the electrode sewed fabric and the mould are significant to carry out before the moulding process as response and sensing element characteristics depend on it. A wooden embroidery hoop, holes kept in moulds and nuts were used (as shown under Figure 7.12) to align the sewed flexible electrodes with the mould.

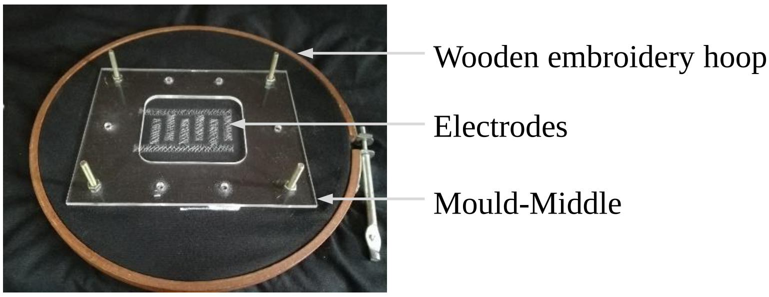

Figure 7.12: Placement of mould in the fabric that flexible electrodes were sewn.

The chemical mixing process described under the Chapter 3 was used with the identified chemical composition in order to mix chemical compounds in ambient temperature and normal pressure, for the silicone based conductive polymer.

A Silicone mould release spray that is commonly used in the industry was thoroughly applied on each mould layer to ease the mould ejection process. Afterwards, a sufficient amount of mixed compound was inserted into the designed space and was compressed using the top-mould layer and nuts. Then, the polymer compound was kept $60 \sim 70$ hours for curing. The fabricated polymer layer after the removal of the top-mould layer is shown and the excess material that went through risers are visible in Figure 7.13.

Figure 7.13: Polymer layer with excess material parts.

The fabricated conductive polymer based tactile sensing element is shown under Figure 7.14 excess material parts were removed during the final fabrication step. In the Figure 7.14, terminal of each electrode is also visible.

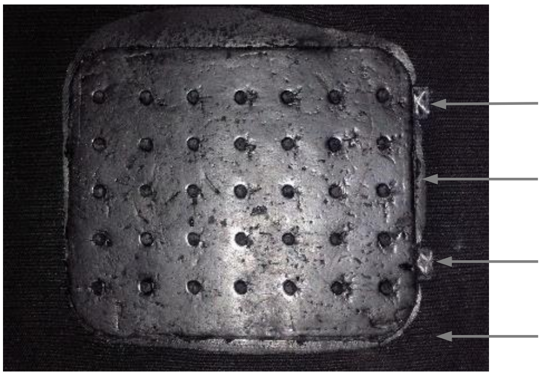

Figure 7.14: Fabricated flexible tactile sensing element with terminals kept for each electrode.

7.6 Development of the controller for the proposed knee brace

The introduction of a controller for the device is essential as data acquisition, signal processing and data processing is required from the system in order to filter-out useful findings from the device.

7.6.1 System layout of the controller

A micro-controller based controller was developed to use with the knee brace. It is capable of acquiring sensor data, conducting initial signal processing and storing data for real-time and post monitoring. The layout of the controller is shown in Figure 7.15.

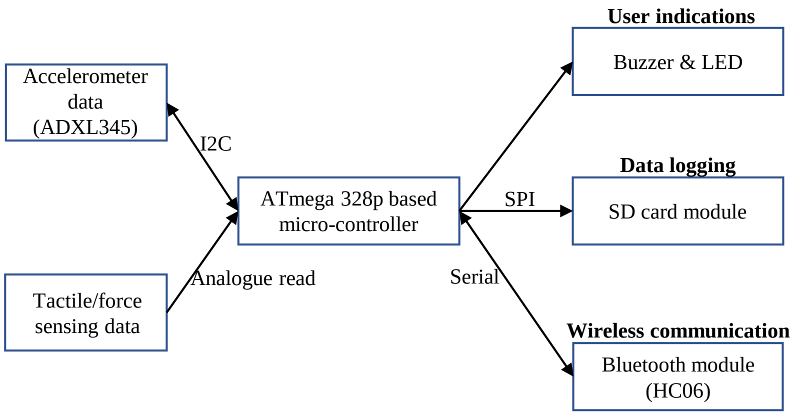

Figure 7.15: Layout of the developed controller.

7.6.2 Data acquisition and signal processing

The controller itself is capable of carrying out the data acquisition and the initial signal conditioning stages. The developed controller is shown in Figure 7.16 and dimensions of the controller were decided so it allows being placed with the developed knee brace. Component arrangement inside the controller is shown under the Figure 7.17.

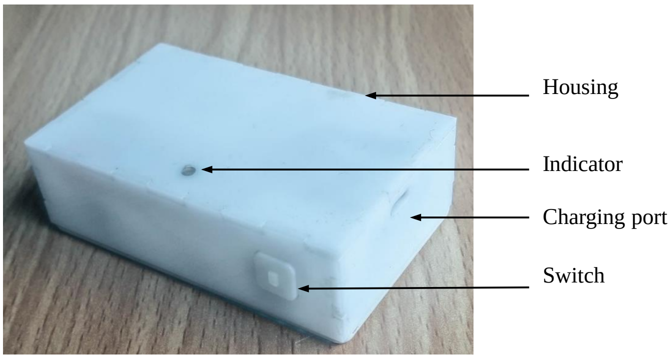

Figure 7.16: The controller developed for the knee brace.

The accelerometer was incorporated into the controller in order to acquire accel-

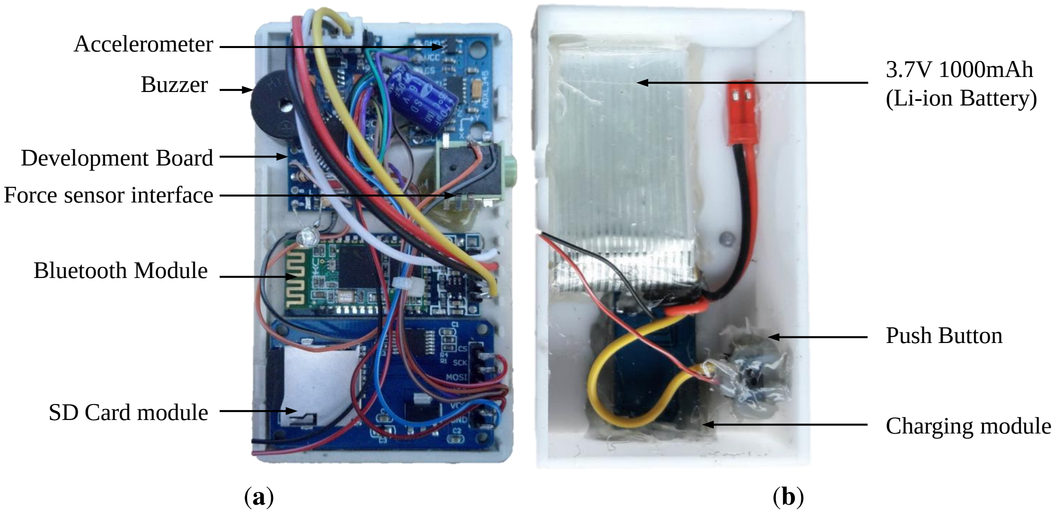

Figure 7.17: Inside view of the developed controller: (**a**) right side; (**b**) left side.

eration data which provide activity related information of the user. Having both accelerometer and force sensing data, the user could precisely identify activities. The controller was designed to power-up with a rechargeable Li-ion battery as it will be useful in continuous running. A buzzer and a LED indicator were incorporated into the controller as it allows to transfer of notifications to the user. The controller is capable of acquiring and logging force sensor and accelerometer data in $15ms$ intervals (Refer Appendix 8 for the Arduino based program.).

Specifications of the controller are listed down in the Table 7.5 and the complete schematic diagram is shown in Appendix 8.

7.6.3 Communication and user interface

Although the system comprises a SD card module for data logging, a Bluetooth module was introduced to the controller in order to enable real-time data monitoring. Wirelessly transmitted serial data was processed with the NI-VISA enabled LabVIEW program in order to process and monitor in real-time. Also, the user interface is capable of logging transmitted data into a file. The developed front panel and the block diagram of the LabVIEW program is shown in the Figure 7.18 and Figure 7.19 respectively.

Table 7.5: Specifications of the controller.

Specification	Details
Controller	ATmega 368p
Communication	Bluetooth via HC-06 module
Sensors	Force Sensor data 3-Axis accelerometer data - ADXL345
Data logger	via SD Card module via LabVIEW based GUI
Power	$1000mAh$ $3.7V$ (Li-ion Battery) - Rechargeable
Charging	via micro USB interface

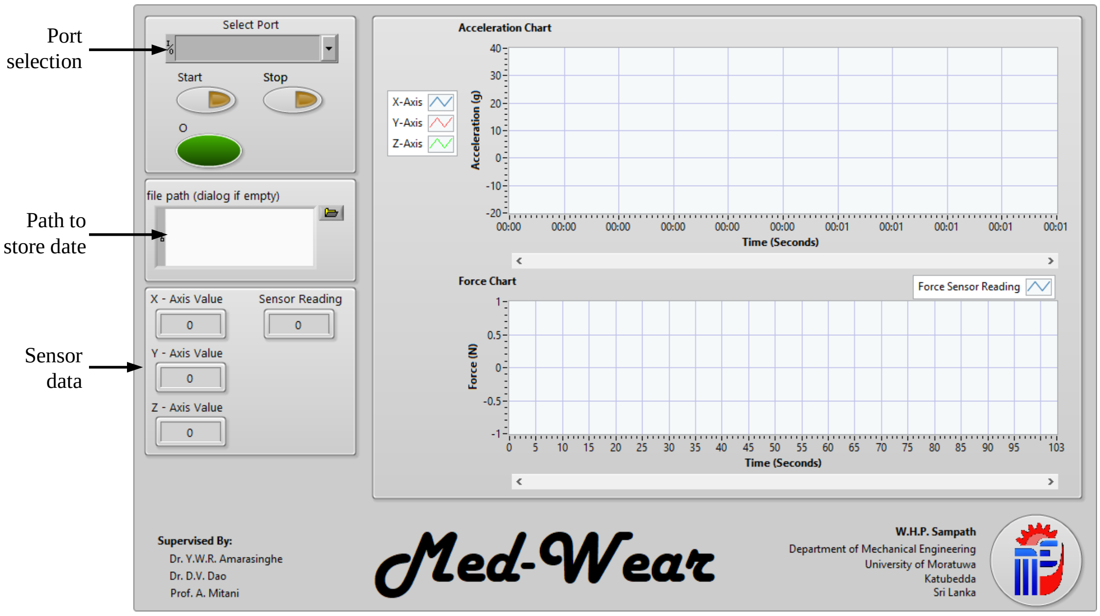

Figure 7.18: Front panel of the developed LabVIEW based GUI for the knee brace.

7.7 Development and Assembling the Sensor Embedded Knee Brace

According to the literature survey conducted related to tactile sensors used in the bio-medical field, it was identified that it is required to place and aligned the sensing element with an external structure to a vital pressure area of the human body. It was decided to use the developed flexible sensing element along with a knee brace to align

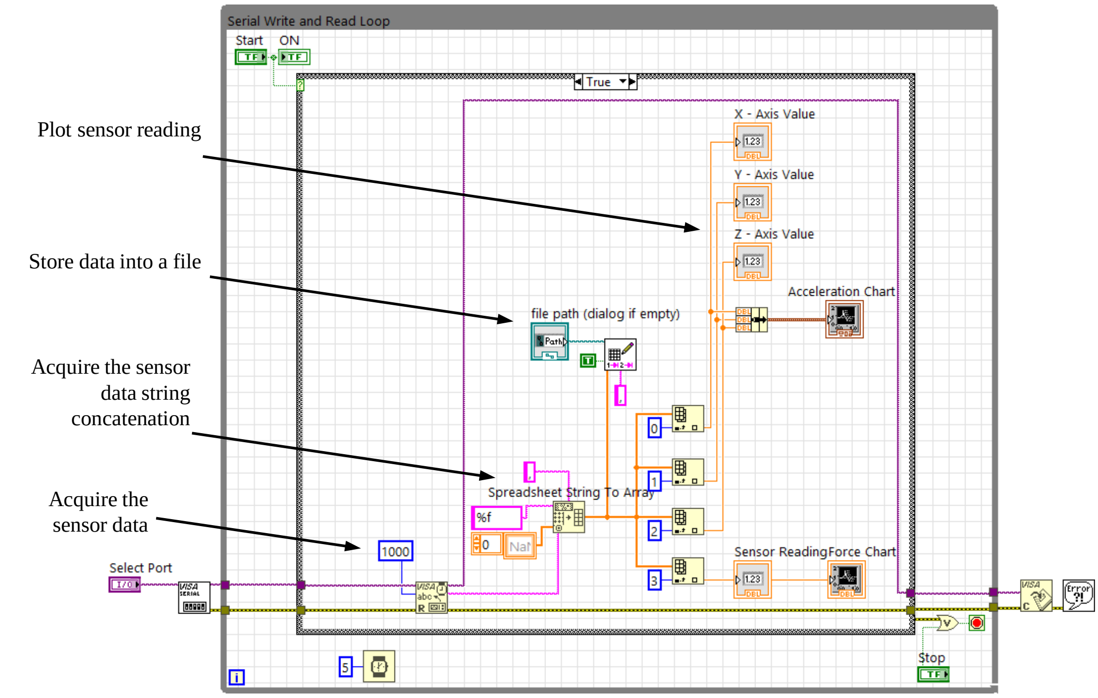

Figure 7.19: Block diagram of the developed LabVIEW based GUI for the knee brace.

and place the sensing element on top of the patella in the knee.

Adjustable knee support designed by OPPO Medical Inc. [79] (shown in Figure 7.20) with an open patella was identified as an external support which allows the flexible sensor to place on top of the patella with the required amount of tension. This knee support is made from Neoprene synthetic rubber.

Figure 7.20: Knee support 1024 by OPPO Medical Inc.

Velcro fastener strips use for clothes were used to adhere to the flexible sensing material to the knee support. It allows the capability to adjust the tension of the fabric that contains the flexible sensing element. Figure 7.21 shows how velcro strips were used in a rectangular arrangement in both sensing element attached fabric and knee support. The controller of the knee brace also attached to the knee support using velcro strips as shown in Figure 7.22.

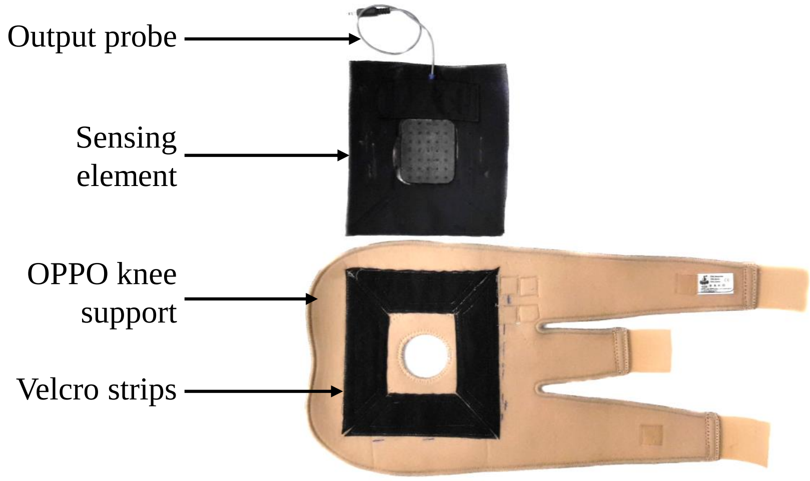

Figure 7.21: Velcro strips were used to attach the sensing element to the knee support.

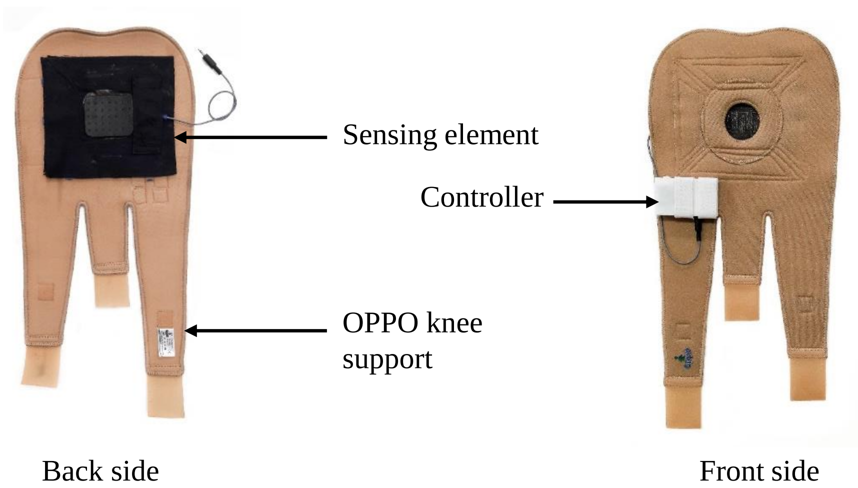

Figure 7.22: Sensors embedded knee brace: front and back side views.

The associated coordinate frame of the “$Med - wear$”, the developed knee brace when it is worn by a user is shown in the Figure 7.23.

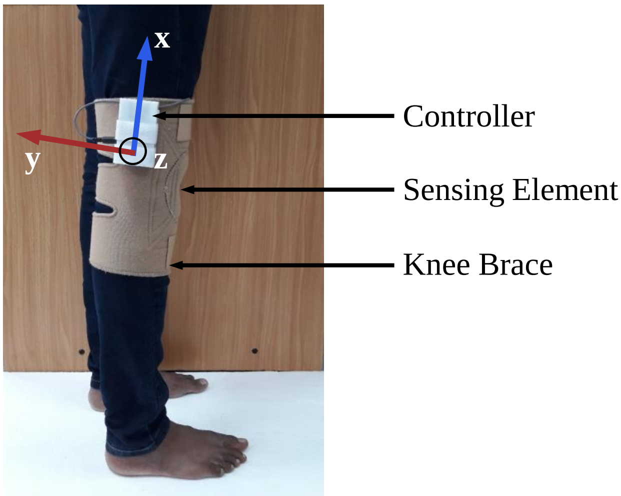

Figure 7.23: Wearing the assembled knee brace “$Med - wear$”.

7.8 Testing Conducted with the Knee Brace and Results

Several preliminary experiments were conducted for the developed sensing element and the developed “$Med - wear$”.

Initially, the developed flexible sensing element was tested with a digital multimeter and possible conductivity changes were observed. Later the sensing element was experimentally tested for equal distribution of materials or compounds throughout the sensing element.

The tactile sensing element was divided into three regions where each region covers an equal amount of electrode regions as shown in Figure 7.24. An external force using the static load test was applied to those regions through a perspex plate.

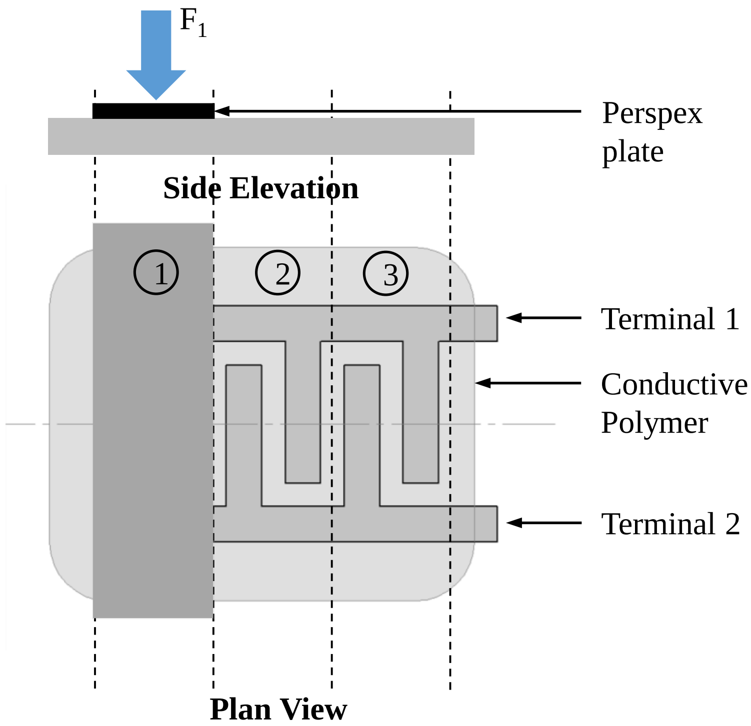

Figure 7.24: A single cylindrical arch design and the arch aspect ratio.

Then the "$Med-wear$" was experimentally tested for its capabilities to differentiate human activities. A human subject who is wearing the "$Med-wear$" was advised to go through a straight path at different speeds while placing steps in approximately the same positions.

Figure 7.25, Figure 7.26 and Figure 7.27 shows the captured sensor readings for a period of 6 seconds. The tactile/force readings of the "$Med-wear$" obtained for each activity can be easily differentiate using the interval between peaks and the amplitude of those peaks (Figure 7.28). Furthermore, the obtained tactile/force readings can be mapped with the accelerometer readings of each activity.

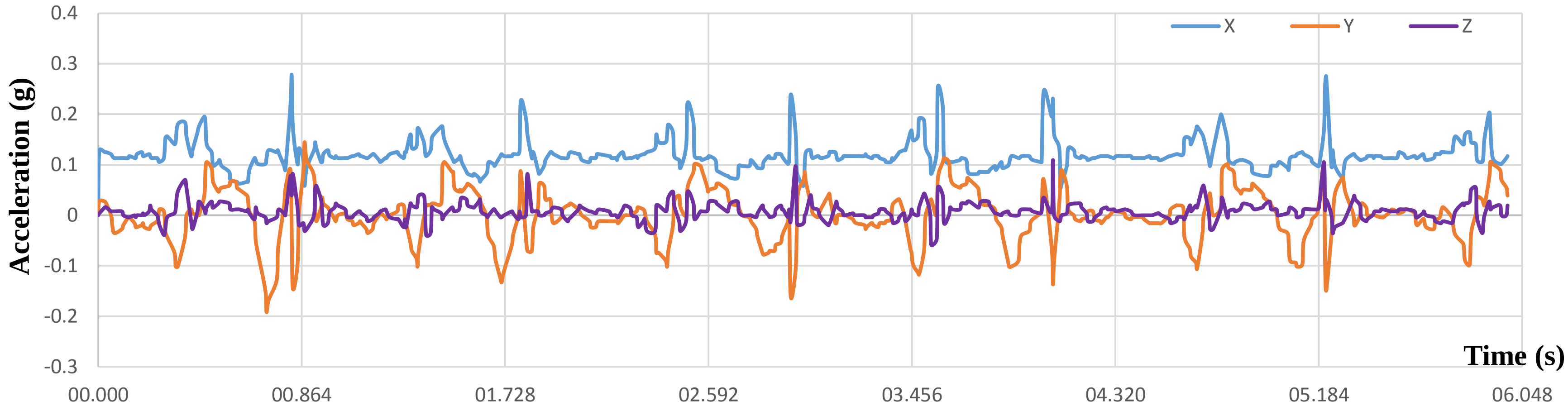

(a)

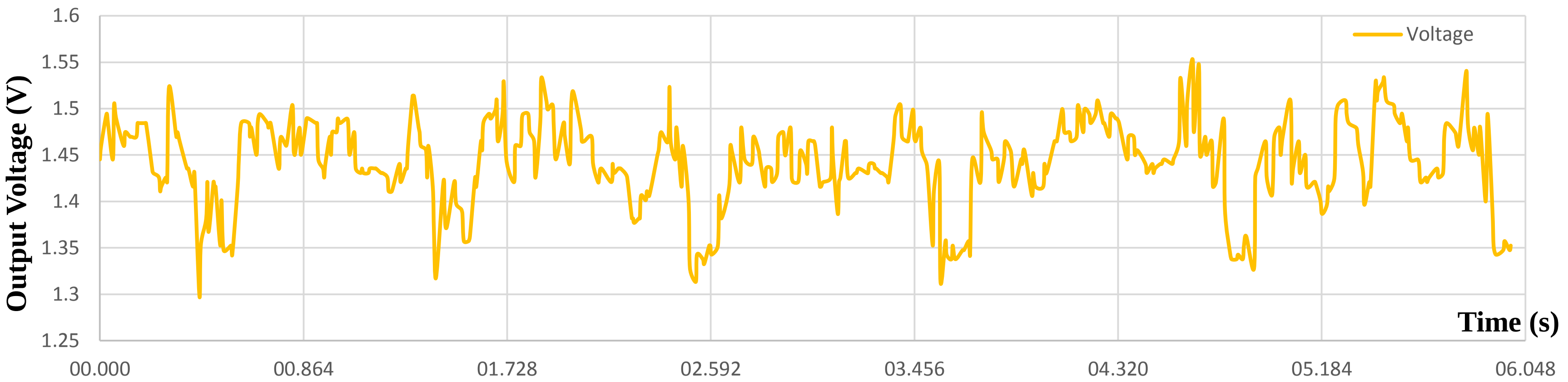

(b)

Figure 7.25: Experimental data for slow walking: (**a**) Accelerometer; (**b**) Tactile/force sensor readings.

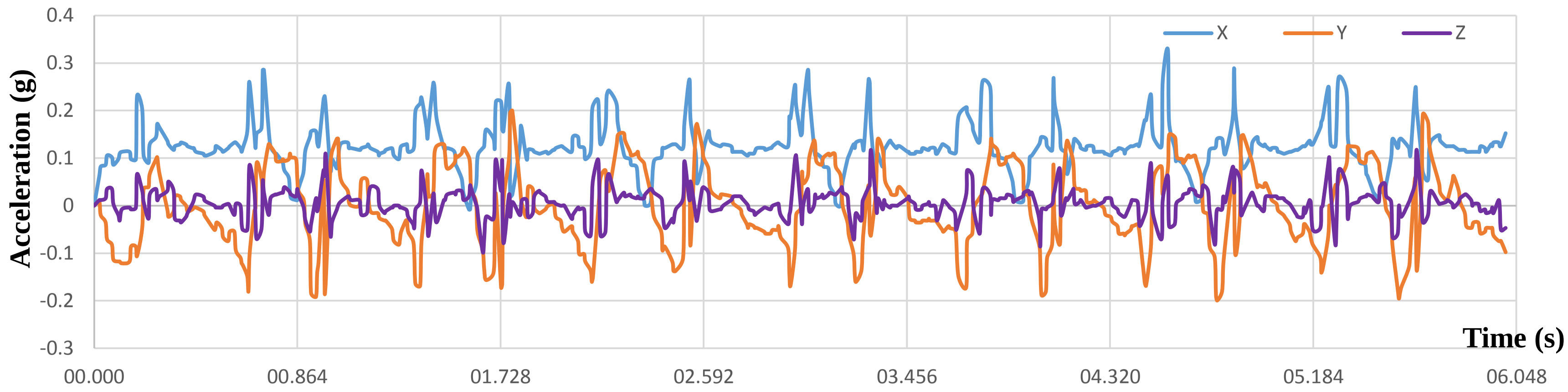

(**a**)

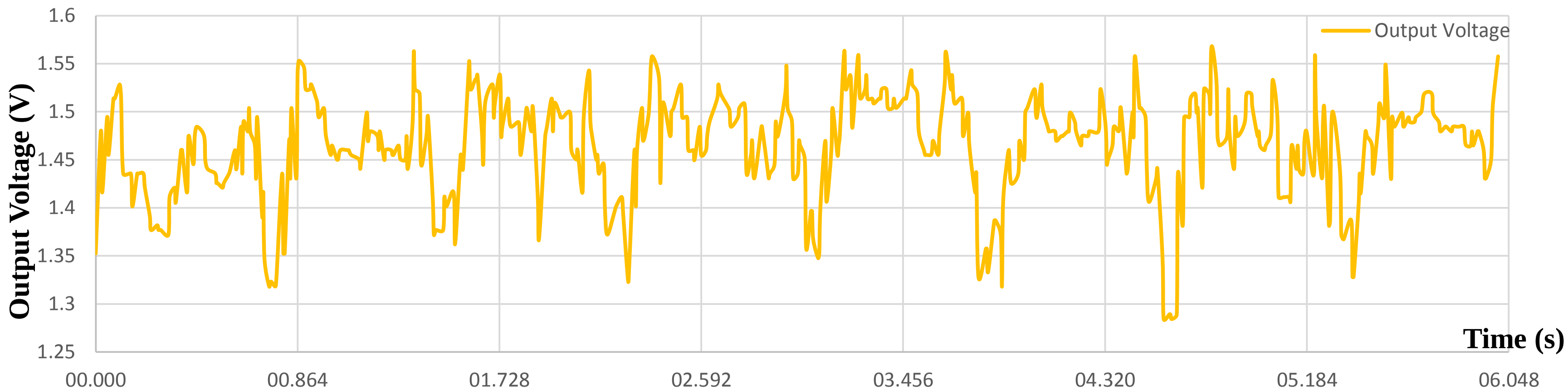

(**b**)

Figure 7.26: Experimental data for walking: (**a**) Accelerometer; (**b**) Tactile/force sensor readings.

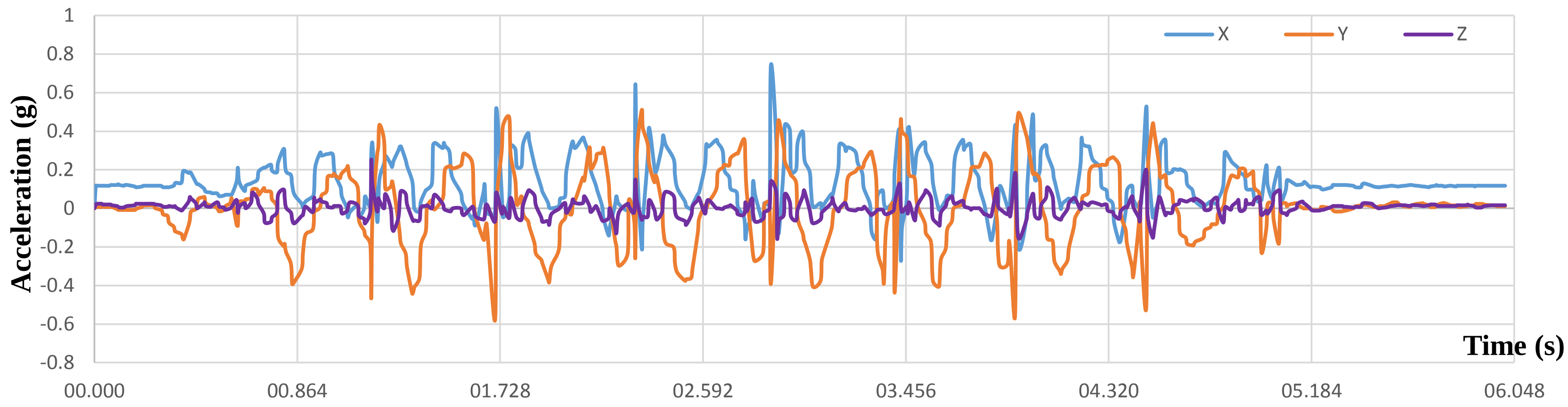

(**a**)

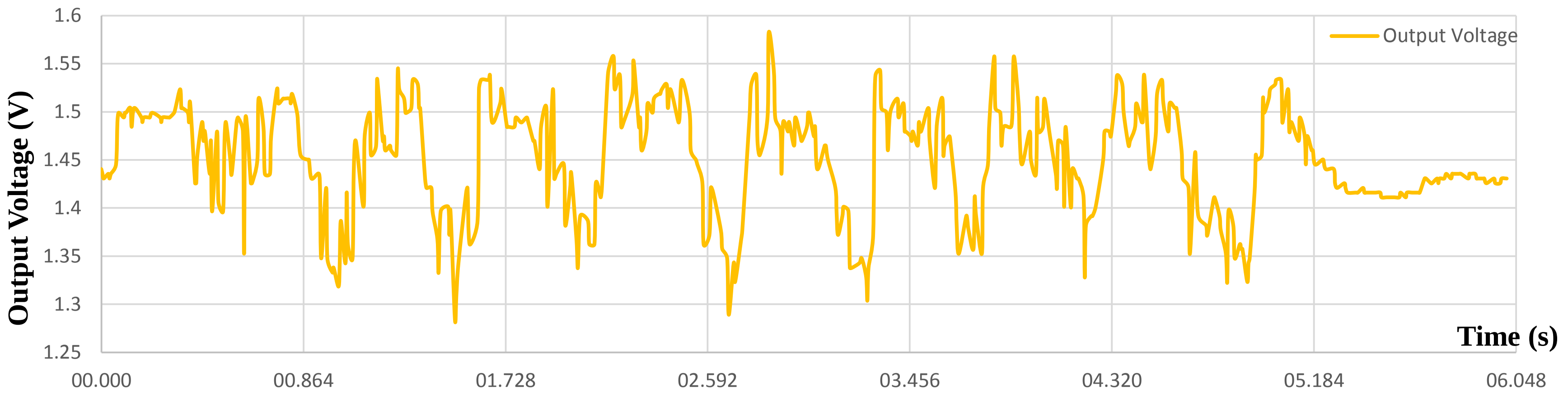

(**b**)

Figure 7.27: Experimental data for running: (**a**) Accelerometer; (**b**) Tactile/force sensor readings.

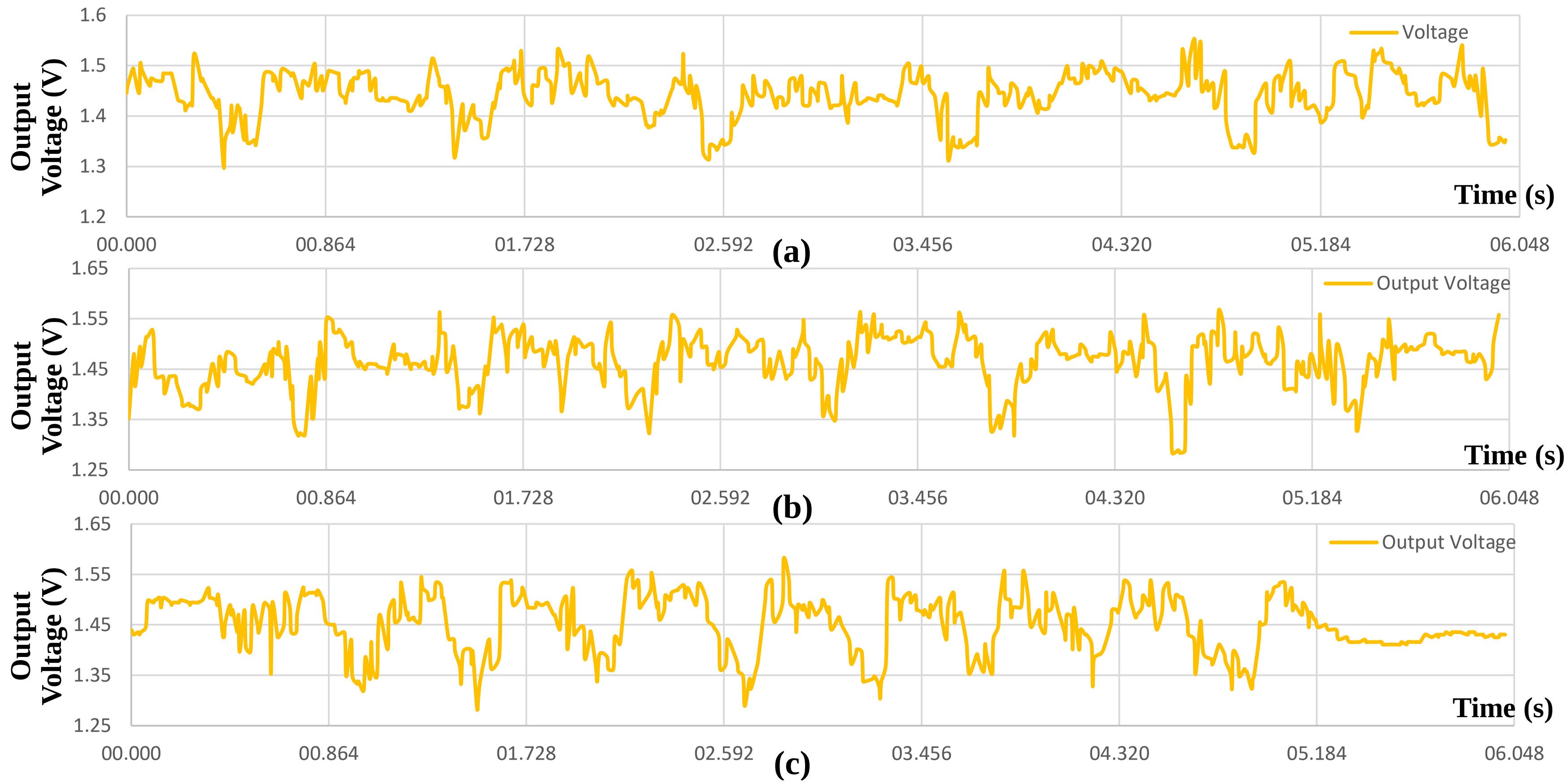

Figure 7.28: A comparison of obtained tactile/force sensing data: (**a**) slow walking; (**b**) walking; (**c**) running.

CHAPTER 8

CONCLUSION

Tactile sensors use the sense of touch to acquire data from the physical environment considering tactile parameters such as force, pressure, temperature, etc. Over the past decades, there have been found many sensing principles that can be incorporated with tactile sensors such as Piezoresistive, piezoelectric, capacitive, etc. These sensing principles have their advantages and disadvantage, hence, it is required to choose optimum sensing principle considering the application to use in a tactile sensor. There can be found many applications of tactile sensors related to robotics, mechatronics, biomedical and industrial field. This is mainly due to the capability of tactile sensors to provide the optimum feedback systems for those applications. Considering the biomedical field, tactile sensors are widely used in tactile imaging and wearable applications.

With the recent advancements of the medical industry, wearable devices are used to support in controlling long-term or repetitive diseases or a disease that comes with time (i.e. chronic diseases) such as heart related diseases, diabetes and asthma by providing information on vital signs. Those vital signs can be heart rate, blood pressure, temperature in the body, blood oxygen level, etc. Other than that wearable biomedical devices are capable of producing smart and intelligent patient monitoring required for several diseases that capable of providing real-time feedback and assist in clinical based decision making. In this research, a novel approach is used to develop conductive polymer based novel tactile sensors to be used with such monitoring devices.

A conductive polymer based sensing element that poses piezoresistive behaviour of composites was successfully developed and tested for its material and mechanical characteristics in this research. Further, the approach to use conductive polymer based sensing elements in different applications were discussed as characteristics such as size, geometry and range can be easily altered during the fabrication process. In order to use it for biomedical applications, its capabilities to incorporate in point based and area based force/pressure measurement systems were discussed in this research with the usage of rigid and flexible sensing structures.

A cylindrical arch spring structure simulated and analysed using FEA tools and fabricated using 3D printing technology was introduced to the conductive polymer based sensing element. This 1 DOF sensor is capable of controlling the deflection of the sensing element to vary within the required deflection range. Due to the manufacturing techniques that have been followed multiple force scaling structures can be 3D printed on a surface to fabricate sensor arrays. Another tactile sensor with a 3D printed square type spring structure was developed and tested for the capabilities to use as a sensor array in biomedical applications.

In the context of flexible sensing structures, a tactile sensor was developed where its electrodes were sewn using conductive yarns on a garment and polymer was moulded on top of that. This fabricated sensor was incorporated into a knee brace in order to monitor force/pressure variations that occurred during human activities. This developed knee brace can differentiate human activities such as slow walking, walking and running w.r.t. peaks and intervals in the acquired signal.

Future work of the research lies in the development of pattern recognition system and the use of artificial intelligence in order to correctly and autonomously identify human activities and use for biomedical monitoring applications.

LIST OF PUBLICATIONS

(01). Development of a conductive polymer based novel 1-DOF tactile sensor with cylindrical arch spring structure using 3D printing technology, **Sampath, W.H.P.**; De Silva, A.H.T.E.; Sameera, N.H.L.; Udayanga, T.D.I.; Amarasinghe, Y.W.R.; Weragoda, V.S.C.; Mitani, A.; *Sensors 19 (2), 318*

(02). Design and development of a novel 3D printed 1-DOF tactile sensor with conductive polymer based sensing element, De Silva, A.H.T.E.; **Sampath, W.H.P.**; Sameera, N.H.L.; Udayanga, T.D.I.; Amarasinghe, Y.W.R.; Weragoda, V.S.C.; Mitani, A.;*2016 IEEE SENSORS, 1-3*

(03). Design and development of a conductive polymer based 3D-printed tactile sensor with square type spring structure, **Sampath, W.H.P.**; De Silva, A.H.T.E.; Roshan, T.A.U.; Amarasinghe, Y.W.R.; *2018 International Conference on Artificial ALife and Robotics(ICAROB 2018), 562-565*

(04). Development of a Novel Telecare System, Integrated with Plantar Pressure Measurement System, De Silva, A.H.T.E.; **Sampath, W.H.P.**; Sameera, N.H.L.; Amarasinghe, Y.W.R.; Mitani, A.; *Informatics in Medicine Unlocked*

REFERENCES

[1] Yousef Al-Handarish, Olatunji Mumini Omisore, Tobore Igbe, Shipeng Han, Hui Li, Wenjing Du, Jinjie Zhang, and Lei Wang. A Survey of Tactile-Sensing Systems and Their Applications in Biomedical Engineering. *Advances in Materials Science and Engineering*, 2020:1–17, January 2020.

[2] Gagan Kaur, Raju Adhikari, Peter Cass, Mark Bown, and Pathiraja Gunatillake. Electrically conductive polymers and composites for biomedical applications. *RSC Advances*, 5(47):37553–37567, April 2015.

[3] Marc O. Ernst and Heinrich H. Bülthoff. Merging the senses into a robust percept. *Trends in Cognitive Sciences*, 8(4):162–169, April 2004.

[4] M.I. Tiwana, S.J. Redmond, and N.H. Lovell. A review of tactile sensing technologies with applications in biomedical engineering. *Sensors and Actuators A: Physical*, 179:17–31, June 2012.

[5] A.M. Almassri, W.Z. Wan Hasan, S.A. Ahmad, A.J. Ishak, A.M. Ghazali, D.N. Talib, and C. Wada. Pressure Sensor: State of the Art, Design, and Application for Robotic Hand. *Journal of Sensors*, 2015:1–12, 2015.

[6] M.R. Cutkosky, R.D. Howe, and W.R. Provancher. Force and tactile sensors. In B. Siciliano and O. Khatib, editors, *Springer Handbook of Robotics*, pages 455–476. Springer Berlin Heidelberg, 2008.

[7] M.H. Lee and H.R. Nicholls. Review Article Tactile sensing for mechatronics—a state of the art survey. *Mechatronics*, 9(1):1–31, February 1999.

[8] M.H. Lee. Tactile Sensing: New Directions, New Challenges. *The International Journal of Robotics Research*, 19(7):636–643, July 2000.

[9] N. Wettels, V.J. Santos, R.S. Johansson, and G.E. Loeb. Biomimetic Tactile Sensor Array. *Advanced Robotics*, 22(8):829–849, January 2008.

[10] J.E. Sanders, R.A. Miller, D.N. Berglund, and S.G. Zachariah. A modular six-directional force sensor for prosthetic assessment: a technical note. *Journal of Rehabilitation Research and Development*, 34(2):195–202, April 1997.

[11] C. Liu, Y. Fujimoto, and Y. Tanaka. Flexible Impact Force Sensor. *Journal of Sensor Technology*, 04(02):66–80, 2014.

[12] J. Gerardo and S. Lanceros-Mendez, editors. *Sensors: Focus on Tactile Force and Stress Sensors*. InTech, December 2008.

[13] Liang Zou, Chang Ge, Z. Wang, Edmond Cretu, and Xiaoou Li. Novel Tactile Sensor Technology and Smart Tactile Sensing Systems: A Review. *Sensors*, 17(11):2653, November 2017.

[14] Pressure Sensor Catalog, PPS, 2016. [Online]. Available: https://pressureprofile.com/catalog-2/. [Accessed on 04-Dec-2016].

[15] R.S. Fearing. Tactile Sensing Mechanisms. *The International Journal of Robotics Research*, 9(3):3–23, June 1990.

[16] "Peratech — What is QTC", Peratech Holdco Limited, 2016. [Online]. Available: https://www.peratech.com/what-is-qtc.html. [Accessed on 04-Dec-2016].

[17] J.G. da Silva, A.A. de Carvalho, and D.D. da Silva. A strain gauge tactile sensor for finger-mounted applications. *IEEE Transactions on Instrumentation and Measurement*, 51(1):18–22, February 2002.

[18] "INASTOMER (Pressure Conductive Sensor) | INABA RUBBER", Inaba—rubber.co.jp, 2010. [Online]. Available: http://www.inaba-rubber.co.jp/en/b_products/inastomer/index.html. [Accessed on 04-Dec-2016].

[19] Zengxi Pan and Zhenqi Zhu. Flexible full-body tactile sensor of low cost and minimal output connections for service robot. *Industrial Robot: An International Journal*, 32(6):485–491, December 2005.

[20] "FlexiForce Load/Force Sensors and Systems", Tekscan, 2016. [Online]. Available: https://www.tekscan.com/flexiforce-load-force-sensors-and-systems. [Accessed on 04-Dec-2018].

[21] P. Dario, D. De Rossi, C. Domenici, and R. Francesconi. Ferroelectric polymer tactile sensors with anthropomorphic features. In *Proceedings. 1984 IEEE International Conference on Robotics and Automation*, volume 1, pages 332–340, Atlanta, GA, USA, 1984. IEEE.

[22] R.D. Howe and M.R. Cutkosky. Dynamic tactile sensing: perception of fine surface features with stress rate sensing. *IEEE Transactions on Robotics and Automation*, 9(2):140–151, April 1993.

[23] A. Persichetti, F. Vecchi, and M.C. Carrozza. Optoelectronic-Based Flexible Contact Sensor for Prosthetic Hand Application. In *2007 IEEE 10th International Conference on Rehabilitation Robotics*, pages 415–420, Noordwijk, Netherlands, June 2007. IEEE.

[24] M.R. Wolffenbuttel and P.P.L. Regtien. Polysilicon bridges for the realization of tactile sensors. *Sensors and Actuators A: Physical*, 26(1-3):257–264, March 1991.

[25] Z. Chu, P.M. Sarro, and S. Middelhoek. Silicon three-axial tactile sensor. *Sensors and Actuators A: Physical*, 54(1-3):505–510, June 1996.

[26] H.K. Lee, S.I. Chang, and E. Yoon. A Flexible Polymer Tactile Sensor: Fabrication and Modular Expandability for Large Area Deployment. *J. Microelectromech. Syst.*, 15(6):1681–1686, December 2006.

[27] M.Y. Cheng, C.L. Lin, Y.T. Lai, and Y.J. Yang. A Polymer-Based Capacitive Sensing Array for Normal and Shear Force Measurement. *Sensors*, 10(11):10211–10225, November 2010.

[28] C. Ge and E. Cretu. MEMS transducers low-cost fabrication using SU-8 in a sacrificial layer-free process. *J. Micromech. Microeng.*, 27(4):045002, April 2017.

[29] S.C.B. Mannsfeld, B.C.K. Tee, R.M. Stoltenberg, C.V.H. Chen, S. Barman, B.V.O. Muir, A.N. Sokolov, C. Reese, and Z. Bao. Highly sensitive flexible pressure sensors with microstructured rubber dielectric layers. *Nature Mater*, 9(10):859–864, October 2010.

[30] M. Shikida, T. Shimizu, K. Sato, and K. Itoigawa. Active tactile sensor for detecting contact force and hardness of an object. *Sensors and Actuators A: Physical*, 103(1-2):213–218, January 2003.

[31] Y Hasegawa, M. Shikida, T. Shimizu, T. Miyaji, H. Sasaki, K. Sato, and K. Itoigawa. Amicromachined active tactile sensor for hardness detection. *Sensors and Actuators A: Physical*, 114(2-3):141–146, September 2004.

[32] T. Frank, L. Doering, G. Heinrich, N. Thronicke, C. Löbner, St. Völlmeke, A. Steinke, and S. Reich. Silicon cantilevers with piezoresistive measuring bridge for tactile line measurement. *Microsyst Technol*, 20(4-5):927–931, April 2014.

[33] Y. Luo, Q. Xiao, and B. Li. A Stretchable Pressure-Sensitive Array Based on Polymer Matrix. *Sensors*, 17(7):1571, July 2017.

[34] S.H. Park, S.Y. Kim, J.H. Kim, and I. Kang. Carbon nano artificial neuron system for flexible tactile sensing. In *2013 10th International Conference on Ubiquitous Robots and Ambient Intelligence (URAI)*, pages 728–729, Jeju, Korea (South), October 2013. IEEE.

[35] Y. Huang, M. Wang, H. Qiu, B. Xiang, and Y. Zhang. Research and Preparation Method of Flexible Tactile Sensor Material. In J. Gerardo and S. Lanceros-Mendez, editors, *Sensors: Focus on Tactile Force and Stress Sensors*. InTech, December 2008.

[36] D. Damjanovic. Ferroelectric, dielectric and piezoelectric properties of ferroelectric thin films and ceramics. *Reports on Progress in Physics*, 61(9):1267–1324, sep 1998.

[37] R. Bao, C. Wang, L. Dong, R. Yu, K. Zhao, Z.L. Wang, and C. Pan. Flexible and controllable piezo-phototronic pressure mapping sensor matrix by zno nw/p-polymer led array. *Advanced Functional Materials*, 25(19):2884–2891, 2015.

[38] Sadao Omata and Yoshikazu Terunuma. New tactile sensor like the human hand and its applications. *Sensors and Actuators A: Physical*, 35(1):9 – 15, 1992.

[39] G. M. Krishna and K. Rajanna. Tactile sensor based on piezoelectric resonance. *IEEE Sensors Journal*, 4(5):691–697, Oct 2004.

[40] M. A. Qasaimeh*, S. Sokhanvar, J. Dargahi, and M. Kahrizi. Pvdf-based microfabricated tactile sensor for minimally invasive surgery. *Journal of Microelectromechanical Systems*, 18(1):195–207, 2009.

[41] C. Li, P. Wu, S. Lee, A. Gorton, M. J. Schulz, and C. H. Ahn. Flexible dome and bump shape piezoelectric tactile sensors using pvdf-trfe copolymer. *Journal of Microelectromechanical Systems*, 17(2):334–341, April 2008.

[42] B. Choi, H.R. Choi, and S. Kang. Development of tactile sensor for detecting contact force and slip. In *2005 IEEE/RSJ International Conference on Intelligent Robots and Systems*, pages 2638–2643, Edmonton, Alta., Canada, 2005. IEEE.

[43] B. Choi, S. Lee, H. Choi, and S. Kang. Development of Anthropomorphic Robot Hand with Tactile Sensor : SKKU Hand II. In *2006 IEEE/RSJ International Conference on Intelligent Robots and Systems*, pages 3779–3784, Beijing, China, October 2006. IEEE.

[44] N. Wettels, J.A. Fishel, and G.E. Loeb. Multimodal Tactile Sensor. In R. Balasubramanian and V.J. Santos, editors, *The Human Hand as an Inspiration for Robot Hand Development*, volume 95, pages 405–429. Springer International Publishing, Cham, 2014.

[45] D. Tan, Q. Wang, R. Song, X. Yao, and Y. Gu. Optical fiber based slide tactile sensor for underwater robots. *Journal of Marine Science and Application*, 7(2):122–126, June 2008.

[46] J. Zhang, W. Liu, L. Gao, Y. Zhang, and W. Tang. Design, Analysis and Experiment of a Tactile Force Sensor for Underwater Dexterous Hand Intelligent Grasping. *Sensors*, 18(8):2427, July 2018.

[47] T.D.I. Udayanga, D.A.M.R. Fernando, H.L.P.L. Chathuranga, Y.W.R. Amarasinghe, and D.V. Dao. Development of a Quantum Tunneling Composite based 1-DOF Tactile Sensor. *International Journal of Advanced Information Science and Technology*, 4(8):99–104, August 2015.

[48] T.D.I. Udayanga, D.A.M.R. Fernando, H.L.P.L. Chaturanga, B.A.D.J.C.K. Basnayake, and Y.W.R. Amarasinghe. Design and Development of Quantum Tunneling Composite based Tactile Sensors. *Proceedings of International Conference on Artificial Life and Robotics*, 23:570–573, February 2018.

[49] T. Mei, W.J. Li, Y. Ge, Y. Chen, L. Ni, and M.H. Chan. An integrated MEMS three-dimensional tactile sensor with large force range. *Sensors and Actuators A: Physical*, 80(2):155–162, March 2000.

[50] J.H. Shan, T. Mei, L. Sun, D.Y. Kong, Z.Y. Zhang hu, L. Ni, M Meng, and J.R. Chu. The design and fabrication of a flexible three-dimensional force sensor skin. In *2005 IEEE/RSJ International Conference on Intelligent Robots and Systems*, pages 1818–1823, Edmonton, Alta., Canada, 2005. IEEE.

[51] T. Someya, T. Sekitani, S. Iba, Y. Kato, H. Kawaguchi, and T. Sakurai. A large-area, flexible pressure sensor matrix with organic field-effect transistors for artificial skin applications. *Proceedings of the National Academy of Sciences*, 101(27):9966–9970, July 2004.

[52] T. Nezakati, A. Seifalian, A. Tan, and A.M. Seifalian. Conductive Polymers: Opportunities and Challenges in Biomedical Applications. *Chemical Reviews*, 118(14):6766–6843, July 2018.

[53] W. Luheng, D. Tianhuai, and W. Peng. Influence of carbon black concentration on piezoresistivity for carbon-black-filled silicone rubber composite. *Carbon*, 47(14):3151–3157, November 2009.

[54] T.H. Speeter. A Tactile Sensing System for Robotic Manipulation. *The International Journal of Robotics Research*, 9(6):25–36, December 1990.

[55] M.Y. Cheng, C.M. Tsao, and Y.J. Yang. An anthropomorphic robotic skin using highly twistable tactile sensing array. In *2010 5th IEEE Conference on Industrial Electronics and Applications*, pages 650–655, Taichung, Taiwan, June 2010. IEEE.

[56] A.H.T.E. De Silva, W.H.P. Sampath, N.H.L. Sameera, Y.W.R. Amarasinghe, and A. Mitani. Development of a wearable tele-monitoring system with IoT for bio-medical applications. In *2016 IEEE 5th Global Conference on Consumer Electronics*, pages 1–2, Kyoto, Japan, October 2016. IEEE.

[57] A.H.T.E. De Silva, W.H.P. Sampath, N.H.L. Sameera, Y.W.R. Amarasinghe, and A. Mitani. Development of a novel telecare system, integrated with plantar pressure measurement system. *Informatics in Medicine Unlocked*, 12:98–105, 2018.

[58] "a Step-by-Step Guide to Compression Moulding Rubber Machinery — Rubber Asia", Rubber Asia, 2015. [Online]. Available: https://rubberasia.com/2015/07/29/a-step-by-step-guide-to-compression-moulding-rubber-machinery/. [Accessed on 04-Dec-2018].

[59] M. Ohmukai, Y. Kami, and R. Matsuura. Electrode for Force Sensor of Conductive Rubber. *Journal of Sensor Technology*, 02(03):127–131, 2012.

[60] J. Castellanos-Ramos, R. Navas-González, H. Macicior, T. Sikora, E. Ochoteco, and F. Vidal-Verdú. Tactile sensors based on conductive polymers. *Microsystem Technologies*, 16(5):765–776, May 2010.

[61] Stratasys® ABSplus, Matweb.com,, 2019. [Online]. Available: http://www.matweb.com/search/datasheet_print.aspx?matguid=14193b776a7b4c1ca6d4ecf86497204b. [Accessed on 20-Feb-2019].

[62] Stratasys® ABS, Matweb.com,, 2019. [Online]. Available: http://www.matweb.com/search/datasheet_print.aspx?matguid=e415f92d1e7047a08b86836459822929. [Accessed on 20-Feb-2019].

[63] "PLA low-cost renewable plastic material for Stratasys 3D Printers", Javelin 3D Solutions, 2019. [Online]. Available: https://www.javelin-tech.com/3d/stratasys-materials/pla/. [Accessed on 20-Feb-2019].

[64] "ABSplus-P430 is a production-grade thermoplastic for Stratasys 3D Printer", Javelin 3D Solutions, 2019. [Online]. Available: https://www.javelin-tech.com/3d/stratasys-materials/absplus-p430/. [Accessed on 20-Feb-2019].

[65] A. Avci, S. Bosch, M. Marin-Perianu, R. Marin-Perianu, and P. Havinga. Activity Recognition Using Inertial Sensing for Healthcare, Wellbeing and Sports Applications: A Survey. In *23th International Conference on Architecture of Computing Systems 2010*, pages 1–10, February 2010.

[66] P.J. Xu, H. Zhang, and X.M. Tao. Textile-structured electrodes for electrocardiogram. *Textile Progress*, 40(4):183–213, December 2008.

[67] M. Ishijima. Cardiopulmonary monitoring by textile electrodes without subject-awareness of being monitored. *Medical & Biological Engineering & Computing*, 35(6):685–690, November 1997.

[68] R. Paradiso, G. Loriga, and N. Taccini. A Wearable Health Care System Based on Knitted Integrated Sensors. *IEEE Transactions on Information Technology in Biomedicine*, 9(3):337–344, September 2005.

[69] S. Choi and Z. Jiang. A novel wearable sensor device with conductive fabric and PVDF film for monitoring cardiorespiratory signals. *Sensors and Actuators A: Physical*, 128(2):317–326, April 2006.

[70] S.M. Lobodzinski and M.M. Laks. Biopotential fiber sensor. *Journal of Electrocardiology*, 39(4):S41–S46, October 2006.

[71] J. W. Zheng, Z. B. Zhang, T. H. Wu, and Y. Zhang. A wearable mobihealth care system supporting real-time diagnosis and alarm. *Medical & Biological Engineering & Computing*, 45(9):877–885, September 2007.

[72] S. Jang, J. Cho, K. Jeong, and G. Cho. Exploring Possibilities of ECG Electrodes for Bio-monitoring Smartwear with Cu Sputtered Fabrics. In *Proceedings of the 12th International Conference on Human-computer Interaction: Interaction Platforms and Techniques*, HCI'07, pages 1130–1137, Berlin, Heidelberg, 2007. Springer-Verlag. event-place: Beijing, China.

[73] M.A. Mestrovic, R.J.N. Helmer, L. Kyratzis, and D. Kumar. Preliminary study of dry knitted fabric electrodes for physiological monitoring. In *2007 3rd International Conference on Intelligent Sensors, Sensor Networks and Information*, pages 601–606, Melbourne, Australia, 2007. IEEE.

[74] E.P. Scilingo, A. Gemignani, R. Paradiso, N. Taccini, B. Ghelarducci, and D. DeRossi. Performance Evaluation of Sensing Fabrics for Monitoring Physiological and Biomechanical Variables. *IEEE Transactions on Information Technology in Biomedicine*, 9(3):345–352, September 2005.

[75] C. Shen, T. Kao, C. Huang, and J. Lee. Wearable Band Using a Fabric-Based Sensor for Exercise ECG Monitoring. In *2006 10th IEEE International Symposium on Wearable Computers*, pages 143–144, Montreux, Switzerland, October 2006. IEEE.

[76] Adafruit industries, "Stainless Medium Conductive Thread - 3 ply - 18 meter/60 ft", Adafruit.com, 2019. [Online]. Available: https://www.adafruit.com/product/641. [Accessed on 15-Mar-2019].

[77] W. Grover. Interdigitated Array Electrode Sensors: Their Design, Efficiency, and Applications. *University of Tennessee Honors Thesis Projects*, May 1999.

[78] Taina Pola and Jukka Vanhala. Textile Electrodes in ECG Measurement. In *2007 3rd International Conference on Intelligent Sensors, Sensor Networks and Information*, pages 635–639, Melbourne, Australia, 2007. IEEE.

[79] OPPO Medical Inc., 2018. [Online]. Available: http://www.oppomedical.com/index.aspx. [Accessed on 16-Mar-2019].

Appendices

PRODUCTION DRAWINGS - ALUMINIUM MOULD

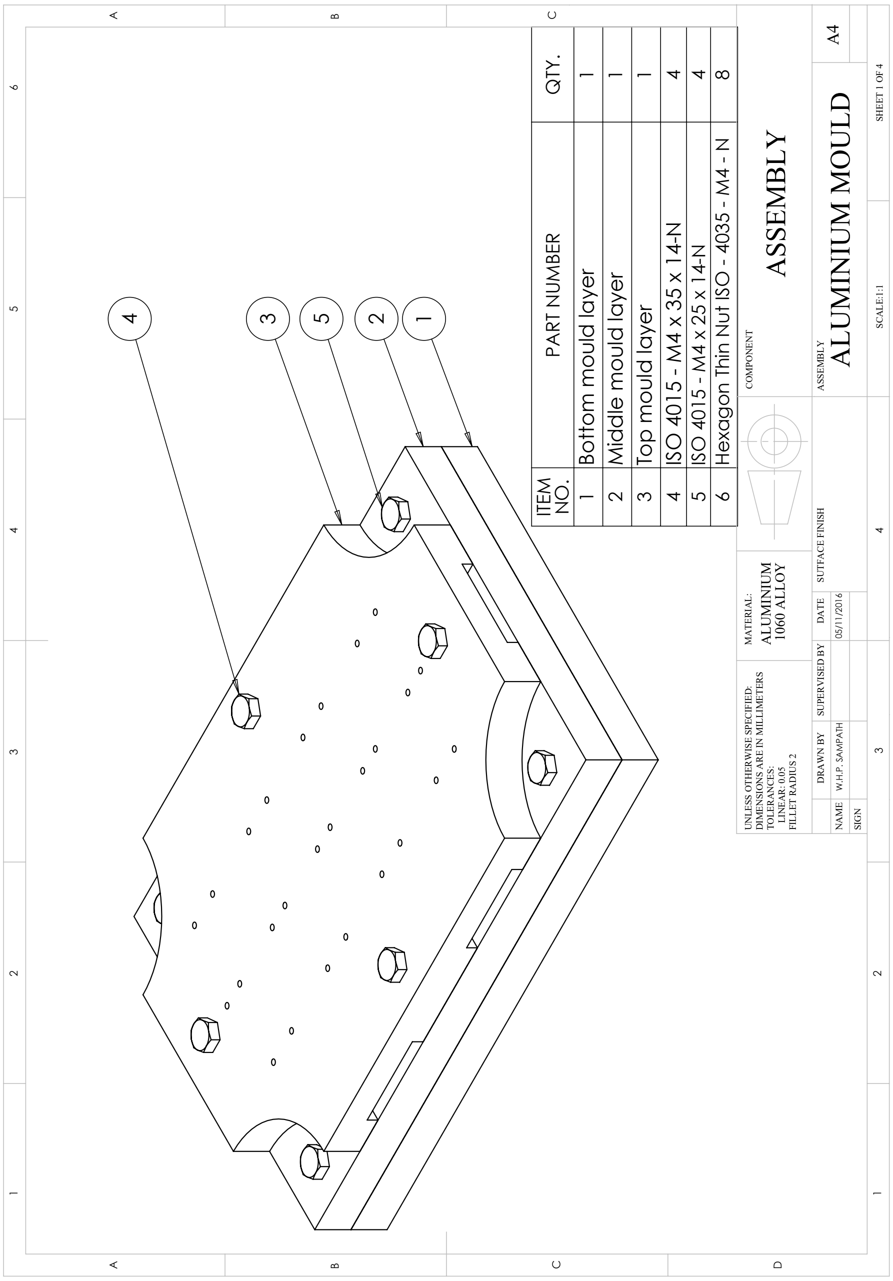

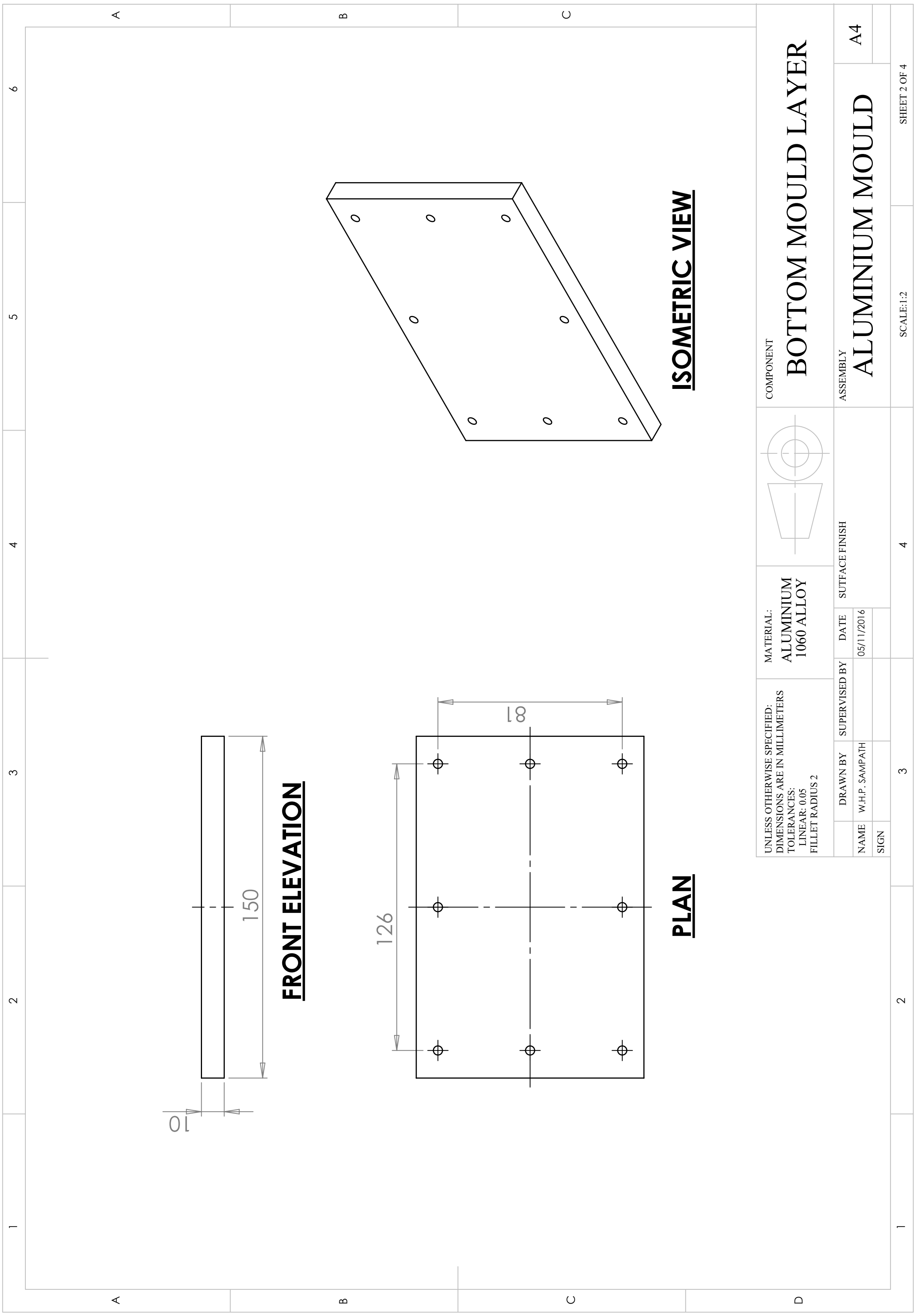
ISOMETRIC VIEW
FRONT ELEVATION
PLAN
150
10
126
81
UNLESS OTHERWISE SPECIFIED:
DIMENSIONS ARE IN MILLIMETERS
TOLERANCES:
LINEAR: 0.05
FILLET RADIUS 2
MATERIAL:
ALUMINIUM
1060 ALLOY
COMPONENT
BOTTOM MOULD LAYER
ASSEMBLY
ALUMINIUM MOULD
A4
DRAWN BY
SUPERVISED BY
DATE
SUTFACE FINISH
NAME
W.H.P. SAMPATH
05/11/2016
SIGN
SCALE:1:2
SHEET 2 OF 4

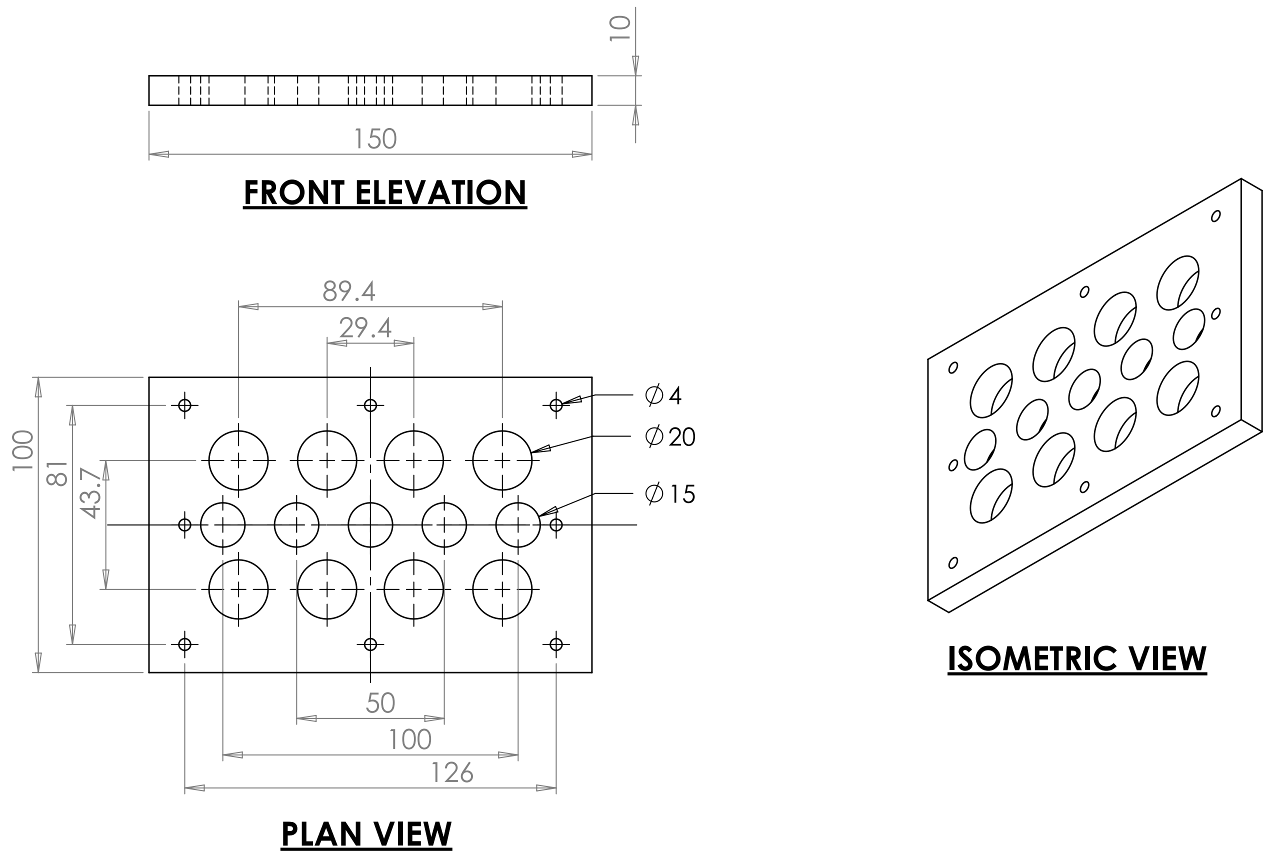

UNLESS OTHERWISE SPECIFIED: DIMENSIONS ARE IN MILLIMETERS TOLERANCES: LINEAR: 0.05 FILLET RADIUS 2		MATERIAL: ALUMINIUM 1060 ALLOY		COMPONENT MIDDLE MOULD LAYER
	DRAWN BY	SUPERVISED BY	DATE	SUTFACE FINISH
NAME	W.H.P. SAMPATH		05/11/2016	ASSEMBLY ALUMINIUM MOULD — A4
SIGN				
SCALE:1:2				SHEET 3 OF 4

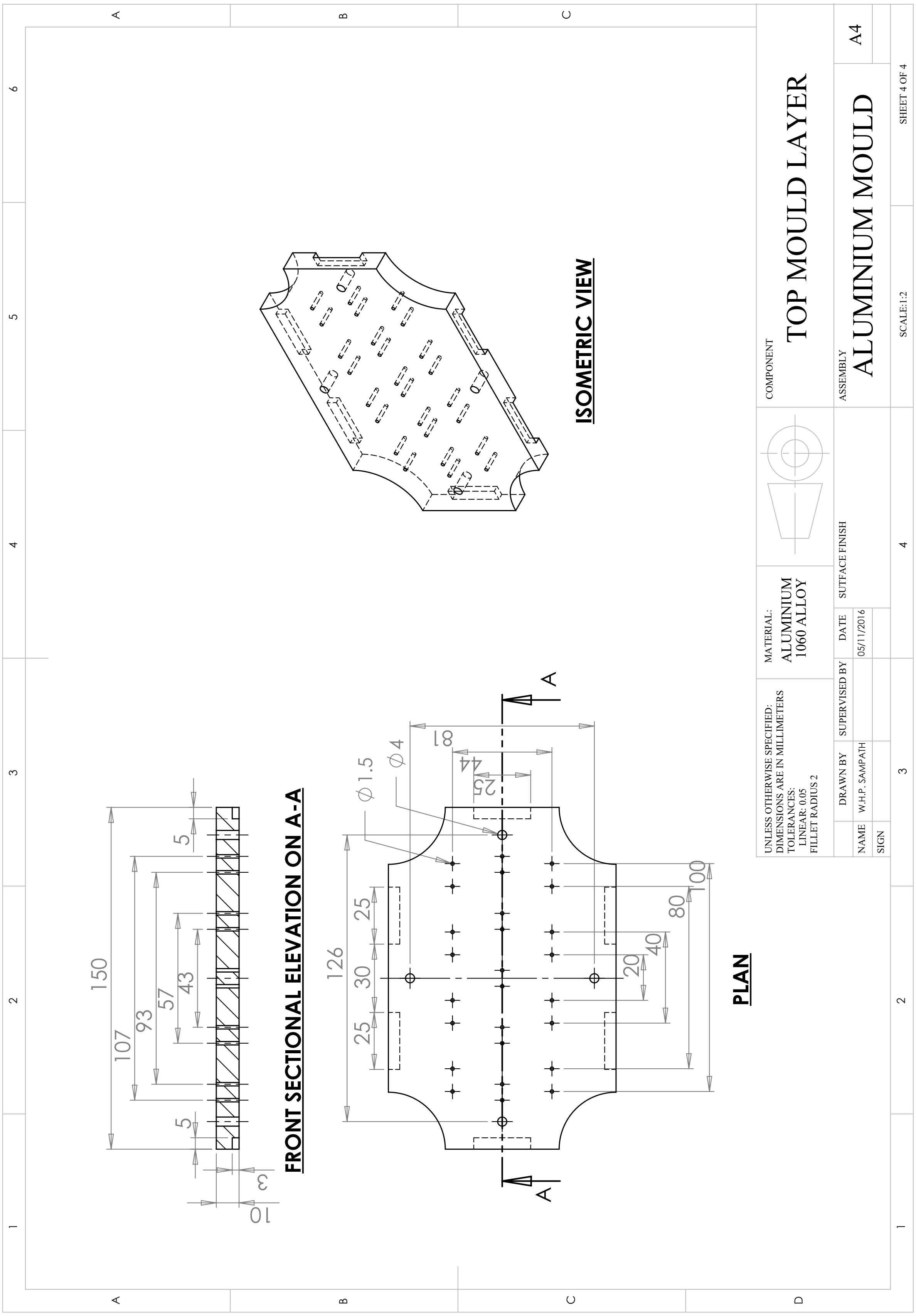
ISOMETRIC VIEW
PLAN
FRONT SECTIONAL ELEVATION ON A-A
A
A
150
107
93
57
43
5
5
3
10
126
25
30
25
Ø1.5
Ø4
81
44
25
100
80
40
20
COMPONENT
TOP MOULD LAYER
ASSEMBLY
ALUMINIUM MOULD
A4
SHEET 4 OF 4
SCALE:1:2
MATERIAL:
ALUMINIUM
1060 ALLOY
SUTFACE FINISH
UNLESS OTHERWISE SPECIFIED:
DIMENSIONS ARE IN MILLIMETERS
TOLERANCES:
LINEAR: 0.05
FILLET RADIUS 2
DRAWN BY
SUPERVISED BY
DATE
NAME
W.H.P. SAMPATH
05/11/2016
SIGN

PRODUCTION DRAWINGS - CYLINDRICAL ARCH SPRING

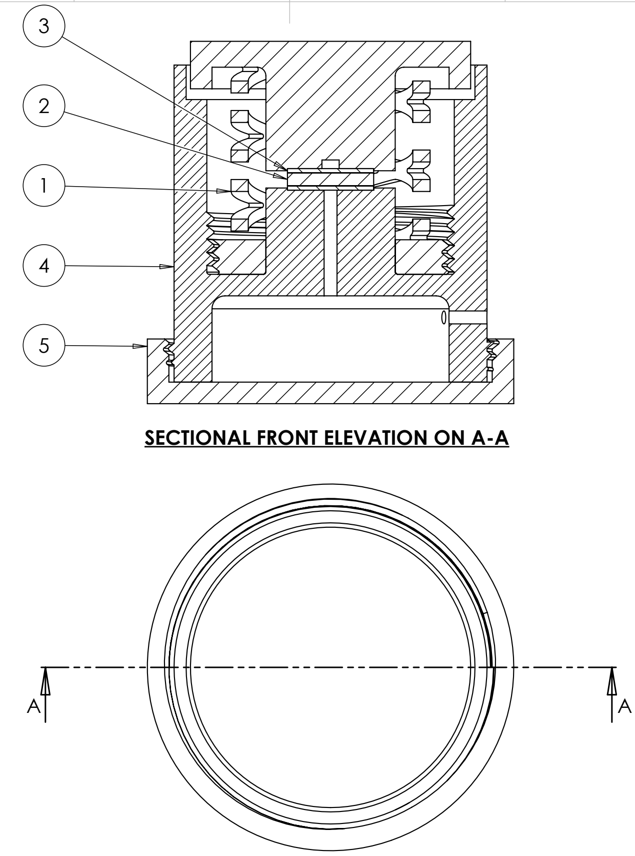

SECTIONAL FRONT ELEVATION ON A-A

PLAN

ITEM NO.	PART NUMBER	QTY.
1	Spring structure	1
2	Polymer pill	1
3	Electrodes	2
4	Outer protection	1
5	Bottom pad	1

UNLESS OTHERWISE SPECIFIED:
DIMENSIONS ARE IN MILLIMETERS
SURFACE FINISH:
TOLERANCES:
LINEAR: 0.1

MATERIAL:

TITLE: ASSEMBLY

TACTILE SENSOR

A4

	NAME	DATE
1	W.H.P. SAMPATH	05/11/2016
2		

SCALE:2:1

SHEET 1 OF 4

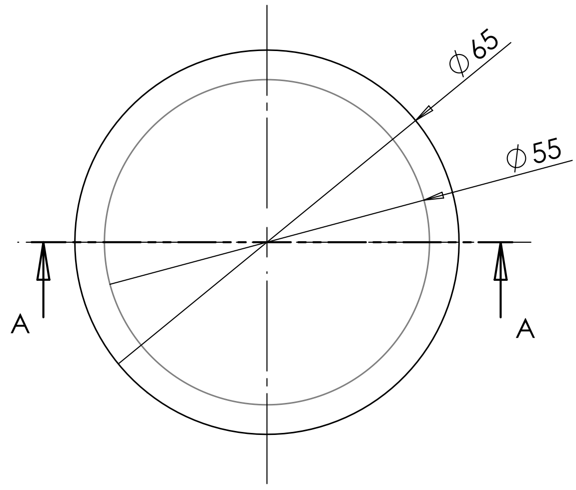

PLAN

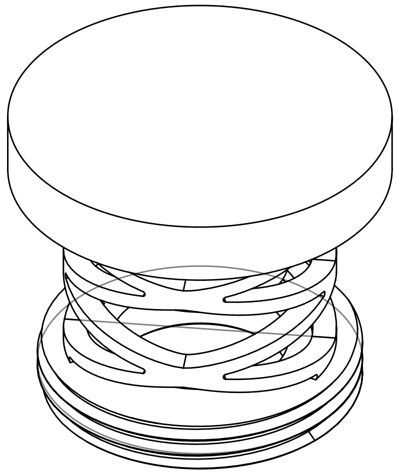

ISOMETRIC VIEW

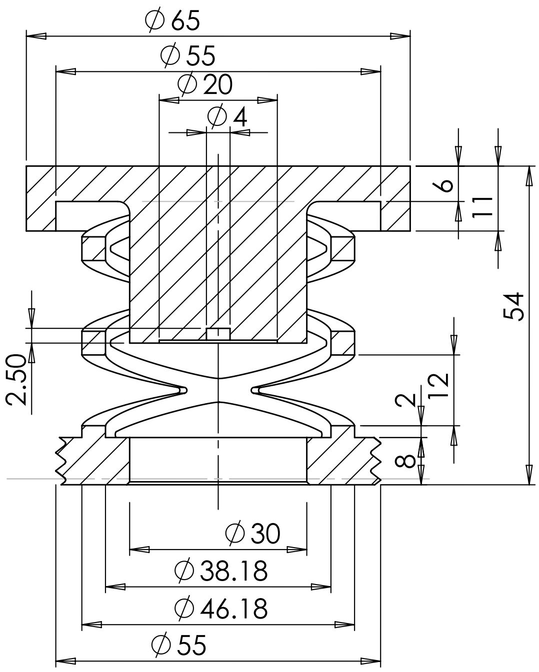

FRONT SECTIONAL ELEVATION ON A-A

UNLESS OTHERWISE SPECIFIED:
DIMENSIONS ARE IN MILLIMETERS
SURFACE FINISH:
TOLERANCES:
LINEAR: 0.1

MATERIAL:
STRATASYS ABSPLUS

TITLE:
SPRING STRUCTURE

TACTILE SENSOR

A4

	NAME	DATE
1	W.H.P. SAMPATH	05/11/2016
2		

SCALE:2:1

SHEET 2 OF 4

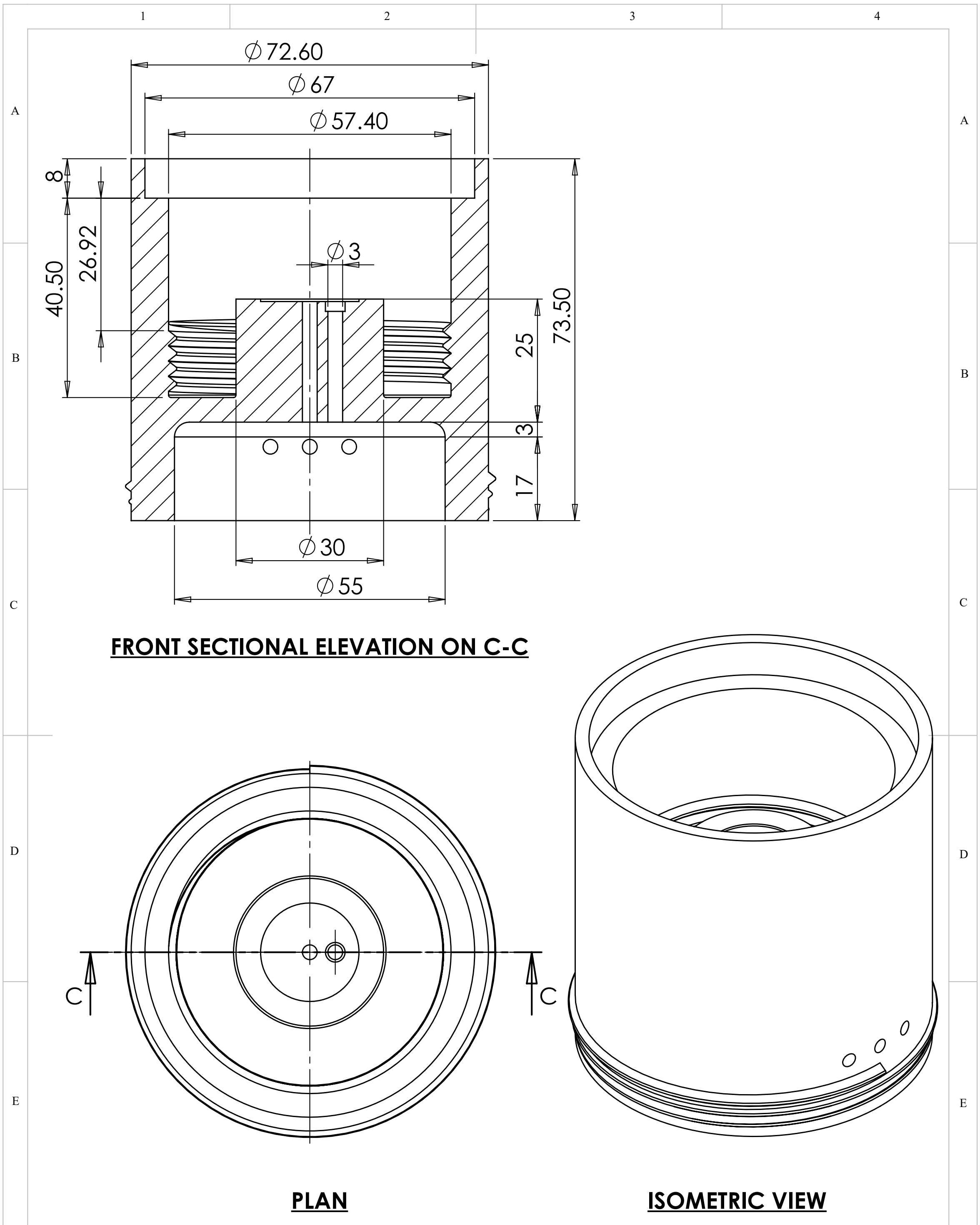

UNLESS OTHERWISE SPECIFIED: DIMENSIONS ARE IN MILLIMETERS SURFACE FINISH: TOLERANCES: LINEAR: 0.1	MATERIAL: STRATASYS ABS		TITLE: OUTER PROTECTION

	NAME	DATE			
1	W.H.P. SAMPATH	05/11/2016		TACTILE SENSOR	A4
2					
	1		2	SCALE:2:1	SHEET 3 OF 4

F

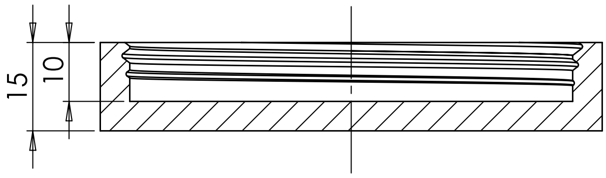

FRONT SECTIONAL ELEVATION ON C-C

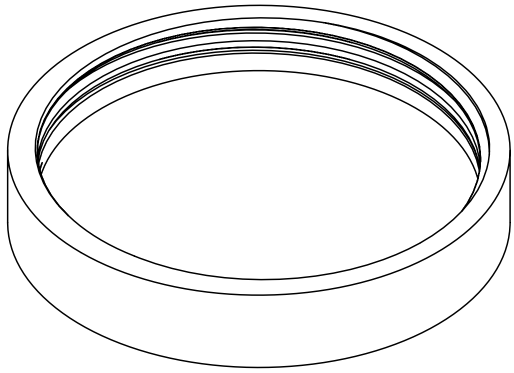

ISOMETRIC VIEW

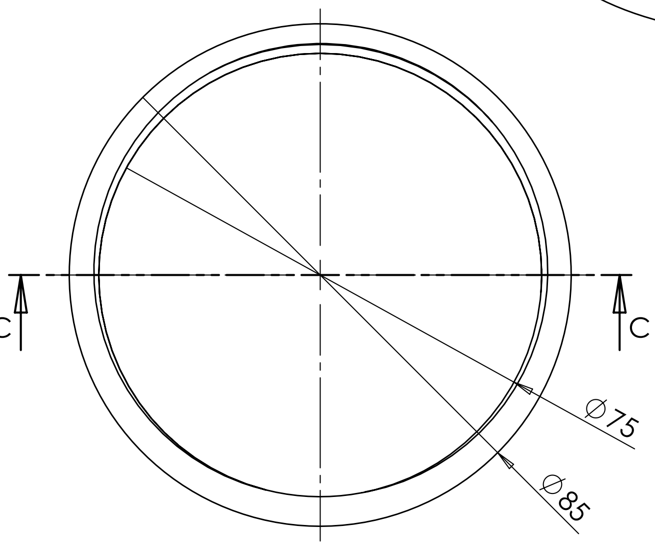

PLAN

UNLESS OTHERWISE SPECIFIED: DIMENSIONS ARE IN MILLIMETERS SURFACE FINISH: TOLERANCES: LINEAR: 0.1		MATERIAL: STRATASYS ABS	TITLE: BOTTOM PAD	
	NAME	DATE	TACTILE SENSOR	A4
1	W.H.P. SAMPATH	05/11/2016		
2				
			SCALE:2:1	SHEET 4 OF 4

PRODUCTION DRAWINGS - PERSPEX MOULD

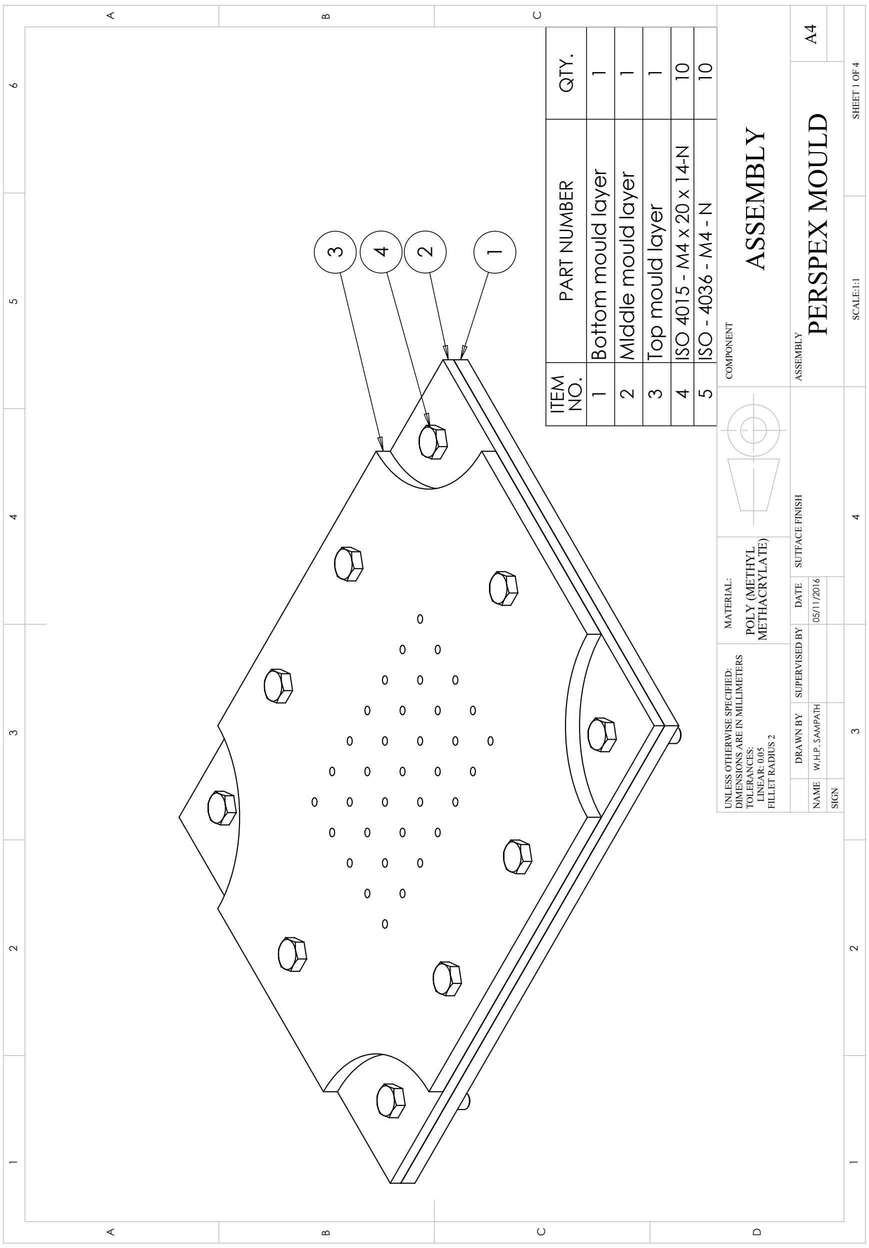

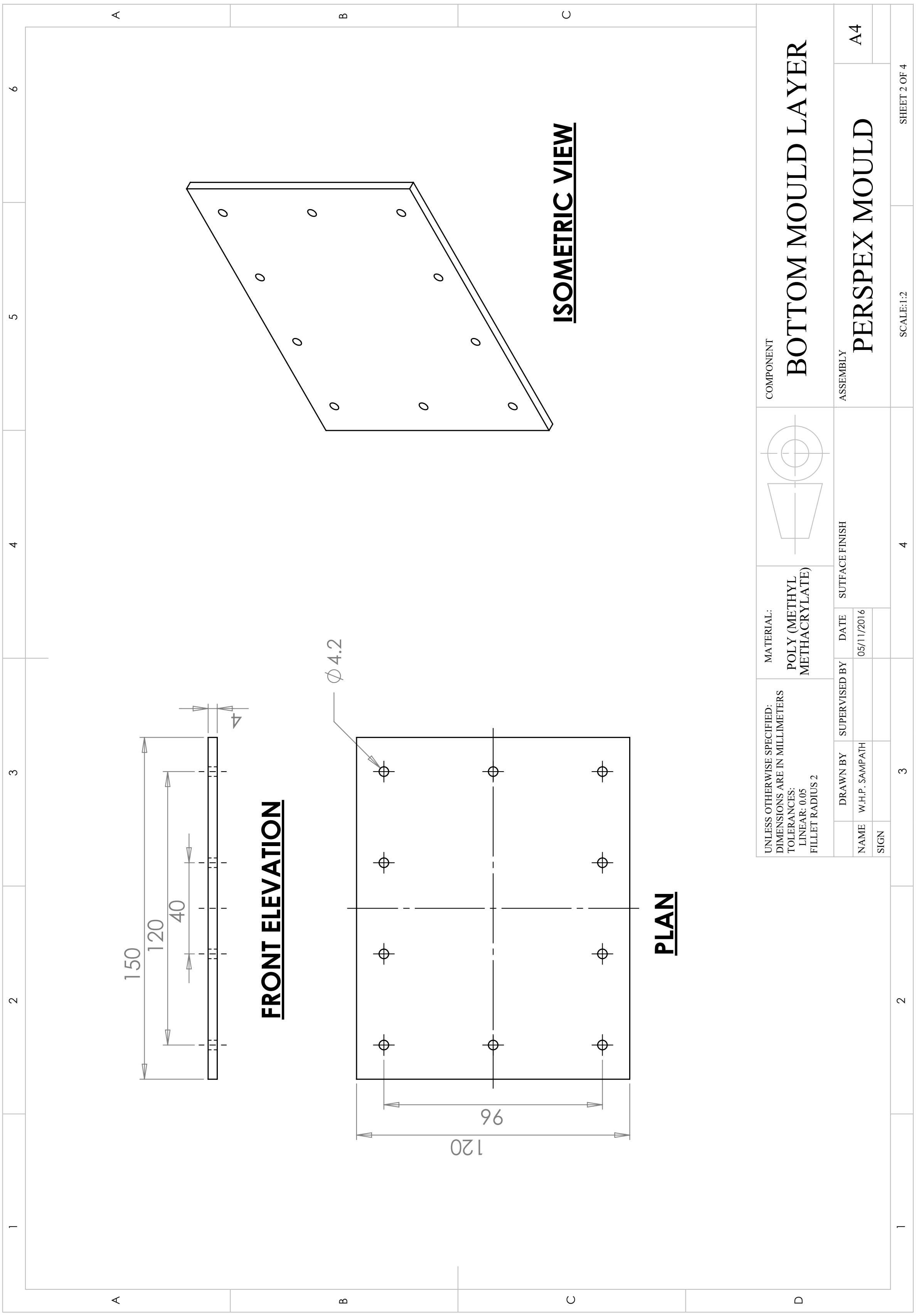
ISOMETRIC VIEW
FRONT ELEVATION
PLAN
150
120
40
4
⌀4.2
96
120
UNLESS OTHERWISE SPECIFIED:
DIMENSIONS ARE IN MILLIMETERS
TOLERANCES:
LINEAR: 0.05
FILLET RADIUS 2
MATERIAL:
POLY (METHYL METHACRYLATE)
COMPONENT
BOTTOM MOULD LAYER
ASSEMBLY
PERSPEX MOULD
A4
DRAWN BY
SUPERVISED BY
DATE
SUTFACE FINISH
NAME
W.H.P. SAMPATH
05/11/2016
SIGN
SCALE:1:2
SHEET 2 OF 4

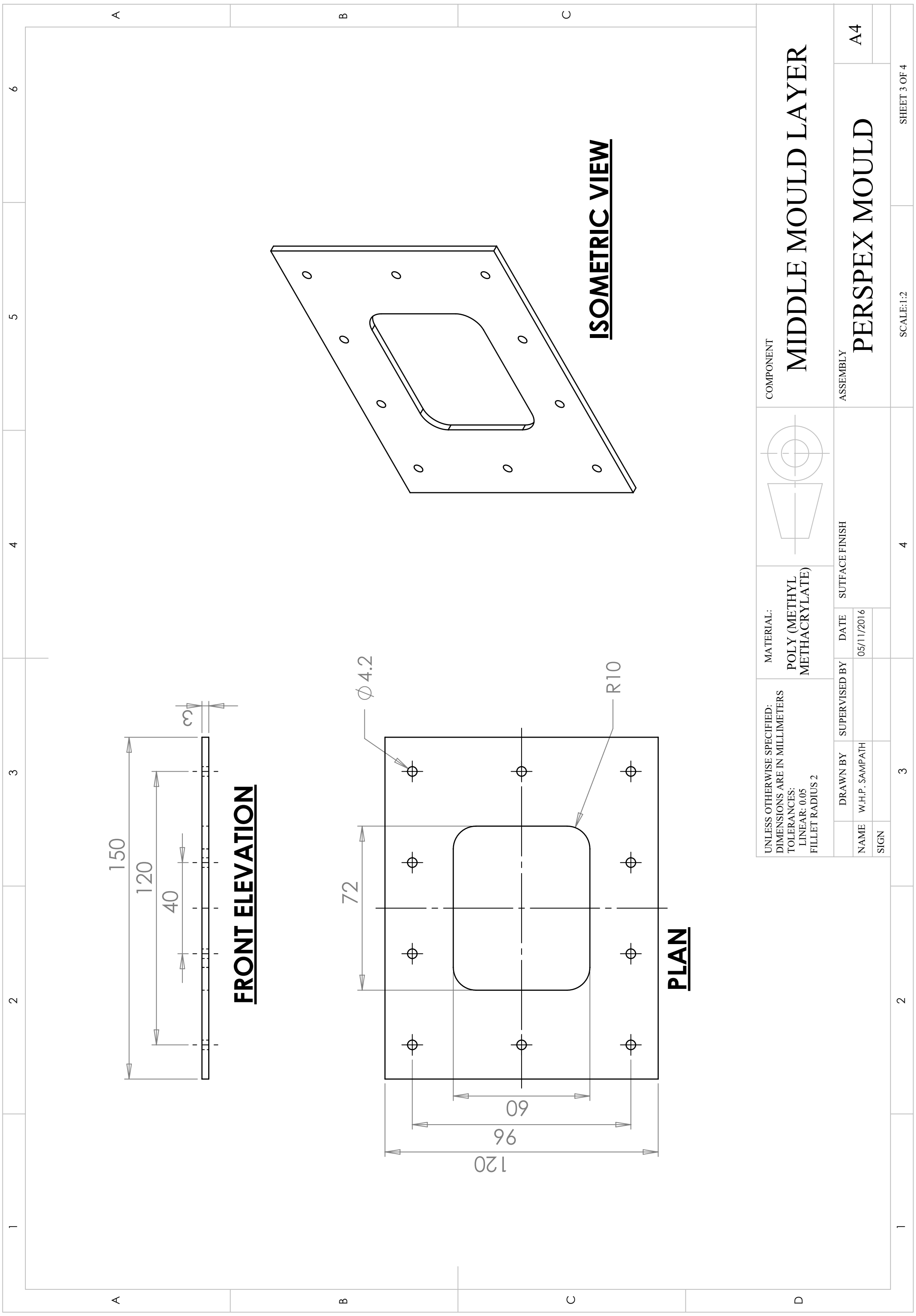
ISOMETRIC VIEW
FRONT ELEVATION
PLAN
150
120
40
3
72
Ø4.2
R10
60
96
120
UNLESS OTHERWISE SPECIFIED:
DIMENSIONS ARE IN MILLIMETERS
TOLERANCES:
LINEAR: 0.05
FILLET RADIUS 2
MATERIAL:
POLY (METHYL METHACRYLATE)
COMPONENT
MIDDLE MOULD LAYER
ASSEMBLY
PERSPEX MOULD
A4
DRAWN BY
SUPERVISED BY
DATE
SUTFACE FINISH
NAME
W.H.P. SAMPATH
05/11/2016
SIGN
SCALE:1:2
SHEET 3 OF 4

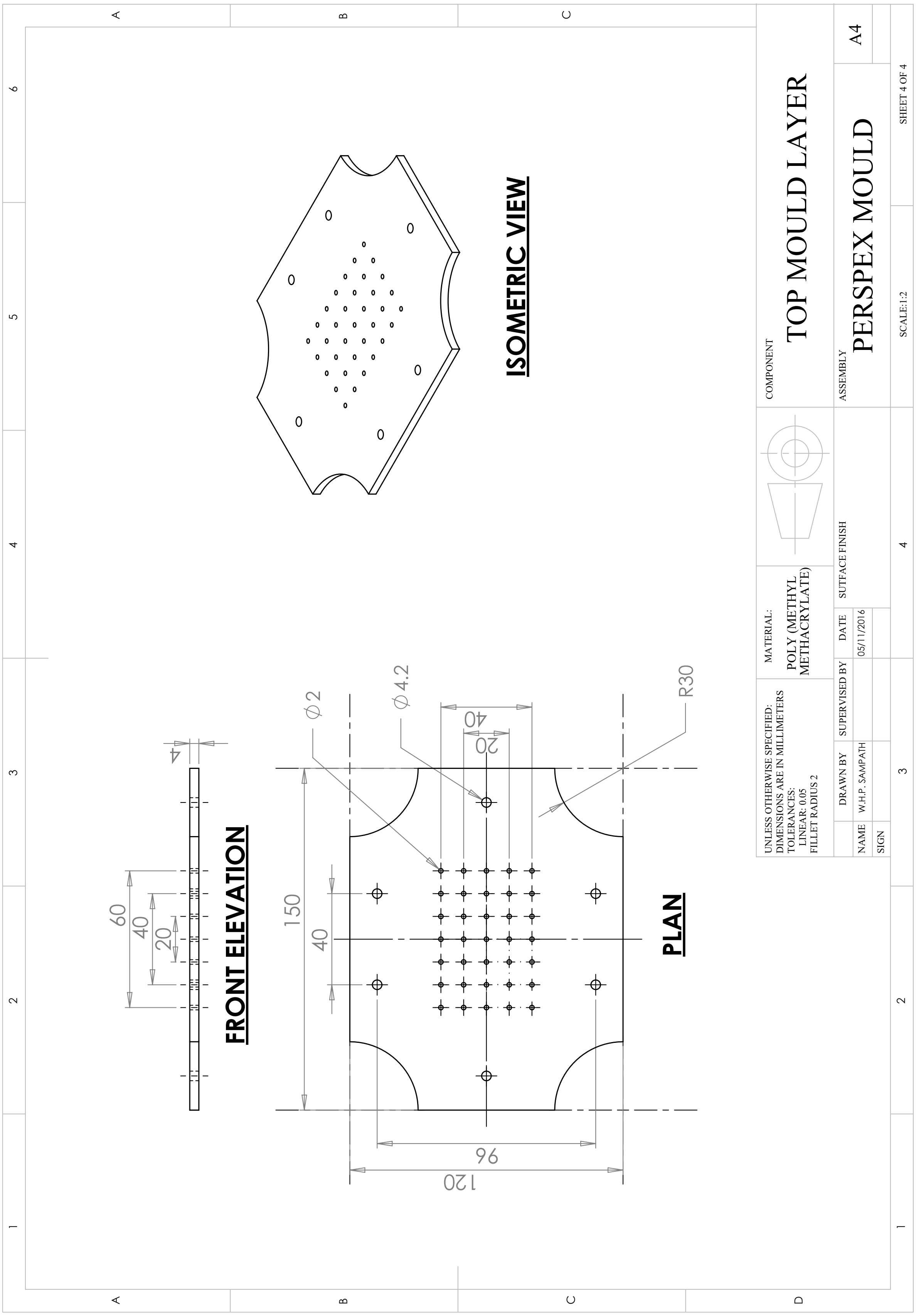
ISOMETRIC VIEW
FRONT ELEVATION
PLAN
COMPONENT
TOP MOULD LAYER
ASSEMBLY
PERSPEX MOULD
A4
SHEET 4 OF 4
SCALE:1:2
MATERIAL:
POLY (METHYL METHACRYLATE)
UNLESS OTHERWISE SPECIFIED:
DIMENSIONS ARE IN MILLIMETERS
TOLERANCES:
LINEAR: 0.05
FILLET RADIUS 2
SUTFACE FINISH
DRAWN BY
SUPERVISED BY
DATE
NAME
W.H.P. SAMPATH
05/11/2016
SIGN
Ø2
Ø4.2
R30
40
20
150
40
96
120
60
40
20
4

MATERIAL SPECIFICATIONS

Stratasys® ABSplus

Stratasys® ABSplus

Categories: Polymer; Rapid Prototyping Polymer; Thermoplastic; ABS Polymer

Material Notes: ABSplus is up to 40 percent stronger than standard ABS material and is an ideal material for conceptual prototyping through design verification through direct digital manufacturing. The marriage of ABSplus with FDM technology gives you the ability to create Real Parts™ direct from digital files that are stronger, smoother, and with more feature detail.

Information provided by Stratasys®

Physical Properties	Metric	English	Comments
Specific Gravity	1.04 g/cc	1.04 g/cc	ASTM D792

Mechanical Properties	Metric	English	Comments
Tensile Strength, Ultimate	36.0 MPa	5220 psi	Type 1, 2"/min; ASTM D638
Elongation at Break	4.0 %	4.0 %	ASTM D638
Tensile Modulus	2.265 GPa	328.5 ksi	Type 1, 2"/min; ASTM D638
Flexural Strength	52.0 MPa	7540 psi	ASTM D790
Flexural Modulus	2.198 GPa	318.8 ksi	ASTM D790
Izod Impact, Notched	0.960 J/cm	1.80 ft-lb/in	ASTM D256

Thermal Properties	Metric	English	Comments
CTE, linear	88.2 µm/m-°C @Temperature 20.0 °C	49.0 µin/in-°F @Temperature 68.0 °F	ASTM D696
Deflection Temperature at 0.46 MPa (66 psi)	96.0 °C	205 °F	ASTM D648
Deflection Temperature at 1.8 MPa (264 psi)	82.0 °C	180 °F	ASTM D648

Stratasys® ABS

Stratasys® ABS (discontinued **)

Categories: Polymer; Rapid Prototyping Polymer; Thermoplastic; ABS Polymer

Material Notes: ABS is a strong, durable production-grade thermoplastic used across many industries. ABS is an ideal material for conceptual prototyping through design verification through direct digital manufacturing. The marriage of ABS with FDM technology gives you the ability to create Real Parts™ direct from digital files, in a variety of standard and custom colors. Refer to the FDM System Material Availability spec sheet for system availability and color options.

Information provided by Stratasys®

Vendors:

Physical Properties	Metric	English	Comments
Specific Gravity	1.05 g/cc	1.05 g/cc	ASTM D792

Mechanical Properties	Metric	English	Comments
Hardness, Rockwell R	105	105	ASTM D785
Tensile Strength, Ultimate	22.0 MPa	3190 psi	Type 1, 2"/min; ASTM D638
Elongation at Break	6.0 %	6.0 %	ASTM D638
Tensile Modulus	1.627 GPa	236.0 ksi	ASTM D638
Flexural Strength	41.0 MPa	5950 psi	ASTM D790
Flexural Modulus	1.834 GPa	266.0 ksi	ASTM D790
Izod Impact, Notched	1.0678 J/cm	2.0004 ft-lb/in	ASTM D256
Izod Impact, Unnotched	2.1356 J/cm	4.0009 ft-lb/in	ASTM D256

Electrical Properties	Metric	English	Comments
Dielectric Constant	2.4 @Frequency 60.0 Hz	2.4 @Frequency 60.0 Hz	IEC 60250
Dielectric Strength	32.0 kV/mm	813 kV/in	IEC 60112

Thermal Properties	Metric	English	Comments
CTE, linear	101 µm/m-°C @Temperature 20.0 °C	56.0 µin/in-°F @Temperature 68.0 °F	ASTM D696
Deflection Temperature at 0.46 MPa (66 psi)	90.0 °C	194 °F	ASTM D648
Deflection Temperature at 1.8 MPa (264 psi)	76.0 °C	169 °F	ASTM D648
Glass Transition Temp, Tg	104 °C	219 °F	DSC (SSYS)
Flammability, UL94	HB	HB	

**

Materials flagged as discontinued (⊘) are no longer part of the manufacturer's standard product line according to our latest information. These materials may be available by special order, in distribution inventory, or reinstated as an active product. Data sheets from materials that are no longer available remain in MatWeb to assist users in finding replacement materials.

Users of our Advanced Search (registration required) may exclude discontinued materials from search results.

Some of the values displayed above may have been converted from their original units and/or rounded in order to display the information in a consistent format. Users requiring more precise data for scientific or engineering calculations can click on the property value to see the original value as well as raw conversions to equivalent units. We advise that you only use the original value or one of its raw conversions in your calculations to minimize rounding error. We also ask that you refer to MatWeb's terms of use regarding this information. Click here to view all the property values for this datasheet as they were originally entered into MatWeb.

Stratasys® PLA

MECHANICAL PROPERTIES[1]	TEST METHOD	ENGLISH		METRIC	
		XZ AXIS	*ZX AXIS*	*XZ axis*	*ZX axis*
Tensile Strength, Yield (Type 1, 0.125", 0.2"/min)	ASTM D638	6,580 psi	3,790 psi	45 MPa	26 MPa
Tensile Strength, Ultimate (Type 1, 0.125", 0.2"/min)	ASTM D638	6,990 psi	3,830 psi	48 MPa	26 MPa
Tensile Modulus (Type 1, 0.125", 0.2"/min)	ASTM D638	440,730 psi	368,200 psi	3,039 MPa	2,539 MPa
Elongation at Break (Type 1, 0.125", 0.2"/min)	ASTM D638	2.5%	1.0%	2.5%	1.0%
Elongation at Yield (Type 1, 0.125", 0.2"/min)	ASTM D638	1.5%	1.0%	1.5%	1.0%
Flexural Strength (Method 1, 0.05"/min)	ASTM D790	12,190 psi	6,570 psi	84 MPa	45 MPa
Flexural Modulus (Method 1, 0.05"/min)	ASTM D790	425,010 psi	358,290 psi	2,930 MPa	2,470 MPa
Flexural Strain at Break	ASTM D790	4.1%	1.9%	4.1%	1.9%
IZOD impact - notched (Method A, 23 °C)	ASTM D256	0.5 ft-lb/in	N/A	27 J/m	N/A
IZOD impact - unnotched (Method A, 23 °C)	ASTM D256	3.6 ft-lb/in	N/A	192 J/m	N/A

THERMAL PROPERTIES	TEST METHOD	ENGLISH	METRIC
Heat Deflection (HDT) @ 66 psi	ASTM D648	127 °F	53 °C
Heat Deflection (HDT) @ 264 psi	ASTM D648	124 °F	51 °C
Vicat Softening Temperature (Rate B/50)	ASTM D1525	129 °F	54 °C
Glass Transition Temperature (Tg)	DMA (SSYS)	145 °F	63 °C
Coefficient of Thermal Expansion (flow)	ASTM E831	56×10^{-06} µin/(in·°F)	101×10^{-06} µm/(m·°C)
Coefficient of Thermal Expansion (xflow)	ASTM E831	57×10^{-06} µin/(in·°F)	102×10^{-06} µm/(m·°C)

SCHEMATIC DIAGRAM OF THE CONTROLLER

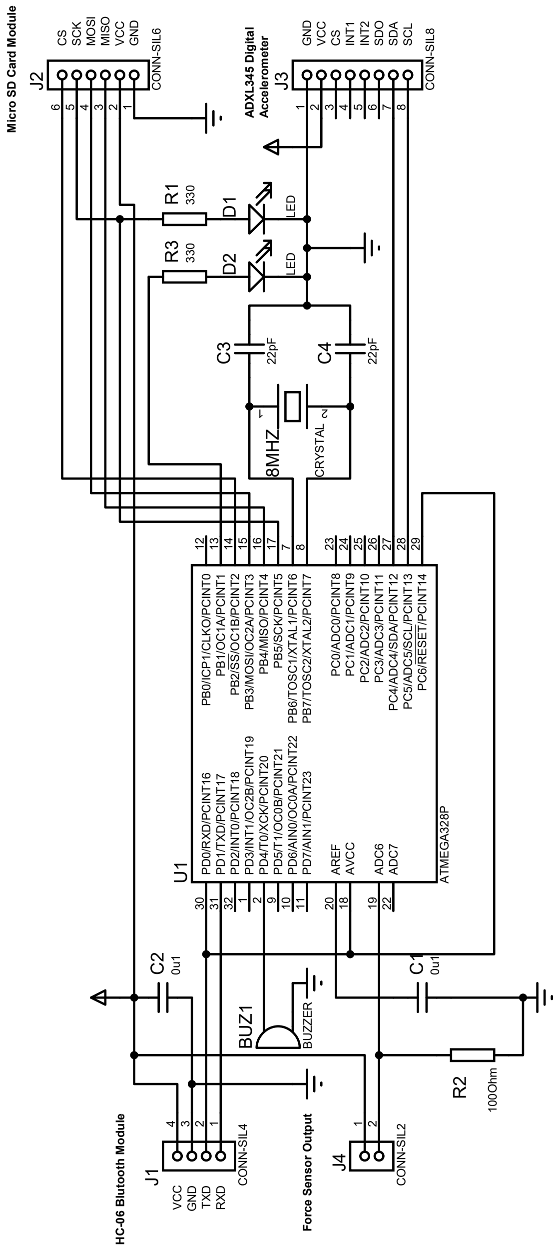

HARDWARE SPECIFICATIONS

8 bit micro-controller (Device: ATmega328p)

Atmel

ATmega328P

8-bit AVR Microcontroller with 32K Bytes In-System Programmable Flash

Features

- High performance, low power AVR® 8-bit microcontroller
- Advanced RISC architecture
  - 131 powerful instructions – most single clock cycle execution
  - 32 × 8 general purpose working registers
  - Fully static operation
  - Up to 16MIPS throughput at 16MHz
  - On-chip 2-cycle multiplier
- High endurance non-volatile memory segments
  - 32K bytes of in-system self-programmable flash program memory
  - 1Kbytes EEPROM
  - 2Kbytes internal SRAM
  - Write/erase cycles: 10,000 flash/100,000 EEPROM
  - Optional boot code section with independent lock bits
    - In-system programming by on-chip boot program
    - True read-while-write operation
  - Programming lock for software security
- Peripheral features
  - Two 8-bit Timer/Counters with separate prescaler and compare mode
  - One 16-bit Timer/Counter with separate prescaler, compare mode, and capture mode
  - Real time counter with separate oscillator
  - Six PWM channels
  - 8-channel 10-bit ADC in TQFP and QFN/MLF package
    - Temperature measurement
  - Programmable serial USART
  - Master/slave SPI serial interface
  - Byte-oriented 2-wire serial interface (Phillips I^2C compatible)
  - Programmable watchdog timer with separate on-chip oscillator
  - On-chip analog comparator
  - Interrupt and wake-up on pin change
- Special microcontroller features
  - Power-on reset and programmable brown-out detection
  - Internal calibrated oscillator
  - External and internal interrupt sources
  - Six sleep modes: Idle, ADC noise reduction, power-save, power-down, standby, and extended standby

- I/O and packages
  - 23 programmable I/O lines
  - 32-lead TQFP, and 32-pad QFN/MLF
- Operating voltage:
  - 2.7V to 5.5V for ATmega328P
- Temperature range:
  - Automotive temperature range: –40°C to +125°C
- Speed grade:
  - 0 to 8MHz at 2.7 to 5.5V (automotive temperature range: –40°C to +125°C)
  - 0 to 16MHz at 4.5 to 5.5V (automotive temperature range: –40°C to +125°C)
- Low power consumption
  - Active mode: 1.5mA at 3V - 4MHz
  - Power-down mode: 1μA at 3V

3-axis accelerometer (Device: ADXL 345)

ANALOG DEVICES

3-Axis, ±2 *g*/±4 *g*/±8 *g*/±16 *g* Digital Accelerometer

ADXL345

FEATURES

Ultralow power: as low as 40 μA in measurement mode and 0.1 μA in standby mode at V_S = 2.5 V (typical)
Power consumption scales automatically with bandwidth
User-selectable resolution
- **Fixed 10-bit resolution**
- **Full resolution, where resolution increases with *g* range, up to 13-bit resolution at ±16 *g* (maintaining 4 m*g*/LSB scale factor in all *g* ranges)**

Embedded, patent pending FIFO technology minimizes host processor load
Tap/double tap detection
Activity/inactivity monitoring
Free-fall detection
Supply voltage range: 2.0 V to 3.6 V
I/O voltage range: 1.7 V to V_S
SPI (3- and 4-wire) and I^2C digital interfaces
Flexible interrupt modes mappable to either interrupt pin
Measurement ranges selectable via serial command
Bandwidth selectable via serial command
Wide temperature range (−40°C to +85°C)
10,000 *g* shock survival
Pb free/RoHS compliant
Small and thin: 3 mm × 5 mm × 1 mm LGA package

APPLICATIONS

Handsets
Medical instrumentation
Gaming and pointing devices
Industrial instrumentation
Personal navigation devices
Hard disk drive (HDD) protection
Fitness equipment

FUNCTIONAL BLOCK DIAGRAM

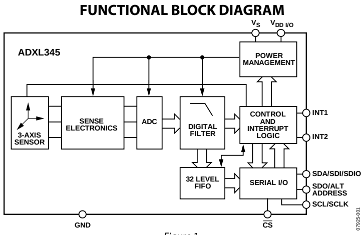

Figure 1.

ARDUINO IDE BASED PROGRAMME FOR THE CONTROLLER

```
#include <SPI.h>
#include <SD.h>
#include <SparkFun_ADXL345.h>          // SparkFun ADXL345 Library

const int chipSelect = 10;
const int Buzzer = 4;
const int LED = 9;
const int SensorPin =6;
ADXL345 adxl = ADXL345();              // Use for I2C Communication
int x,y,z;                             // Accelerometer Readings

String dataString = "";                // Making a string for assembling the data to log:

void setup()
{
  pinMode(Buzzer, OUTPUT);             // Initialize digital pin Buzzer as an output.
  pinMode(LED, OUTPUT);                // Initialize digital pin Buzzer as an output.

  Initiate();                          // Initiation notification via the buzzer

  Serial.begin(9600);                  // Serial initiation
  while (!Serial)
  {
    ;                                  // Waiting serial port to connect.
  }

  adxl.powerOn();                      // Power on the ADXL345

  adxl.setRangeSetting(16);            // Range settings of the accelerometer
                                       // Accepted values are 2g, 4g, 8g or 16g
                                       // Higher Values = Wider Measurement Range
                                       // Lower Values = Greater Sensitivity
/*// Configure the device to be in 4 wire SPI mode when set to '0' or 3 wire SPI mode when set to 1*/
  adxl.setSpiBit(0);
                                       // Default: Set to 1
}
```

```
void loop()                                // The loop function runs over and over again forever
{
 if(millis()%15==0)                        // Reading in 15 mili-second intervals
 {
    Accelerometer();                       // Reading and writing accellerometer values

    pinMode(5, OUTPUT);                    // Adjust the resistor vautes in the vltage devider
    pinMode(7, INPUT);
    pinMode(8, INPUT);
    digitalWrite(5,HIGH);

    int sensor = analogRead(SensorPin);    // Reading the sensor pin

    dataString += String(sensor);          // Amend the string
    Serial.println(dataString);
   }
}

void Accelerometer()
{
 adxl.readAccel(&x, &y, &z);               // Read the accelerometer values and store them in variables declared above x,y,z

 dataString = "";                          // Output Results to Serial

 dataString += x;                          // Accelerometer values
 dataString += ",";

 dataString += y;
 dataString += ",";

 dataString += z;
 dataString += ",";
}

void Initiate()                            // Short && Long Beeps
{
 digitalWrite(Buzzer, HIGH);
 digitalWrite(LED, HIGH);
 delay(20);
 digitalWrite(Buzzer, LOW);
 digitalWrite(LED, LOW);
 delay(30);
 digitalWrite(Buzzer, HIGH);
 digitalWrite(LED, HIGH);
 delay(100);
 digitalWrite(Buzzer, LOW);
 digitalWrite(LED, LOW);
}
```